Structure and Function of Enzymes Involved in Tetrapyrrole Biosynthesis

Von der Fakultät für Lebenswissenschaften

der Technischen Universität Carolo-Wilhelmina

zu Braunschweig

zur Erlangung des Grades einer

Doktorin der Naturwissenschaften

(Dr. rer. nat.)

genehmigte

D i s s e r t a t i o n

von Ilka Ursula Heinemann
aus Osnabrück

1. Referent: Prof. Dr. Dieter Jahn
2. Referent: Prof. Dr. Michael Steinert
eingereicht am: 20.08.2007
mündliche Prüfung (Disputation) am: 21.09.2007

Druckjahr 2007

VORVERÖFFENTLICHUNGEN DER DISSERTATION

Teilergebnisse aus dieser Arbeit wurden mit Genehmigung der Fakultät für Lebenswissenschaften, vertreten durch den Mentor der Arbeit in folgenden Beiträgen vorab veröffentlicht:

PUBLIKATIONEN

Buchenau, B., Kahnt, J., **Heinemann, I.U.**, Jahn, D., Thauer, R.K. Heme biosynthesis in *Methanosarcina barkeri* via a pathway involving two methylation reactions. *J. Bacteriol.* 2006 Dec;188(24):8666-8.

Heinemann, I.U., Diekmann, N., Masoumi, A., Koch, M., Messerschmidt, A., Jahn, M., Jahn, D. Functional definition of the tobacco protoporphyrinogen IX oxidase substrate-binding site. *Biochem. J.* 2007 Mar 15;402(3):575-80.

EINGEREICHTE PUBLIKATIONEN

Tan, F.C., Cheng, Q., Saha, K., **Heinemann, I.U.**, Jahn, M., Jahn, D. and Smith, A.G. Identification of the *Arabidopsis* gene encoding the tetrapyrrole biosynthesis enzyme uroporphyrinogen III synthase by functional complementation of a yeast mutant. *Under revision in Biochemical Journal.*

Masoumi, A., **Heinemann, I.U.**, Rhode, M., Jahn, M., Jahn, D. Metabolic channeling of photoreactive protoporphyrinogen IX in *Thermosynechococcus elongatus* during the ultimate steps in porphyrin biosynthesis. *Under revision in Journal of Bacteriology.*

Heinemann, I.U., Schulz, C., Jaffe, E., Schubert, W.D., Wachi, M., Jahn, M., Jahn, D. Structure of the *Pseudomonas aeruginosa* porphobilinogen synthase in complex with the antibiotic alaremycin. *Under review.*

TAGUNGSBEITRÄGE

Heinemann, I.U., Schulz, C., Jaffe, E., Schubert, W.D., Wachi, M., Jahn, M., and Jahn, D. The molecular target of the antibiotic alaremycin. Implications from ist crystal structure with porphobilinogen synthase and kinetic parameters. (Poster) Gordon Research Conference, Enzymes, Coenzymes and Metabolic Pathways, Biddeford, USA. (2007)

Heinemann, I.U., Schulz, C., Jaffe, E., Schubert, W.D., Wachi, M., Heinz, D., Jahn, M., and Jahn, D. Crystal structure of *Pseudomonas aeruginosa* porphobilinogen synthase (PBGS) in complex with the novel antibiotic alaremycin. (Poster) VAAM-Jahrestagung, Osnabrück, Germany. (2007)

Heinemann, I.U., Diekmann, N., Masoumi, A., Koch, M., Jahn, M. and Jahn, D. Functional definition of the active site of protoporphyrinogen IX oxidase involved in tetrapyrrole biosynthesis. (Poster) VAAM-Jahrestagung, Jena, Germany. (2006)

Heinemann, I.U., Jahn, M., Moser, J., Schubert, W.D., Heinz, D., Warren, M., Thauer, R.K. and Jahn, D. Towards the elucidation of the late pathway to heme. (Poster) Gordon Research Conference, Archaea: Ecology, Metabolism & Molecular Biology, Oxford, Great Britain. (2006)

Heinemann, I.U., Jahn, M. and Jahn, D. Structure-based mutagenesis of tobacco protoporphyrinogen IX oxidase. Porphyrins and Porphyrias. (Poster) Cape town, South Africa. (2005)

Meiner Familie

„Nicht Kunst und Wissenschaft allein,
Geduld muss bei dem Werke sein.“

Johann Wolfgang von Goethe
Faust, Der Tragödie erster Teil, Hexenküche

TABLE OF CONTENTS

ABBREVIATIONS

A	ampere
Å	Ångström
ALA	5-aminolevulinic acid
ALAS	5-aminolevulinic acid synthase
amp	ampicillin
APS	ammonium peroxidisulfate
AtUROS	*Arabidopsis thaliana* uroporphyrinogen III synthase
ATP	adenosine triphosphate
BLAST	basic local alignment search tool
bp	base pair
BTP	1,3,-bis-[tris(hydroxymethyl)-methylamino]propane
C	Celsius (°C)
CPO	coproporphyrinogen III oxidase
Da	Dalton
ddNTP	didesoxy nucleotide triphosphate
DMBA	4-dimethylbenzaldehyde
DNA	desoxyribonucleic acid
dNTP	desoxy nucleotide triphosphate
Dnase	desoxyribonuclease
EDTA	ethylenediamine tetraacetic acid
et al.	*et alteri* (and others)
e. g.	*exempli gratia* (for example)
FAD	flavin adenine dinucleotide
FMN	flavin adenine mononucleotide
FC	ferrochelatase
Fig.	figure
FPLC	fast performance liquid chromatography
fwd	forward
g	→*centrifugation:* earth gravity (x *g*) → *weight*: gram

GST	glutathione-S-transferase
GluTR	glutamyl-tRNA-reductase
GSA	glutamate-1-semialdehyde
GSAM	glutamate-1-semialdehyde-2,1-aminomutase
h	hour
HEPES	4-(2-hydroxyethyl)-piperazine-1-ethane sulfonic acid
HsPBGS	*Homo sapiens* porphobilinogen synthase
IC_{50}	inhibitor concentration reducing enzyme activity to 50 %
IPTG	isopropyl-β-D-thiogalactopyranoside
k	kilo
kan	kanamycin
k_{cat}	catalytic constant
K_M	Michaelis Menten constant
L	liter
LA	levulinic acid
λ	wavelength
LB	Luria Bertani
m	milli
M	molar (mol/L)
MALDI-TOF	matrix-assisted laser desorption/ionization – time of flight
μ	micro
MbPBGS	*Methanosarcina barkeri* porphobilinogen synthase
MES	2-(N-morpholino)ethanesulfonic acid
MIC	minimal inhibitory concentration
min	minute
M_r	relative molecular mass
NAD(P)	nicotine adenine dinucleotide (phosphate), reduced form
n.d.	not detectable
Ni-IDA	nickel agarose with tridentate chelating agent iminodiacetic acid
Ni-NTA	nickel agarose with chelating agent nitrilo-tri-acetic acid
NtPPO2	mitochondrial protoporphyrinogen IX oxidase from *Nicotiana tabacum*
rpm	rotation per minute
OD_λ	optical density at a wavelength λ in nm

PaPBGS	*Pseudomonas aeruginosa* porphobilinogen synthase
PBGS	porphobilinogen synthase
PBGD	porphobilinogen deaminase
PBS	phosphate buffered saline
PCR	polymerase chain reaction
PEG	polyethyleneglycol
PMSF	phenylmethanesulfonyl fluorid
rev	reverse
RNase	ribunuclease
PPO	protoporphyrinogen IX oxidase
ORF	open reading frame
RT	room temperature
s	second
SAM	*S*-adenosyl-*L*-methionine
SCV	small colony variants
SDS	sodium dodecyl sulfate
SDS-PAGE	sodium dodecyl sulfate polyacrylamide gel electrophoresis
sp.	species
Tab.	table
TEMED	tetramethylen diamine
Tris	Tris-(hydroxymethyl)-aminomethane
U	unit
UROD	uroporphyrinogen III decarboxylase
UROS	uroporphyrinogen III synthase
UV	ultraviolet
V	volt
v_{max}	maximal velocity
VP	variegate porphyria
v/v	volume per volume
WT	wildtype
w/v	weight per volume

1 INTRODUCTION

1.1 Tetrapyrroles

1.1.1 Structure and Function of Naturally Occurring Tetrapyrroles

Tetrapyrroles consist of four pyrrolic rings, in general attached to each other in a cyclic or linear form *via* methine bridges. One exception are the corrinoids which lack one brigde carbon. The basic structure of a cyclic tetrapyrrole is the porphyrin macrocycle shown in Fig. 1.

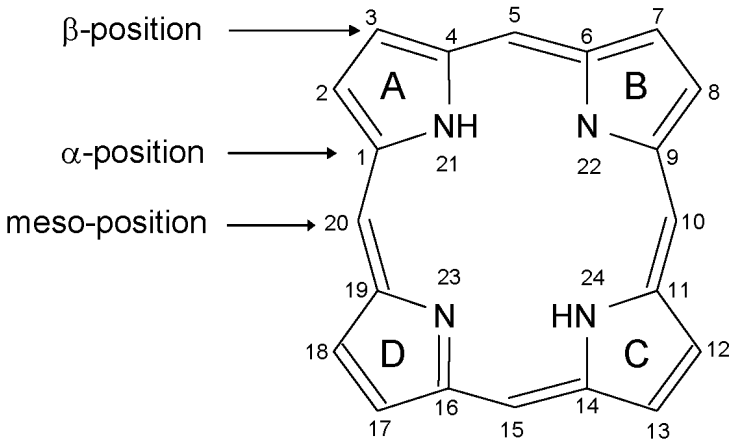

Fig. 1: Basic structure of cyclic tetrapyrroles, the porphyrin ring.
Pyrrole rings are denoted A-D, carbon and nitrogen atoms are numbered.

The pyrrole rings of the macrocycle are denoted A – D around the circle in clockwise direction. Within the pyrrole ring, carbon atoms adjacent to the nitrogens are named α-carbons (*e.g.* C_1). Carbon atoms in distal position to the nitrogens are β-carbons (*e.g.* C_2) while the methine bridge carbons are in meso-position. The macrocyclic tetrapyrrole contains a system of fully conjugated double bonds, resulting in the red color of human blood and the green color of plants. Another important property of porphyrins is their ability to chelate diverse divalent metal ions such as Fe^{2+}, Mg^{2+}, Ni^{2+} or Co^{2+}. *In vivo*, the cyclic tetrapyrroles differ in the oxidation state of their ring systems, the nature of the chelated metal ion and the ring substituents (Frankenberg *et al.*, 2003, Jahn *et al.*, 1996).

Hemes are true porphyrins whereas tetrapyrroles with variations of the basic porphyrin structure are known as porphinoids. Examples include more reduced cyclic tetrapyrroles such as chlorophylls (a chlorin), bacteriochlorophylls (chlorins or bacteriochlorins), siroheme (an isobacteriochlorin), coenzyme F_{430} and heme d_1 (Raux *et al.*, 2003, Thauer and Bonacker, 1994). Finally, tetrapyrroles like vitamin B_{12} belong to the class of corrinoids

characterized by a missing methine bridge in the porphyrin ring (Banerjee and Ragsdale, 2003). Linear tetrapyrroles like bilins also contain only three bridge carbons and all result from the cleavage of previously cyclic tetrapyrroles. The structures of important representatives of natural occurring porphyrins, porphinoids and corrinoids are depicted in Fig. 2.

Tetrapyrroles fulfill diverse functions and are essential compounds for almost all living organisms. Iron-containing heme as a cofactor of hemoglobin coordinates molecular oxygen and carbon dioxide and is responsible for their transport in the cardiovascular system from the lungs to the tissues and *vice versa*. Many enzymes such as peroxidases and catalases also rely on heme as prosthetic group. Furthermore, heme plays an important role in respiration, since heme-containing cytochromes are part of various electron transfer chains (Panek and O'Brian, 2002). Heme proteins can serve as sensors for diatomic gases such as O_2, CO and NO and for CO_2 in signal transduction pathways (Rodgers, 1999). Magnesium-chelating chlorophylls – the origin of the green color in plants – and bacteriochlorophylls are essential to the photosynthetic apparatus of plants and bacteria (Beale, 1999). The yellow nickel-containing coenzyme F_{430} is the cofactor of methylcoenzyme M reductase involved in methane formation (Thauer and Bonacker, 1994).

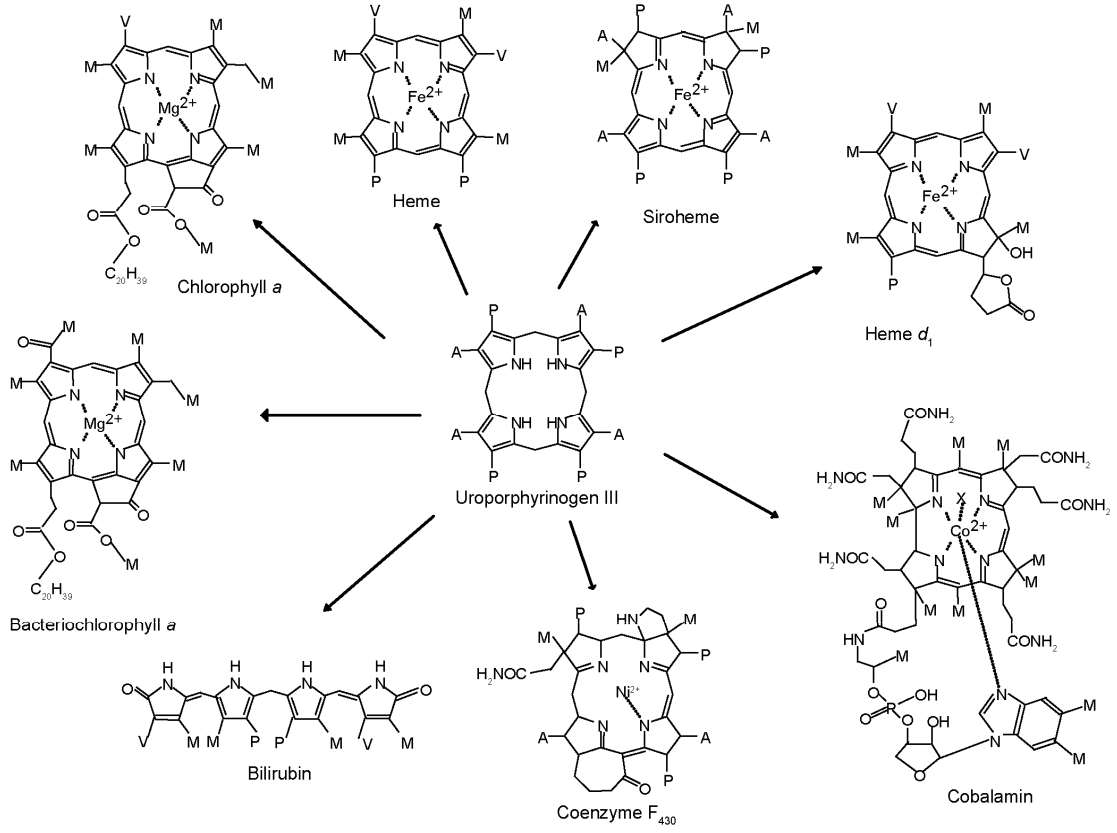

Fig. 2: Structures of important tetrapyrrole representatives.
Depicted are naturally occurring tetrapyrroles and their common precursor molecule uroporphyrinogen III. A = acetate side chain; P = propionate side chain; M = methyl group; V = vinyl group.

Derivatives of the cobalt-containing vitamin B_{12} are the cofactors of a number of enzymes that catalyze radical-dependent reactions such as methyl transfer reactions or nucleotide reduction (Banerjee and Ragsdale, 2003). The iron chelating siroheme is a greenish cofactor involved in reactions during assimilatory nitrite or sulfite reduction (Raux *et al.*, 2003). In contrast, linear tetrapyrroles do not contain a tightly bound metal. They are employed as chromophoric photoreceptors in cyanobacterial and higher-plant light-harvesting systems (Frankenberg and Lagarias, 2003). The variety of functions fulfilled by tetrapyrroles underscores their importance in nature, and explains the extensive effect of disorders in tetrapyrrole anabolism.

1.1.2 Biosynthesis of Tetrapyrroles

The shared structural core of tetrapyrroles intuitively implies a related biosynthetic pathway. All tetrapyrroles derive from the common precursor molecule 5-aminolevulinic acid (ALA) and the initial biosynthetic steps are highly conserved. The major branching point occurs after the formation of uroporphyrinogen III, the first cyclic intermediate. It is either converted into protoporphyrin IX or precorrin-2. Protoporphyrin IX is utilized to synthesize hemes, chlorophylls and bacteriochlorophylls, while precorrin-2 gives rise to siroheme, heme d_1, coenzyme F_{430} and corrinoids. An overview of the divergent biochemical pathways of tetrapyrroles is given in Fig. 3.

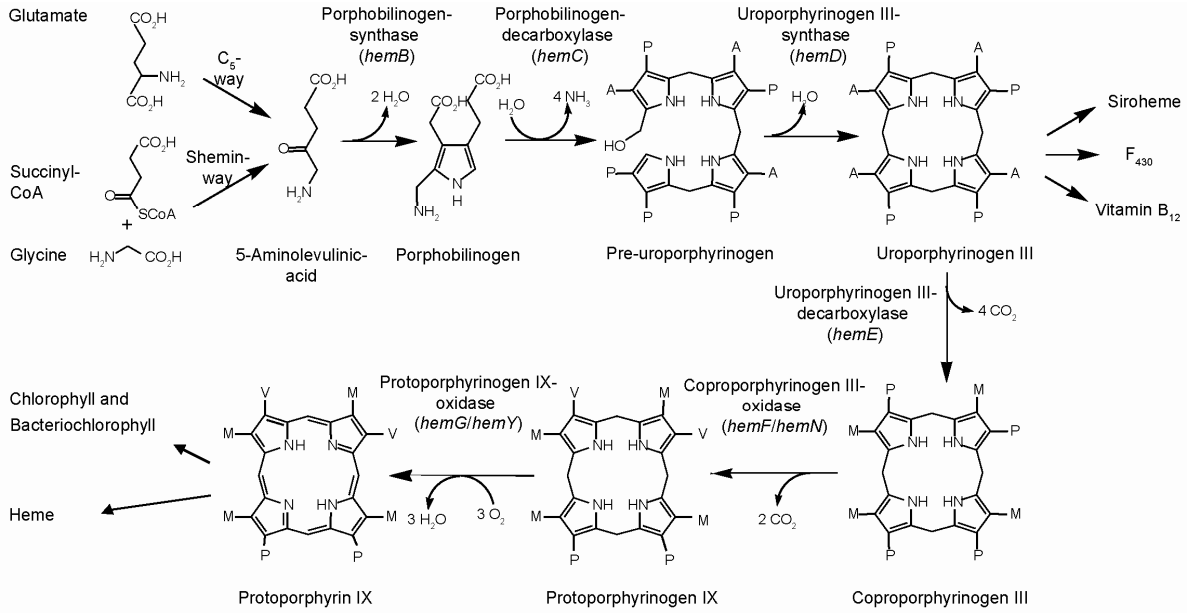

Fig. 3: The biosynthesis of tetrapyrroles.
The names of the enzymes and their respective genes (bacterial) are given above the arrows. A = acetate side chain; P = propionate side chain; M = methyl group; V = vinyl group.

In eukaryotes, tetrapyrrole biosynthesis is limited to the formation of heme, siroheme, chlorophyll and bilins. Prokaryotes additionally synthesize complicated tetrapyrroles as corrinoids, coenzyme F_{430} and heme d_1 (Jahn *et al.*, 1996).

1.1.3 Heme Biosynthesis

1.1.3.1 Biosynthesis of 5-Aminolevulinc Acid

The biosynthesis of all tetrapyrroles (Fig. 3) starts with the formation of ALA. This small molecule is the sole source of all carbon and nitrogen atoms required for the formation of the tetrapyrrolic macrocycle. There are, however, two alternate routes leading to ALA formation. Of these, the "Shemin pathway" was discovered first. It is formed in non photosynthetic eukaryotes such as animals and fungi as well as in the α-group of proteobacteria (Shemin and Russel, 1953). The pyridoxal-5'-phosphate dependent enzyme ALA synthase (ALAS; encoded by *hemA*; EC 2.3.1.37) synthesizes ALA in a single step through condensation of glycine and succinyl-CoA under elimination of carbon dioxide (Kikuchi *et al.*, 1958, O´Brian and Thöny-Meyer, 2002). The second route of ALA formation is the "C_5 - pathway" found in most bacteria, archaea and plants (Beale and Castelfranco, 1973). Here, glutamyl-tRNA serves as initial substrate and two enzymatic steps are required to form ALA (Jahn *et al.*, 1992). The first enzyme of this path, glutamyl-tRNA reductase (GluTR; encoded by *hemA*; EC 6.1.1.17), is NADPH dependent and catalyzes the reduction of glutamyl-tRNA to the instable glutamate-1-semialdehyde (GSA) (Jahn *et al.*, 1991, Moser *et al.*, 1999). In the following step glutamate-1-semialdehyde-2,1-aminomutase (GSAM; encoded by *hemL*; EC 5.4.3.8) converts GSA to ALA in a pyridoxal-5'-phosphate-dependent transamination reaction (Ilag and Jahn, 1992). Thus, the 5-carbon skeleton of glutamate is incorporated into ALA, giving rise to the name "C_5 - pathway". Since GSA is a highly reactive aldehyde, a coordinated action of the two enzymes is required. This led to the proposal of a GluTR/GSAM complex, which is in line with the structural complementarity of the two enzymes (Moser *et al.*, 2001). This complex was shown to exist *in vivo* (Luer *et al.*, 2005) and allows direct channeling of the instable intermediate to prevent solvent exposure. The photosynthetic phytoflagellate *Euglena gracilis* is currently the only organism reported to use both the C_5 - pathway and ALAS for heme biosynthesis. Here, ALA derived by ALAS is incorporated into mitochondrial tetrapyrroles, whereas plastidic pigments are made from ALA synthesized by the C_5 - pathway (Weinstein and Beale, 1983). Both pathways for ALA were also discovered in

Streptomyces nodosus subsp. *askuaensis*. However, the ALA produced *via* the Shemin way is utilized exclusively for the production of the antibiotic asukamycin and is not incorporated into heme (Petricek *et al.*, 2006).

1.1.3.2 The Central Pathway from 5-Aminolevulinic Acid to Uroporphyrinogen III

The following three steps in heme biosynthesis are common to the biosynthesis of all tetrapyrroles. Two molecules of ALA are asymmetrically condensed to yield the pyrrole derivative porphobilinogen. This reaction is catalyzed by porphobilinogen synthase (PBGS; encoded by *hemB*; EC 4.2.1.24). PBGS enzymes from different organisms are all metal-dependent but variable regarding the nature of the utilized cations. Four molecules of porphobilinogen are linked consecutively by porphobilinogen deaminase (PBGD; encoded by *hemC*; EC 4.3.1.8) to produce the linear tetrapyrrole pre-uroporphyrinogen. Interestingly, porphobilinogen is both the substrate as well as a component of the cofactor for PBGD. The dipyrromethane cofactor is a porphobilinogen dimer covalently attached to the enzyme through its free amino group (Jordan and Warren, 1987, Warren and Jordan, 1988). It primes the sequential addition and deamination of the tetrapolymerization with a transient porphobilinogen hexamer of which pre-uroporphyrinogen is hydrolyzed (McNeill and Shoolingin-Jordan, 1998). Pre-uroporphyrinogen is passed directly on to uroporphyrinogen III synthase (UROS; encoded by *hemD*; EC 4.2.1.75), which converts it to uroporphyrinogen III, the first cyclic intermediate of the pathway. UROS catalyzes the inversion of ring D of pre-uroporphyrinogen *via* a spiro-mechanism with spiro-pyrrolenine as an intermediate creating uroporphyrinogen III (Chadwick, 1994, Shoolingin-Jordan and Cheung, 1999). The inversion of ring D at this point causes cyclic tetrapyrroles to be asymmetric molecules.

1.1.3.3 Conversion of Uroporphyrinogen III into Heme

The conversion of uroporphyrinogen III to heme is outlined in Fig. 3. Uroporphyrinogen III decarboxylase (UROD; encoded by *hemE;* EC 4.1.1.37) catalyzes the sequential decarboxylation of the four acetate residues of uroporphyrinogen III to yield the corresponding methyl groups of the product coproporphyrinogen III. The decarboxylations proceed in an ordered manner beginning with the acetate side chain of ring D, followed by A, B and finally C (Akhtar, 1991, Luo and Lim, 1993). Genes encoding UROD have been isolated from various sources (Chelstowska *et al.*, 1992, Hansson and Hederstedt, 1992,

Kiel *et al.*, 1990, Nishimura *et al.*, 1993, Romana *et al.*, 1987, Romana *et al.*, 1987). So far identified proteins have been found to be highly conserved and are likely to function in a very similar way. In the next step, coproporphyrinogen III oxidase (CPO; encoded by *hemF/N*; EC 1.3.3.3) catalyzes the transformation of coproporphyrinogen III to protoporphyrinogen IX. During this reaction the propionate side chains on rings A and B are oxidatively decarboxylated to the corresponding vinyl groups (Dailey, 2002). Eukaryotic CPOs are structurally conserved and require oxygen for the oxidative reaction (HemF). Most bacteria also contain an oxygen-independent CPO (HemN), which was shown to be a "Radical-SAM" enzyme (Layer *et al.*, 2002). Protoporphyrinogen IX oxidase (PPO; encoded by *hemG/Y*; EC 1.3.3.4) converts protoporphyrinogen IX to protoporphyrin IX, which requires the elimination of six electrons and results in the formation of a system of completely conjugated double bonds. Oxygen-dependent PPO (HemY), found in eukaryotes and some bacteria, is a flavin-containing enzyme that employs molecular oxygen as the final electron acceptor (Hansson and Hederstedt, 1994, Koch *et al.*, 2004). Oxygen independent PPO (HemG) is a rather small protein with a relative molecular mass of 21,000 with flavin mononucleotide (FMN) as cofactor, which transfers electrons to fumarate *via* menaquinone (Sasarman *et al.*, 1979, Sasarman *et al.*, 1993, Möbius *et al.*, unpublished data). The last step of heme biosynthesis is the insertion of iron into protoporphyrin IX which is catalyzed by ferrochelatase (FC; encoded by *hemH*; EC 4.99.1.1) (Dailey, 2002). Metabolic channeling between PPO and FC has only recently been shown to exist *in vivo* and prevents solvent exposure of the photoreactive protoporphyrin IX in *Thermosynechococcus elongatus* (Masoumi *et al.*, unpublished data).

1.1.4 Conversion of Uroporphyrinogen III into Siroheme

After formation of uroporphyrinogen III the pathways for vitamin B_{12}, coenzyme F_{430}, heme d_1 and siroheme formation branch from the pathway leading to heme and chlorophyll formation. Siroheme, the prosthetic group of sulphite and nitrite reductases, is synthesized from uroporphyrinogen III in three steps as outlined in Fig. 4. Uroporphyrinogen III is therefore converted into precorrin-2, a 2,7-dimethyl derivative, *via* two consecutive methylation reactions. These are catalyzed by uroporphyrinogen III methyltransferase (EC 2.1.1.107) with *S*-adenosyl-*L*-methionine (SAM) as methyl donor under release of *S*-adenosyl-*L*-homocysteine. The second step resulting in an overall oxidation of the macrocycle is catalyzed by precorrin-2 dehydrogenase (EC 1.3.1.76), which requires NAD^+ as a cofactor. Finally, siroheme is synthesized by insertion of ferrous iron into

sirohydrochlorin in a reaction catalyzed by sirohydrochlorin ferrochelatase (EC 4.99.1.4) (Raux-Deery *et al.*, 2005, Raux *et al.*, 2003). In some bacteria, these three steps are executed by a single multifunctional protein called CysG (Spencer *et al.*, 1993), whereas in *Bacillus megaterium* three separate enzymes are required for each step (Leech *et al.*, 2002).

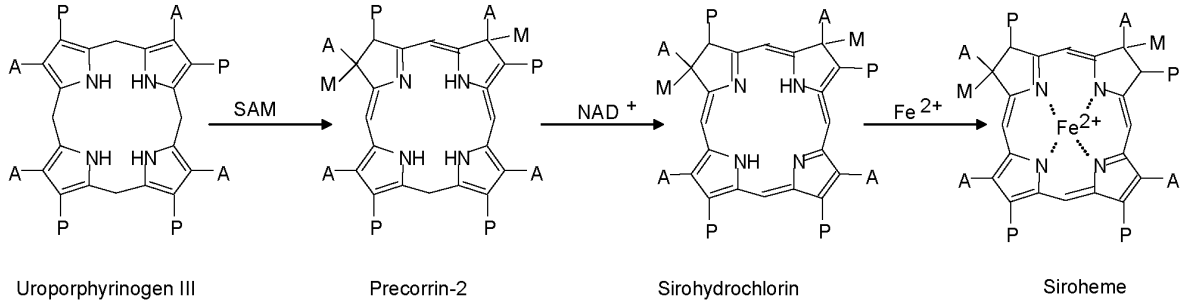

Fig. 4: The biosynthesis of siroheme from uroporphyrinogen III.

Siroheme is formed from uroporphyrinogen III in three steps *via* the intermediates precorrin-2 and sirohydrochlorin. A = acetate side chain; P = propionate side chain; M = methyl group.

1.1.5 Diseases and Growth Defects Caused by Tetrapyrrole Deficiency

Heme is an essential cofactor for most archaea, bacteria and eukaryotes. Consequently, its biosynthesis is an attractive target for antibacterial drug discovery and herbicide treatment (Matringe *et al.*, 1989, Padmanaban and Rangarajan, 2000). Perturbation of the tetrapyrrole anabolism in plants induces photodynamic cell damage due to accumulation of photoreactive chlorophyll intermediates. This can result in a decrease of chlorophyll synthesis and thus lowering of the photosynthesis capacity (Lermontova *et al.*, 1997, Mock and Grimm, 1997, Mock *et al.*, 1999). PPO for example is the target for diphenylether herbicides such as acifluorfen-methyl. The phytotoxicity of these herbicides is based on the accumulation of protoporphyrinogen IX, which is transported from the chloroplasts to other parts of the cell, where it is non-enzymatically oxidized and generates reactive oxygen species, thereby damaging cellular components (Matringe *et al.*, 1989).

On the other hand a variety of genetic disorders concerning the involved enzymes have severe consequences on human health. Mutations in the different human heme biosynthetic genes cause disorders commonly known as porphyrias (Sarkany, 1999, von und zu Fraunberg *et al.*, 2002). Porphyrias are a group of inherited or acquired disorders of certain enzymes in the heme biosynthetic pathway. They are broadly classified as hepatic porphyrias or erythropoietic porphyrias, based on the site of the overproduction and accumulation of the porphyrins or their chemical precursors. Patients suffer from cutaneous photosensitivity and a propensity to develop acute neurovisceral crises (Meissner *et al.*, 1996, Meissner *et al.*, 1986).

1.2 Porphobilinogen Synthase

PBGS from prokaryotes and eukaryotes share a high degree of sequence similarity with each other. All catalyze the asymmetric condensation of two molecules of ALA to yield the first pyrrole porphobilinogen (see Fig. 3) (Frankenberg *et al.*, 2003, Jordan, 1994). PBGS from various organisms have been intensively studied over the past years and crystal structures of many PBGS enzymes have been published (Breinig *et al.*, 2003, Erskine *et al.*, 1999, Erskine *et al.*, 1997, Frankenberg *et al.*, 1999). The enzyme catalyzed reaction is initiated by the formation of Schiff base bonds between the two ALA substrate molecules and two conserved lysine residues in the active site. It involves multiple bond-braking and bond-making events (Erskine *et al.*, 1999). The substrate ALA molecule that becomes the acetyl-substituted half of porphobilinogen is called A-site ALA. The propionyl-coordinating half of porphobilinogen derives from P-site ALA. The corresponding substrate binding sites of PBGS consequently are termed the A-site and P-site, respectively. The PBGS reaction starts with the binding of P-site ALA with subsequent binding of the second substrate molecule to the A-site. A proposed order derived from various crystal structures has recently been published and experimentally underlined and is illustrated in Fig. 5 (Frere *et al.*, 2006).

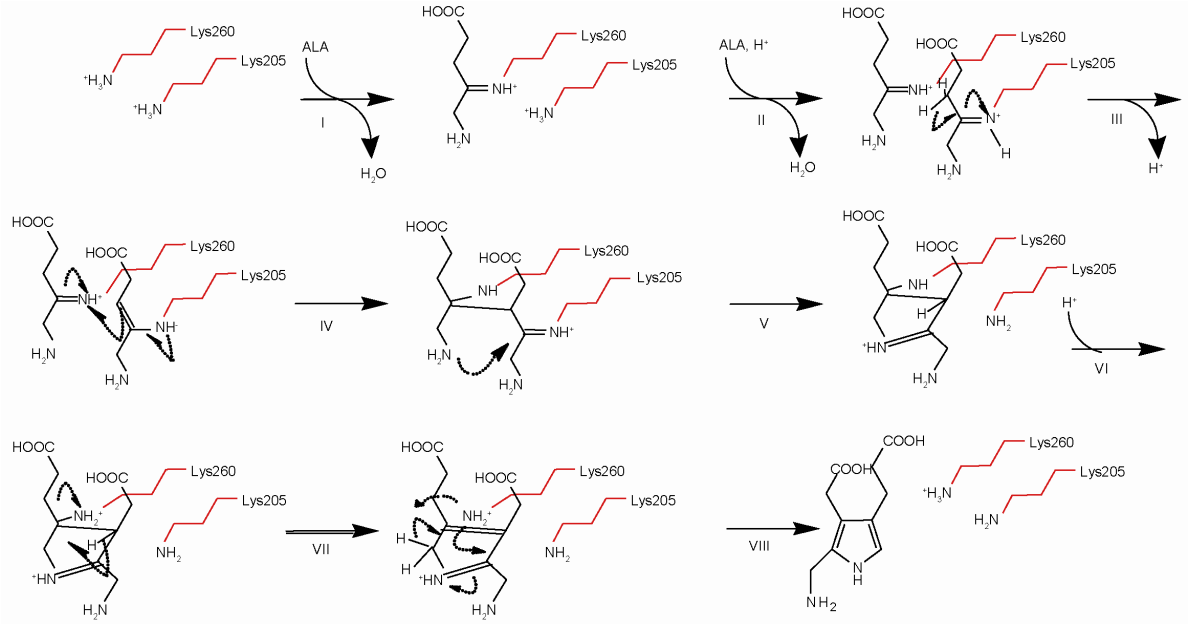

Fig. 5: Proposed catalytic mechanism of the porphobilinogen synthase.
The reaction starts with the binding of P-site ALA (I) and subsequent binding of A-site ALA *via* Schiff base (II). The abstraction of a proton from C_3 of A-site ALA follows yielding an A-site enamine (III). The next step is the aldole addition forming the C-C bond between A-site and P-site ALA (IV), with subsequent Schiff base exchange producing a C-N bond between A-site and P-site ALA (V) with following transfer of a proton to Lys260 (VI). Finally, the trans elimination of P-site lysine occurs (VII) followed by the abstraction of the *pro-R* proton from C_5 of P-site ALA (VIII) with subsequent aromatization and release of the product PBG (Frere *et al.*, 2006).

PBGS are usually enzymes with a relative molecular mass of 280 - 300,000 and are composed of eight identical subunits. They carry a high degree of structural conservation but a considerable diversity in the use of metal ion cofactors. Zinc and magnesium-dependent enzymes have been described (Jaffe, 2000), with each PBGS octamer containing only four functional actives sites (Cheh and Neilands, 1973, Jaffe *et al.*, 1992, Shemin, 1976). *Pseudomonas aeruginosa* PBGS crystallographic data showed an asymmetric dimer as the fundamental structural unit (Frankenberg *et al.*, 1999). A flexible loop covers the active site in the "closed" conformation and separates it from the surrounding medium. The bound Mg^{2+} ion is separated 14 Å from the Schiff base lysine, which is too far to play a direct catalytic role. The "open" conformation of the asymmetric dimer was not shown to contain an Mg^{2+} ion. It was suggested that the open and closed conformation of each monomer is governed by Mg^{2+} binding. The dimer is illustrated in Fig. 6. In the active site cavity two lysine residues, *i.e.* Lys205 and Lys260, are responsible for substrate coordination *via* stable Schiff base formation (Frankenberg *et al.*, 1999).

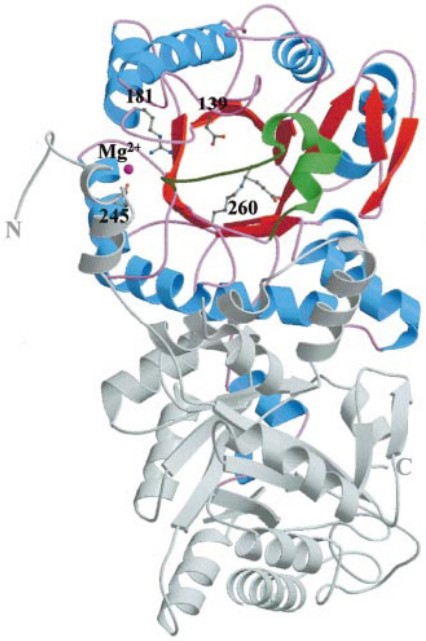

Fig. 6: Crystal structure of *P. aeruginosa* porphobilinogen synthase.
Each PBGS monomer is a TIM barrel with a long N-terminal arm. In monomer A the β-strands are colored in orange, α-helices in blue and loops in pink. The lid (shown in green) sits atop the active site and isolates the center of the barrel from solvent exposure. The side-chains of a number of residues in the active site (Asp139 and Lys260) and the neighboring Mg^{2+}-binding site (Arg181 and Glu245) are also shown. The competitive inhibitor levulinic acid is covalently attached *via* a Schiff base to Lys260. The Mg^{2+} is shown as a sphere colored in magenta. Monomer B is depicted in grey (Frankenberg *et al.*, 1999).

1.2.1 Alaremycin, an Antibiotic Structurally Related to 5-Aminolevulinic Acid

The lately discovered antibiotic alaremycin (Awa *et al.*, 2005) was isolated from the culture broth of the actinomycete strain *Streptomyces sp.* A012304. Its structure was determined as 5-acetamido-4-oxo-5-hexenoic acid and is thus structurally related to ALA (Fig. 7) (Awa *et al.*, 2005). The biosynthesis pathway has not been solved but attempts in this direction are currently being made (Masaaki Wachi, Tokyo Institute of Technology, Japan, personal

communication). Alaremycin revealed enhanced antimicrobial activity against *Escherichia coli* in the presence of ALA (Awa *et al.*, 2005), and was proposed to execute its antimicrobial activity *via* the inhibition of tetrapyrrole biosynthesis. Firstly it was proposed that alaremycin competes with ALA and inhibits PBGS, which utilizes ALA as substrate. However, excessive addition of ALA to the medium did not relieve the lethal effect of alaremycin, but in contrast enhanced the antibacterial effect (Awa *et al.*, 2005). Thus, it was suggested that alaremycin affects the heme biosynthetic pathway by a mechanism other than competitive inhibition of PBGS or that the antibacterial activity is caused by a mechanism indifferent to heme biosynthesis. Until now, no further attempts have been made to resolve the mode of action.

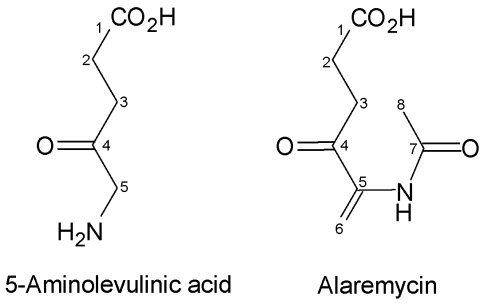

Fig. 7: Structure of 5-aminolevulinic acid and alaremycin.
The structural core of the novel isolated antibiotic alaremycin resembles the structure of 5-aminolevulinic acid, the first common precursor of tetrapyrrole biosynthesis. Carbon atoms are numbered.

1.3 Uroporphyrinogen III Synthase

Another open question in heme biosynthesis regards the identity of the fourth enzyme in chlorophyll and heme biosynthesis, UROS, in plants. Although UROS has been cloned from many organisms, the level of sequence conservation between them is very low. No gene from plants has been assigned to UROS so far and no obviously recognizable homolog has been identified from the *Arabidopsis thaliana* genome.

UROS catalyzes the cyclization of pre-uroporphyrinogen with a concomitant inversion of the fourth ring of the porphyrin macrocycle to give rise to uroporphyrinogen III (Battersby, 1979). In the absence of UROS, pre-uroporphyrinogen cyclizes non-enzymatically to form toxic uroporphyrinogen I without any rearrangement of the fourth pyrrole ring. Since it is not a precursor for biologically active tetrapyrroles, uroporphyrinogen I cannot be metabolized past the following step in the pathway. Congenital erythropoetic porphyria, a human disease caused by UROS deficiency, is characterized by the accumulation of uroporphyrin I and coproporphyrin I in the plasma, tissues, and red blood cells. This leads to severe photosensitivity with skin fragility, hypertrichosis, and lesions on light-exposed areas (Desnick *et al.*, 1998, Kappas, 1995). In bacteria, the genes encoding PBGD (*hemC*) and

UROS (*hemD*) are usually organized in an operon, leading to a coordinated expression of both genes. This might be necessary for a direct substrate transfer of the instable intermediate pre-uroporphyrinogen III from PBGD to UROS to prevent solvent exposure and spontaneous cyclization to uroporphyrinogen I (Hansson *et al.*, 1991, Mohr *et al.*, 1994). UROS has been purified from a variety of sources including the bacterium *E. coli* (Alwan *et al.*, 1989), the protozoan *Euglena gracilis* (Hart and Battersby, 1985), rat liver (Kohashi *et al.*, 1984), and human erythrocytes (Tsai *et al.*, 1987). In all cases, the purified enzyme was a monomer with a molecular mass of about 30,000 Da. Interestingly, the UROS from different sources were all found to be remarkably susceptible to heat denaturation. This is in contrast to other enzymes of the biosynthetic pathway, which are rather thermostable (Noriega *et al.*, 2002, Sasarman *et al.*, 1987). A comparison between UROS sequences showed that there are seven invariant residues and conservative substitutions in further 15 positions. The crystal structure of the human enzyme revealed that it consists of two α/β domains linked by a β-ladder as depicted in Fig. 8 (Mathews *et al.*, 2001). The active site appears to be located between the domains suggesting an enzyme mechanism including variations in the relative domain positions.

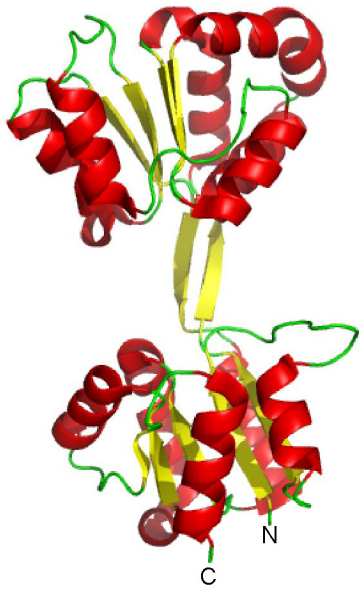

Fig. 8: Structure of the human uroporphyrinogen III synthase.
Human UROS consists of two α/β domains linked by a β-ladder. The active site is located between these two domains. The C- and the N-terminus are labeled.

However, the overall amino acid sequence similarity between UROSs from different organisms is low. For example the *Bacillus subtilis* and mouse amino acid sequences share less than 22 % identity. Furthermore, both show very little homology to *E. coli* UROS. This is in contrast to other tetrapyrrole biosynthesis enzymes, such as PBGD and CPO that are up to 55 – 60 % identical between prokaryotes and eukaryotes. Primary amino acid sequence conservation is a necessary prerequisite to identify putative orthologues by sequence

database miming. The lack of similarities between the various known UROSs reduced the possibility to identify a UROS gene from higher plants by simple BLAST searching, even after the publication of the complete genome sequence of *A. thaliana* (The Arabidopsis Genome Initiative, 2000, O´Brian and Thöny-Meyer, 2002). However, UROS activity has been described for plants and is necessary for chlorophyll biosynthesis (Higuchi and Bogorad, 1975).

1.4 Protoporphyrinogen IX Oxidase

The penultimate step in heme biosynthesis is the oxygen-dependent aromatization of protoporphyrinogen IX to protoporphyrin IX (see Fig. 3) catalyzed by PPO (Brenner and Bloomer, 1980). It is the last common step of tetrapyrrole biosynthesis for the formation of hemes and chlorophylls. Initially, the enzyme was characterized from yeast (Poulson and Polglase, 1975) and mammalian liver (Dailey and Karr, 1987, Poulson, 1976). The six-electron oxidation of protoporphyrinogen IX is catalyzed by PPO using a flavin cofactor and molecular oxygen as terminal electron acceptor, resulting in a fully conjugated tetrapyrrole macrocycle. PPO belongs to a flavin adenine dinucleotide (FAD) superfamily that also includes monoamine oxidase and phytoene desaturase (Dailey and Dailey, 1998). PPO has been described as soluble monomer in *Bacillus subtilis* (Hansson and Hederstedt, 1992), as membrane-associated monomer in bovine (Siepker *et al.*, 1987) or as homodimer in *Myxococcus xanthus* and humans (Dailey and Dailey, 1996, Dailey and Dailey, 1996, Maneli *et al.*, 2003). In eukaryotes PPO is associated with the outer surface of the inner mitochondrial membrane (Deybach *et al.*, 1985), while the plant enzyme is additionally located in chloroplasts (Dailey, 2002, Jacobs and Jacobs, 1984). In humans, partial PPO deficiency causes a disease known as variegate porphyria (VP, OMIN^{TM} accession number 176200) that is inherited as an autosomal dominant trait displaying incomplete penetrance (Mustajoki, 1980). The biochemical abnormalities found in VP patients include overproduction and increased excretion of porphyrins and porphyrin precursors. VP manifests clinically with photosensitivity and acute attacks, which includes various neuropsychiatric symptoms (Dean, 1971). In South Africa VP is common due to a founder effect, where mainly one amino acid exchange from Arg59 to tryptophan causes the disease (Meissner *et al.*, 1996, Roberts *et al.*, 1998, Warnich *et al.*, 1996). However, there are various additional mutations known to cause VP (von und zu Fraunberg *et al.*, 2002).

1.4.1 Tobacco Protoporphyrinogen IX Oxidase

In plants two isoforms of PPO, plastidic PPO (PPO1) and mitochondrial PPO (PPO2) have been found (Beale, 1999, Jacobs and Jacobs, 1984, Lermontova *et al.*, 1997). They share an amino acid sequence identity of less than 30 %. Both enzymes operate as homodimers and use FAD as cofactor. The crystal structure of *Nicotiana tabacum* mitochondrial PPO (NtPPO2) with the bound inhibitor 4-bromo-3-(5'-carboxy-4'-chloro-2'-fluoro-phenyl)-1-methyl-5-trifluoromethyl-pyrazol and non-covalently bound FAD has been solved recently (Fig. 9) (Koch *et al.*, 2004). Furthermore, the *M. xanthus* structure was published recently (Corradi *et al.*, 2006). The structure of NtPPO2 revealed a loosely associated dimer, each monomer consisting of a membrane-, a FAD- and a substrate-binding domain, respectively. The inhibitor was found to be located in the active site domain and consists of a phenyl- and pyrazol-ring system. Even though the FAD is not covalently bound to the enzyme it was found in close proximity to the co-crystallized inhibitor in the active site cavity. A potential reaction mechanism was proposed based on the fact that the substrate has only limited space to rotate in the active site. The six electron oxidation of protoporphyrinogen IX to protoporphyrin IX is supposedly catalyzed *via* three steps. Three times the FAD cofactor is reduced by two electrons from the tetrapyrrole ring and re-oxidized by molecular oxygen which in turn is reduced to H_2O_2. The reduction is proposed to start at the C_{20} atom of the tetrapyrrole *via* enamine-imine-tautomerisation and H-rearrangements (Koch *et al.*, 2004).

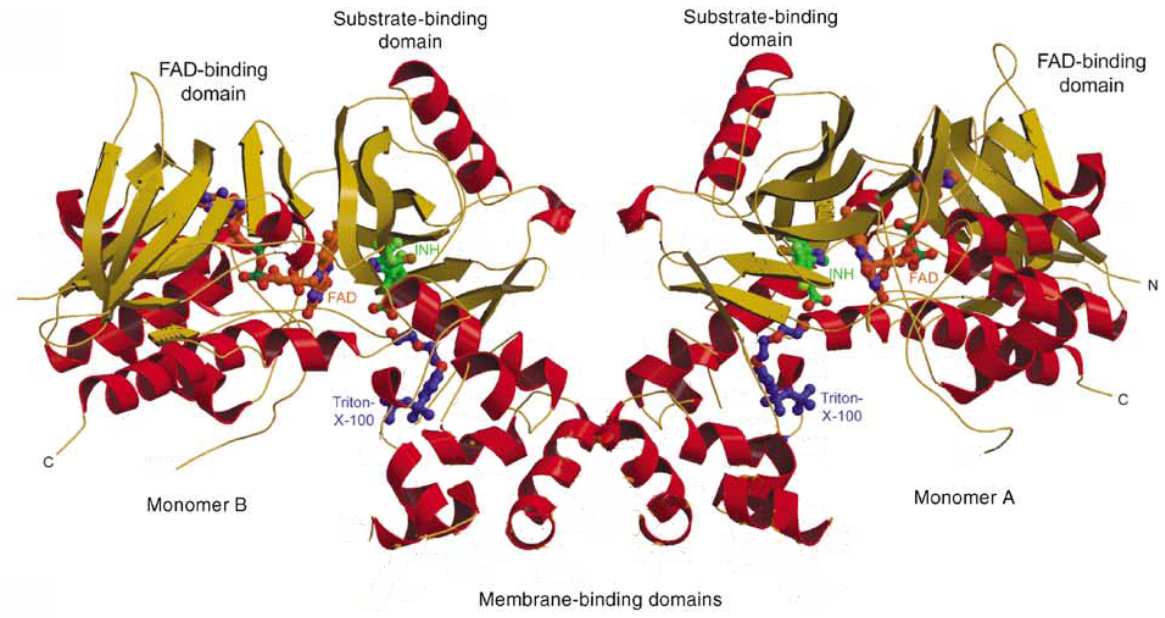

Fig. 9: Dimeric structure of mitochondrial tobacco protoporphyrinogen IX oxidase.
The three-domain monomer consists of a FAD-binding, a substrate-binding and a membrane-binding domain. The inhibitor (green) binds into the active site cavity near the cofactor FAD (red–orange). The product channel in the membrane-binding domain starts at the bound Triton X-100 detergent molecule (blue). (modified from Koch *et al.*, 2004).

Very recently PPO has been shown to build a tight complex with FC *in vivo* (Masoumi *et al.*, unpublished data). This complex has been postulated for a long time since the intermediate protoporphyrin IX is highly photoreactive and induces cell death when released to the cell.

1.5 Heme Biosynthesis in Archaea

Despite the fact that heme biosynthesis has been investigated for a long time, there are still various fundamental questions to be answered. One concerns heme biosynthesis in archaea. Archaea have been shown to possess hemes and heme-dependent proteins (Gartner, 1991, Lubben and Morand, 1994, Schutz *et al.*, 2000). Furthermore, essential metabolic pathways such as methanogenesis in methanogenic archaea are dependent on tetrapyrrole cofactors, such as F_{430} (Thauer and Bonacker, 1994). Nevertheless, the genes necessary for the late steps of heme biosynthesis could not be identified (see Tab. 1).

Tab. 1: Genes for heme biosynthesis in different organisms (modified after Panek and O'Brian, 2002).
The letters B, C, D etc. refer to *hemB*, *hemC*, *hemD*, and so on. Since there are two pathways leading to ALA formation, genes for the corresponding enzymes Glu and L for the C_5 pathway and A for the Shemin pathway are given.

Organism	**Genes present [*hem*]**
Eukarya	
Homo sapiens sapiens	A, B, C, D, E, F, Y, H
Bacteria	
Escherichia coli	Glu, L, B, C, D, E, F/N, G, H
Pseudomonas aeruginosa	Glu, L, B, C, D, E, F, N, H
Staphylococcus aureus	Glu, L, B, C, D, E, N, Y, H
Bacillus subtilis	Glu, L, B, C, D, E, N, Y, H
Aquifex aeolicus	Glu, L, B, C, D, E, N, Y, H
Desulfovibrio vulgaris	B, C, D
Archaea	
Sulfolobus solfataricus	Glu, L, B, C, D
Archaeoglobus fulgidus	Glu, L, B, C, D
Methanosarcina barkeri	Glu, L, B, C, D
Halobacterium sp. NRC-1	Glu, L, B, C, D
Thermoplasma volcanium	Glu, L, B, C, D, E, N, H

Biochemical and genomic information indicate that heme biosynthesis starts from ALA which is synthesized from glutamate, and proceeds *via* porphobilinogen, pre-

uroporphyrinogen and uroporphyrinogen III as intermediates (Diekert *et al.*, 1981, Friedmann and Thauer, 1987, Galagan *et al.*, 2002). At this stage the pathway appears to deviate from that known to be operative in eukaryotes and most bacteria. In the conventional pathway, the four methyl groups of the porphyrin are derived from decarboxylation of the acetate groups of uroporphyrinogen III to yield coproporphyrinogen III. Thus, all methyl groups and carbons are derived from ALA. Nevertheless, most archaeal genomes lack gene homologs of *hemE*, *hemF* or *N*, *hemG* or *Y* and *hemH* encoding the enzymes catalyzing the successive conversion of uroporphyrinogen III *via* coproporphyrinogen III, protoporphyrinogen IX and protoporphyrin IX to protoheme (Tab. 1) (Panek and O'Brian, 2002). One exception is the genome of *Thermoplasma volcanium* in which gene homologs of *hemE, hemN*, and *hemH* are present (Kawashima *et al.*, 2000, Panek and O'Brian, 2002).

1.5.1 A Second Pathway for Heme Biosynthesis in *Desulfovibrio vulgaris*

The absence of typical late heme biosynthesis genes in most archaea raises the question for an alternate biosynthetic route. For the sulfate-reducing *Desulfovibrio vulgaris* utilizing cytochromes *b* and *c*, *hemE*, *hemF* or *N*, *hemG* or *Y* and *hemH* genes have not been identified in its known genome sequence (Heidelberg *et al.*, 2004, Matias *et al.*, 2005). The synthesis of protoheme in *D. vulgaris* has been shown to involve precorrin-2 as intermediate (Akutsu *et al.*, 1993, Ishida *et al.*, 1998). The formation of precorrin-2, which is a 2,7-dimethyl derivative of uroporphyrinogen III, is known to proceed in two consecutive methylation reactions with SAM as methyl donor (Vevodova *et al.*, 2004). The so far observed pathway thus resembles the initial steps of siroheme biosynthesis rather than the late steps of heme biosynthesis (see Fig. 10).

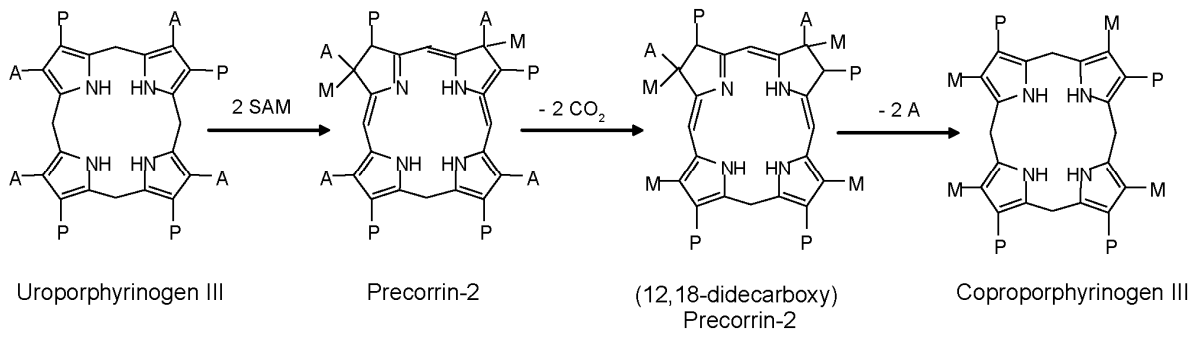

Fig. 10: Proposed alternate pathway of porphyrin biosynthesis in *D. vulgaris*.
An alternate pathway for porphyrin biosynthesis from uroporphyrinogen III to coproporphyrinogen III was proposed for *D. vulgaris* (Ishida *et al.*, 1998). A, M, P stand for acetate group, methyl group and propionyl group, respectively.

The intermediates and proteins involved in precorrin-2 conversion into protoheme in *D. vulgaris* have not yet been identified. In cell extracts of this organism precorrin-2 was converted under strictly anaerobic conditions into 12,18-didecarboxyprecorrin-2 indicating that the following step is a decarboxylation reaction (Ishida *et al.*, 1998). These are first indications for a novel, but most likely ancient pathway, which may apply to archaea as well. In Fig. 10 the tetrapyrrole pathway postulated by Ishida and coworkers (Ishida *et al.*, 1998) for *D. vulgaris* is depicted. They proposed that porphyrin biosynthesis reenters the common pathway at the step of coproporphyrinogen III.

1.6 Aim of the Study

Several open questions related to various steps of heme biosynthesis in bacteria, archaea and plants had to be investigated in the cause of this thesis.

1. The target of the inhibitory capacity of the antibiotic alaremycin should be explored using inhibition studies with various bacteria and recombinant, purified porphobilinogen synthases from various sources. Finally, a crystal structure of alaremycin bound to its target enzyme was the ultimate goal.

2. The previously unknown uroporphyrinogen III synthase from plants should be functionally identified in close cooperation with the group of Alison Smith at Cambridge, UK.

3. The substrate binding of tobacco protoporphyrinogen IX oxidase should be defined using site directed mutagenesis and kinetic testing, all based on the known crystal structure of the enzyme.

4. Finally, the principal biosynthetic route for the late steps of archaeal heme biosynthesis was of interest.

2 MATERIALS AND METHODS

2.1 Instruments and Chemicals

2.1.1 Instruments

Agarose gel electrophoresis	Agagel	Biometra
Agarose gel documentation	GelDoc	Bio-Rad
Anaerobic chamber	Type B Flexible vinyl chamber	Coy Laboratories
Autoclave	LVSA 50/70	Zirbus
Blotting equipment	Semidry-Blot Trans-Blot®SD	BioRad
Centrifuges	5415 C	Eppendorf
	Minispin	Eppendorf
	RC 5B Plus	Sorvall
	L8-70M ultracentrifuge	Beckman
	Speed Vac SPD 110B	Savant
DNA sequencing	Genetic Analyzer ABI Prism™ 310	Applied Biosystems
Electrophoresis power supply	PowerPac 300	BioRad
Electroporation	Gene Pulser II ™	BioRad
Fluorescence spectrometer	PA LS50B	PerkinElmer
FPLC	Äkta Purifier™	Amersham Biosciences
French press	French® Pressure Cell Press	Amersham Biosciences
pH-determination	pH meter C 6840 B	Schott
Photometer	Ultrospec 2000	Amersham Bioscience
Protein concentration cells	Amicon 8010	Millipore
	Amicon 8050	Millipore
Scales	BL 1500	Sartorius
	BL 61S	Sartorius
	SBA 52	Scaltec
Scintillation analyzer	Tri-Carb 2900 TR	Bio-Rad
SDS-PAGE-system	Mini Protean II	Bio-Rad
Thermocycler	Tpersonal	Biometra
	Tgradient	Biometra
Thermomixer	Thermomixer compact	Eppendorf
Ultrasonic bath		Merck eurolab
Ultrasound device	Sonoplus HD 2070	Bandelin
UV/visible spectrophotometer	Ultrospec 2000	Amersham Biosciences
	Lambda 2	PerkinElmer
Vortex	Vortex-Genie 2	Scientific Industries
Water purification	Milli-Q System	Millipore

2.1.2 Chemicals and Kits

5-aminolevulinic acid	Sigma
[^{14}C]-5-aminolevulinic acid	PerkinElmer
BigDye Terminater v1.1 Cycle Sequencing Kit	Applied Biosystems
Coproporphyrin IX	Porphyrin Products
Crystal Screen and Crystal Screen 2	Hampton Research
CrystalClear strip racks	Douglas Instruments
Enzymes for molecular biological applications	MBI Fermentas, New England Biolabs, Amersham Biosciences, Promega, Qiagen
FAD	Sigma
Fibrous cation exchange resign	Whatman
Dialysis visking, type 27/32 exclusion 14000	Roth
Glutathione sepharose XK26 column	Amersham Biosciences
Hemin	Fluka
L-[*methyl*-^{14}C]methionine	Amersham Biosciences
L-[*methyl*-D_3]methionine	Sigma
Micro BCA Protein Assay Kit	Pierce
Ni-IDA resign	Macherey Nagel
Ni-chelating Sepharose Fast Flow	Amersham Biosciences
Opti-Phase HiSafe2 (scintillation cocktail)	PerkinElmer
Porphobilinogen	Porphyrin Products
Prepacked PD10 columns	General Electric Company
PreScission™ Protease	Amersham Biosciences
Protoporphyrin IX	Porphyrin Products
QIAquick Gel Extraction Kit	Qiagen
QIAquick PCR Purification Kit	Qiagen
S•Tag Rapid Assay Kit	Merck
S-adenosyl-*L*-[*methyl*-^{14}C]methionine	Amersham Biosciences
Size standards for agarose gels	
GeneRuler™ DNA Ladder Mix	MBI Fermentas
MassRuler™ DNA Ladder Mix	MBI Fermentas
Size standards for SDS-PAGE	
Protein Molecular Weight Marker	MBI Fermentas
Superdex 200 HR 10/30	General Electric Company
Uroporphyrin III	Porphyrin Products

Chemicals and reagents not specifically listed here were purchased from the following manufacturers: Amersham Biosciences, Fluka, Gerbu, Merck, Roth, Sigma.

2.2 Strains and Plasmids

All strains and plasmids used for this work are listed in Tab. 2 and Tab. 3.

Tab. 2: Employed bacterial and archaeal strains.

Strain	Description	Reference
Escherichia coli DH10b	F^- *mcr*A Δ(*mrr-hsd*RMS-*mcr*BC) Φ80*lac*ZΔM15 Δ*lac*X74 *rec*A1 *end*A1 *ara*Δ139 Δ(*ara*, *leu*)7697 *gal*U *gal*K λ^- *rps*L (Str^R) *nup*G	Invitrogen
Escherichia coli BL21(DE3)RIL	F^- *omp*T *hsd*S(rB^- mB^-) dcm^+ Tet^r *gal* Δ(DE3) *end*A The[*arg*U *ile*Y *leu*W Cam^r]	Stratagene
Escherichia coli EV61	*thr*-l *ara*-14 *leu*B6 A(*gpt-pro*A)62 *lac*Yl *tsx*-33 *sup*E44 *gal*K2 Rac^- *his*G4 *rfb*Dl *mgl*-51 *rps*L31 *kdg*K51 *xyl*-5 *mtl*-l *arg*E3 *thi*-J *rec*B21 *rec*C22 *sbc*BJ5 *sbc*C201 λ^- Δ*hemA*::*kan*, Kan^r	Verkamp and Chelm, 1989
Escherichia coli CSA	Hemepermable variant of *E. coli* EV61 designed by chemical mutagenesis Δ*hemA*, *env*	Claudia Schulz, TU Braunschweig
Bacillus subtilis JH652	*trp*C2 *phe*A1	*Bacillus* Genetic Stock Center 1A96
Bacillus megaterium DSM 319		Hunger and Claus, 1981
Pseudomonas aeruginosa strain PAO1		Dunn and Holloway, 1971
Staphylococcus aureus DSM 20714		Schleifer and Kocur, 1973
Streptomyces sp. A012304		Awa *et al.*, 2005
Streptomyces coelicolor DSM 40233		Berger and Edberg, 1987, Skerman *et al.*, 1980
Streptomyces avermitilis DSM 46492		Burg *et al.*, 1979
Methanosarcina barkeri strain Fusaro, DSM 804		Kandler and Hippe, 1977

Tab. 3: Plasmids used in this study.

Plasmid	Description	Reference
pET32a	Expression vector carrying C-terminal His-Tag® and S•tag sequence, T7 promoter, *amp*^{r}	Novagen
pGEX-6P-1	Expression vector carrying N-terminal sequence for GST from *Schistosoma japonicum* and recognition sequence for PreScission™ Protease, *lac* promoter, *amp*^{r}	Amersham Biosciences
pIH45	pET32a derivative encoding PBGS from *M. barkeri*	this work
pGEXPahemB	pGEX-6P-1 derivative encoding *P. aeruginosa* PBGS	Frankenberg *et al.*, 1999
$pUROS_{full}$	pET28a derivative encoding *A. thaliana* UROS	Alison Smith, Cambridge, UK
$pUROS_{mat}$	pET28a derivative encoding *A. thaliana* UROS missing the first 81 amino acids	Alison Smith, Cambridge, UK
pIH41	pETcoco2 derivative enconding *M. barkeri cobA*, *Methanothermobacter thermoautotrophicum hemB* and *B. megaterium hemC* and *hemD*	Evelyne Deery, Kent, UK
pIH1	pET32a derivative encoding mitochondrial PPO from *N. tabacum*; Mutation from lysine 244 to glutamine (K224Q). Resulting protein is referred to as wildtype protein	Koch *et al.*, 2004
pIH2	pIH, with exchange of triplet CGC (nucleotides 292-294) to AAG, protein carries Lys instead of Arg	this work
pIH3	pIH, with exchange of triplet CGC (nucleotides 292-294) to GAG, protein carries Glu instead of Arg	this work
pIH4	pIH, with exchange of triplet CGC (nucleotides 292-294) to GCC, protein carries Ala instead of Arg	this work
pIH5	pIH, with exchange of triplet CTT (nucleotides 1066-1068) to AAT, protein carries Asn instead of Lys	this work
pIH6	pIH, with exchange of triplet CTT (nucleotides 1066-1068) to GTT, protein carries Val instead of Lys	this work
pIH7	pIH, with exchange of triplet CTC (nucleotides 1114-1116) to AAC, protein carries Asn instead of Lys	this work
pIH8	pIH, with exchange of triplet CTC (nucleotides 1114-1116) to GTC, protein carries Val instead of Lys	this work
pIH9	pIH, with exchange of triplet TTT (nucleotides 1174-1176) to CAT, protein carries His instead of Phe	this work
pIH10	pIH, with exchange of triplet TTT (nucleotides 1174-1176) to GAG, protein carries Glu instead of Phe	this work
pIH11	pIH, with exchange of triplet TCT (nucleotides 1120-1122) to GAT, protein carries Asp instead of Ser	this work

pIH12	pIH, with exchange of triplet TCT (nucleotides 1120-1122) to GAT, protein carries Asp instead of Ser and exchange of triplet AAT (nucleotides 199-201) for CGT, protein carries Arg instead of Asn	this work
pIH13	pIH, with exchange of triplet TCT (nucleotides 1120-1122) to GAT, protein carries Asp instead of Ser and exchange of triplet AAT (nucleotides 199-201) for TGG, protein carries Trp instead of Asn	this work
pIH46	pIH, with exchange of triplet AAT (nucleotides 199-201) to CGT, protein carries Arg instead of Asn	this work
pIH47	pIH, with exchange of triplet AAT (nucleotides 199-201) to TGG, protein carries Trp instead of Asn	this work

2.3 Growth Media and Media Additives

2.3.1 Growth Media

As a standard medium for growth of all bacterial strains Luria Bertani (LB) medium was used (Sambrook, 1989), unless indicated otherwise. For the production of recombinant PBGS, UROS and PPO wildtype and mutant proteins, *E. coli* BL21(DE3)RIL carrying the respective plasmids were grown in LB media. Minimal inhibitory concentrations (MIC) for alaremycin were determined in complex and defined media. LB-medium was used for most strains except for *S. avermitilis* which was cultured in medium DSM425 and *S. coelicolor* which was grown in medium DSM65. Minimal media were prepared as following. *P. aeruginosa* was grown in AB minimal medium, *B subtilis*, *B. megaterium*, *S. coelicolor* and *S. avermitilis* in SMM minimal medium, *E. coli* in M9 minimal medium containing 20 µM hemin for *E. coli* CSA. *S. sp*. A012304 was grown in seed medium for 4 days for genomic DNA extraction or in production medium for 5 days for alaremycin production. All strains were grown at 37°C and 200 rpm, except for the *Streptomyces* strains which were cultivated at 25°C and 150 rpm. *M. barkeri* was grown in low salt media under strictly anaerobic conditions for two to seven days at 37°C as described before (Karrasch *et al.*, 1989).

All media were autoclaved for 20 min at 121°C. For solid media 1.5 % (w/v) agar-agar was added before sterilization.

<u>*LB medium*</u>	tryptone	1.0 % (w/v)
	yeast extract	0.5 % (w/v)
	NaCl	0.5 % (w/v)
	in H_2O_{dest}; pH 7.0	
<u>*DSM425 medium*</u>	oat meal	2.0 % (w/v)
	in H_2O_{dest}; pH 7.2	

DSM65 medium	glucose	0.4 % (w/v)
	yeast extract	0.4 % (w/v)
	malt extract	1.0 % (w/v)
	in H_2O_{dest}; pH 7.2	
AB medium	salt solution 1	10.0 % (v/v)
	trace element solution 1	0.1 % (v/v)
	$MgCl_2$ x 6 H_2O	0.02 % (w/v)
	$CaCl_2$ x 6 H_2O	0.0015 % (w/v)
	$FeSO_4$ x 4 H_2O	0.00056 % (w/v)
	$NaNO_3$	0.425 % (w/v)
	glucose	0.36 % (w/v)
	in H_2O_{dest}; pH 7.0	
salt solution 1	$(NH_4)_2SO_4$	2 % (w/v)
	Na_2HPO_4	4.8 % (w/v)
	KH_2PO_4	3 % (w/v)
	NaCl	2.9 % (w/v)
	in H_2O_{dest}; pH 7.0	
trace element solution 1	$CaSO_4$ x 2 H_2O	0.02 % (w/v)
	$FeSO_4$ x 7 H_2O	0.02 % (w/v)
	$MnSO_4$ x H_2O	0.002 % (w/v)
	$CuSO_4$ x 5 H_2O	0.002 % (w/v)
	$ZnSO_4$ x 7 H_2O	0.002 % (w/v)
	$CoSO_4$ x 7 H_2O	0.001 % (w/v)
	Na_2MoO_4 x H_2O	0.001 % (w/v)
	H_3BO_4	0.0005 % (w/v)
	in H_2O_{dest}; pH 7.0	
M9 medium	salt solution 2	10.0 % (v/v)
	glucose	0.02 % (w/v)
	$MgSO_4$	0.012 % (w/v)
	thiamine hydrochloride	0.0005 % (w/v)
	leucine hydrochloride	0.001 % (w/v)
	in H_2O; pH 7.0	
salt solution 2	Na_2HPO_4	6.0 % (v/v)
	KH_2PO_4	3.0 % (w/v)
	NH_4Cl	1.0 % (w/v)
	NaCl	0.5 % (w/v)
	$CaCl_2$	0.003 % (w/v)
	in H_2O; pH 7.0	
SMM medium	$(NH_4)_2SO_4$	0.2 % (w/v)
	K_2HPO_4	1.4 % (w/v)
	KH_2PO_4	0.6 % (w/v)
	Na_3 citrate x 2 H_2O	0.1 % (w/v)
	$MgSO_4$ x 7 H_2O	0.02 % (w/v)
after autoclaving addition of:	SMM mix	10.0 % (v/v)
	trace element solution 2	1.0 % (v/v)
	in H_2O_{dest}; pH 7.0	
SMM mix	thiamine hydrochloride	0.001 % (w/v)
	glucose monohydrate	10.0 % (w/v)
	sodium pyruvate	5.5 % (w/v)
	casamino acids	0.1 % (w/v)
	in H_2O_{dest}; pH 7.0	

trace element solution 2	$CaCl_2$ x 2 H_2O	0.08 % (w/v)
	$FeCl_2$ x 4 H_2O	0.115 % (w/v)
	$MnCl_2$ x 4 H_2O	0.01 % (w/v)
	$ZnCl_2$	0.017 % (w/v)
	$CuCl_2$ x 2 H_2O	0.004 % (w/v)
	$CoCl_2$ x 6 H_2O	0.006 % (w/v)
	Na_2MoO_4 x 2 H_2O	0.006 % (w/v)
	in H_2O_{dest}; pH 7.0	
Seed medium	glucose	4 % (w/v)
	dry bouillon	1 % (w/v)
	soy bean meal	0.3 % (w/v)
	$CaCO_3$	0.3 % (w/v)
	in H_2O_{dest}; pH 7.0	
Production medium	dextrin	6 % (w/v)
	yeast extract	2 % (w/v)
	NaCl	0.3 % (w/v)
	$CaCO_3$	0.3 % (w/v)
	dry bouillon	0.1 % (w/v)
	K_2HPO_4	0.1 % (w/v)
	in H_2O_{dest}; pH 8.5	
Low salt medium	salt solution 3	20 % (v/v)
	trace element solution 3	1 % (v/v)
	vitamin solution	1 % (v/v)
	methanol	1 % (v/v)
	resazurine solution	0.1 % (v/v)
after anaerobization addition of:	cysteine hydrochloride	0.07 % (w/v)
	in H_2O_{dest}; pH 7	
after autoclaving addition of:	sodium sulfide solution	0.002 % (v/v)
salt solution 3	imidazole	1.35 % (w/v)
	NaH_2PO_4 x H_2O	0.0345 % (w/v)
	Na_2HPO_4 x 2 H_2O	0.044 % (w/v)
	$CaCl_2$ x 2 H_2O	0.25 % (w/v)
	$MgCl_2$ x 6 H_2O	0.4 % (w/v)
	NH_4Cl	0.25 % (w/v)
	KCl	0.2 % (w/v)
	NaCl	2 % (w/v)
	in H_2O_{dest}; pH 6.4	
trace element solution 3	tritiplex	0.15 % (w/v)
	pH 6.4 with KOH	
	$MnSO_4$	0.05 % (w/v)
	$FeSO_4$ x 7 H_2O	0.01 % (w/v)
	$CoCl_2$ x 6 H_2O	0.01 % (w/v)
	$ZnSO_4$ x 5 H_2O	0.001 % (w/v)
	$CuSO_4$ x 5 H_20	0.001 % (w/v)
	$AlCl_3$ x 6 H_2O	0.001 % (w/v)
	H_3BO_3	0.001 % (w/v)
	Na_2MoO_4 x 2 H_2O	0.001 % (w/v)
	$NiCl_2$ x 6 H_2O	0.003 % (w/v)
	$NaHSeO_3$	0.0015 % (w/v)
	in H_2O_{dest}; pH 7	

vitamin solution	d-Biotin	0.0002 % (w/v)
	folic acid	0.0002 % (w/v)
	pyridoxin-hydrochloride	0.001 % (w/v)
	thiamine-hydrochloride	0.0005 % (w/v)
	riboflavin	0.0005 % (w/v)
	nicotinic acid	0.0005 % (w/v)
	D-L-Ca-pantothenate	0.0005 % (w/v)
	vitamin B_{12}	0.00001% (w/v)
	p-aminobenzoic acid	0.0005 % (w/v)
	D-L-α-liponate	0.0005 % (w/v)
	in H_2O_{dest}	
resazurine solution	resazurine	0.2 % (w/v)
	in H_2O_{dest}	
sodium sulfide solution	Na_2S	2.8 % (w/v)
	in H_2O_{dest}	

2.3.2 Media Additives

Antibiotics and other additives were prepared as concentrated stock solutions, sterilized by filtration and added to the medium after autoclaving. Solutes and concentrations are summarized in Tab. 4. For the hemin stock solution, hemin was slowly diluted to 50 mL with H_2O and a few drops of 5 M KOH were added to support solubilization.

Tab. 4: Media additives

Substance	Solute	Concentration of stock solution	Final concentration
ampicillin	H_2O	100 mg/mL	100 µg/mL
chloramphenicol	ethanol (70 % (v/v))	34 mg/mL	34 µg/mL
hemin	H_2O; KOH	4 mg/mL	40 µg/mL
isopropyl-1-thio-ß-D-galactopyranoside (IPTG)	H_2O	1 M	100-250 µM
kanamycin	H_2O	50 mg/mL	50 µg/mL

2.4 Microbiological Techniques

2.4.1 Sterilization

All media were vapor sterilized at 121°C and 1 bar positive pressure for 20 min. Other substances and solutions were either vapor sterilized or, if temperature sensitive, sterilized by filtration (pore width 0.2 µm).

2.4.2 Cultivation of Bacteria and Archaea

Cells for recombinant protein production were grown under vigorous aeration. Pre-cultures (volume 100 mL) of *E. coli* BL21(DE3)RIL containing appropriate plasmids were grown overnight at 37°C and 200 rpm. 500 mL cultures were grown at 37°C until induction of

protein production with indicated amounts of IPTG. After induction cultures were incubated at 25°C overnight. For the generation of cell free extracts, strains *P. aeruginosa*, *B. subtilis*, *B. megaterium*, *S. aureus*, *E. coli* and *E. coli* CSA were grown at 37°C for 24 h at 200 rpm. *S. avermitilis*, *S. coelicolor* and *S.* sp. A012304 were grown at 25°C for 48 hours at 150 rpm. Medium for *M. barkeri* was depleted of oxygen prior to inoculation with an actively growing *M. barkeri* culture in an anaerobic chamber. Cells were cultured under strictly anaerobic conditions for two to seven days at 37°C with repeated degassing. Flasks containing *M. barkeri* were submitted to a positive pressure of 0.2 bar to prevent intake of oxygen, since cells exposed to oxygen were hardly recovered for active growth.

Agar plates were either utilized for plating 50 - 100 µL of a bacterial cell suspension with a Drigalski spatula, or for streaking cells with an inoculating loop with liquid culture or with a single colony. Plates were incubated aerobically at 37°C overnight, except for all *Streptomyces* strains which were incubated at 25°C for up to four days.

2.4.3 Determination of Cell Density

The cell density of liquid cultures was determined by measuring the optical density (OD) at a wavelength of 578 nm. For cell densities with an $OD_{578} \geq 0.6$ dilutions were prepared before the measurement. An OD_{578} of 1 corresponds to approximately 1 x 10^9 *E. coli* cells/mL. In microtitre plates the optical density was determined at an OD_{600}.

2.4.4 Storage of Bacterial Strains

Strains were kept on agar plates at 4°C for up to four weeks. For long-term storage glycerol stocks were prepared. For this purpose cultures were grown for 6 to 8 h, cooled on ice for 30 min and 500 µL of the culture mixed with 500 µL of sterile glycerol (80 % (v/v)). Stocks were immediately frozen and kept at - 80°C.

2.4.5 Determination of Minimal Inhibitory Constants

MICs for alaremycin were determined in complex and defined media for *B. subtilis*, *B. megaterium*, *P. aeruginosa*, *E. coli, S. coelicolor*, *S. avermitilis*, *S. sp.* A012304, *S. aureus* and *E. coli* CSA, respectively, using a microdilution technique. An overnight culture was diluted in fresh media to achieve a cell density of an $OD_{578} = 0.2$. A volume of 100 µL cell suspension was then added to 100 µL antibiotic serially diluted in the corresponding medium. For all strains at least four independent growth curves over a time period of 24 h with different alaremycin concentrations were recorded. The MIC was

considered to be the concentration at which the antibiotic prevented turbidity in the well for at least five hours at 37°C.

2.5 Molecular Biology Techniques

2.5.1 Preparation of DNA

2.5.1.1 Preparation of Genomic DNA

The respective strains were grown for an appropriate incubation time to yield 50 mL high density cell suspension and were harvested by centrifugation (5 min at 7,000 x *g*). Cell were washed once in TE buffer and suspended in 4 mL lysis buffer supplemented with 0.2 mg/mL RNase A and 50 µg lysozyme. The samples were incubated at 37°C for 45 min. After addition of 500 µL N-laurosylsarcosinine (20 % (w/v)) and further incubation for 5 min at 37°C the suspension was mixed with one volume of phenol and incubated under constant motion for 30 min at room temperature (RT). After subsequent centrifugation (20 min at 7,000 x *g*) the upper, aqueous phase was transferred into a fresh tube and submitted to 4 mL phenol/chloroform/isoamylalcohol (24:24:1). Following 15 min of incubation, samples were again centrifuged and the phenol-chloroform extraction was repeated. The upper, aqueous phase of this step was again transferred into a fresh tube and DNA precipitation initiated by addition of 10 mL pure ethanol and 500 µL of a 3 M sodium acetate solution (pH 4.8). The sample was centrifuged at 4°C for 30 min (7,000 x *g* and 4°C) and the DNA washed twice with 70 % (v/v) ethanol. After evaporation of residual ethanol, the DNA was solubilized in 200 µL TE buffer and stored at 4°C.

Lysis buffer	NaCl	0.6 % (w/v)
	EDTA	7.3 % (w/v)
	in H_2O_{dest}; pH 8.0	
TE buffer	Tris-HCl	10.0 mM
	EDTA	1.0 mM
	in H_2O_{dest}; pH 8.0	

2.5.1.2 Preparation of Plasmid DNA (Mini Prep)

4.5 mL of an overnight culture were harvested by centrifugation (5 min at 7,000 x *g* and 4°C) and cells suspended in 300 µL of buffer P1. 300 µL of buffer P2 were added, the sample was carefully mixed by inverting the tube and incubated at RT for 5 min. Next, 300 µL of buffer P3 were added, the sample was again carefully mixed and further

incubated in ice for 5 min. Following centrifugation (15 min at 15,000 x *g* and 4°C) 800 µL of the supernatant were added to 600 µL isopropanol in a fresh tube. Precipitation of plasmid DNA was allowed to proceed during a 10 min incubation step at 4°C, followed by a 30 min centrifugation step at 4°C (15,000 x *g*). The DNA was washed twice with 70 % (v/v) ethanol. After all traces of ethanol had evaporated, the DNA was solubilized in 50 - 100 µL H_2O_{dest}.

Buffer P1	Tris-HCl	50.0	mM
	ethylene diamine tetraacetic acid (EDTA)	10.0	mM
	RNaseA	200.	µg/mL
	in H_2O_{dest}; pH 8.0		
Buffer P2	NaOH	200.0	mM
	sodium dodecyl sulfate (SDS)	1.0	% (w/v)
	in H_2O_{dest}; pH 8.0		
Buffer P3	potassium acetate	3.0	M
	in H_2O_{dest}; pH 5.5		

2.5.2 Determination of DNA Concentration

The concentration of a DNA solution was determined by measuring the absorbance at 260 nm and additionally at 280 nm to account for protein impurities. For a pure DNA solution an OD_{260} of one corresponds to a dsDNA concentration of 50 µg/mL. The puritiy of the DNA solution can be deduced from the ratio of OD_{260} to OD_{280}. With an OD_{260}/OD_{280} ratio of 1.8 – 2.0 the DNA was considered as pure.

2.5.3 Transformation of Bacteria by the $RbCl_2$ Method

E. coli cells were grown aerobically in 500 mL vapor sterilized LB medium containing the required additives. When the culture reached an OD_{578} of 0.6 cells were harvested by centrifugation (10 min at 6,000 x *g* and 4°C), suspended in 200 mL TFB1 and incubated on ice for 5 min. After subsequent centrifugation (5 min at 3,000 x *g* and 4°C) cells were suspended in 2 volumes of TFB2 (referring to the volume of the cell sediment), incubated on ice for 30 min and divided into 40 µL aliquots. These were either immediately used for transformation or stored at – 80°C

TFB1	potassium acetate	30	mM
	$CaCl_2$	10	mM
	$MnCl_2$	50	mM
	$RbCl_2$	100	mM
	glycerol	15	% (v/v)
	in H_2O_{dest}; pH 5.8		

TFB2	MOPS	10	mM
	$CaCl_2$	75	mM
	RbCl	10	mM
	glycerol	15	% (v/v)
	in H_2O_{dest}; pH 6.5		

Transformation of chemocompetent cells was applied as standard transformation method. 40 µL of $RbCl_2$-competent cells were combined with 1 - 2 µL DNA solution (50 µg/mL) and subjected to a heat shock for 45 s at 42°C. Immediately after the transformation cells were cooled on ice for 2 min. Afterwards 1 mL of preheated LB medium was added and cells were incubated at 37°C for 1 h. Depending on the expected colony density, different volumes were then streaked on agar plates containing the appropriate antibiotics and plates were incubated overnight at 37°C.

2.5.4 Electrophoretic Separation of DNA

For the analytical separation of DNA fragments, agarose gels consisting of 1 % (w/v) agarose in TAE buffer were prepared. For exceptionally small DNA fragments (below 1000 bp) the agarose concentration was increased to 1.3 % (w/v). Depending on the size of the gel, a voltage of 80 - 100 V was applied. DNA fragments migrate towards the anode with a velocity that is proportional to the negative logarithm of their size. Prior to loading, DNA samples were mixed with loading dye to facilitate loading and to indicate the progress of the samples in the gel. GeneRuler™ DNA Ladder Mix or MassRuler™ DNA Ladder Mix were used as size standard according to the manufacturer's instructions. After electrophoresis, gels were incubated in an ethidium bromide solution for 10 - 30 min, rinsed with H_2O and the DNA was detected *via* its fluorescence under UV light (λ = 312 nm). In cases where DNA fragments were to be extracted from the gel, extraction was carried out using the QIAquick Gel Extraction Kit according to the manufacturer's instructions.

TAE buffer	Tris-acetate	40.0	mM
	EDTA	1.0	mM
	in H_2O_{dest}; pH 8.0		
DNA loading dye	bromphenol blue	0.35	mM
	xylene cyanol FF	0.45	mM
	orange G	0.25	mM
	sucrose	115.0	mM
	in H_2O_{dest}		
ethidium bromide solution	ethidium bromide	0.1	% (v/v)
	in H_2O_{dest}		

2.5.5 Site-Directed Mutagenesis of DNA

Single amino acids in a protein of interest can be exchanged by inserting site-specific mutations into the DNA sequence of the corresponding gene. The QuikChange Site-directed Mutagenesis Kit was employed in this work for mutational analysis of NtPPO2. The method, which is illustrated in Fig. 11, utilizes a dsDNA plasmid carrying the gene of interest and two synthetic oligonucleotide primers which contain the desired mutation (see Tab. 5) and are complementary to opposite strands of the vector. During polymerase chain reaction (PCR) with PfuTurbo DNA polymerase a mutated plasmid is generated. The PCR product is treated with *Dpn*I, an endonuclease specifically digesting partially methylated DNA, here the parental template DNA. This allows isolation of the newly synthesized unmethylated DNA of the mutated plasmid, which is subsequently transformed into a suitable *E. coli* strain where DNA ligase closes the nicked DNA circles.

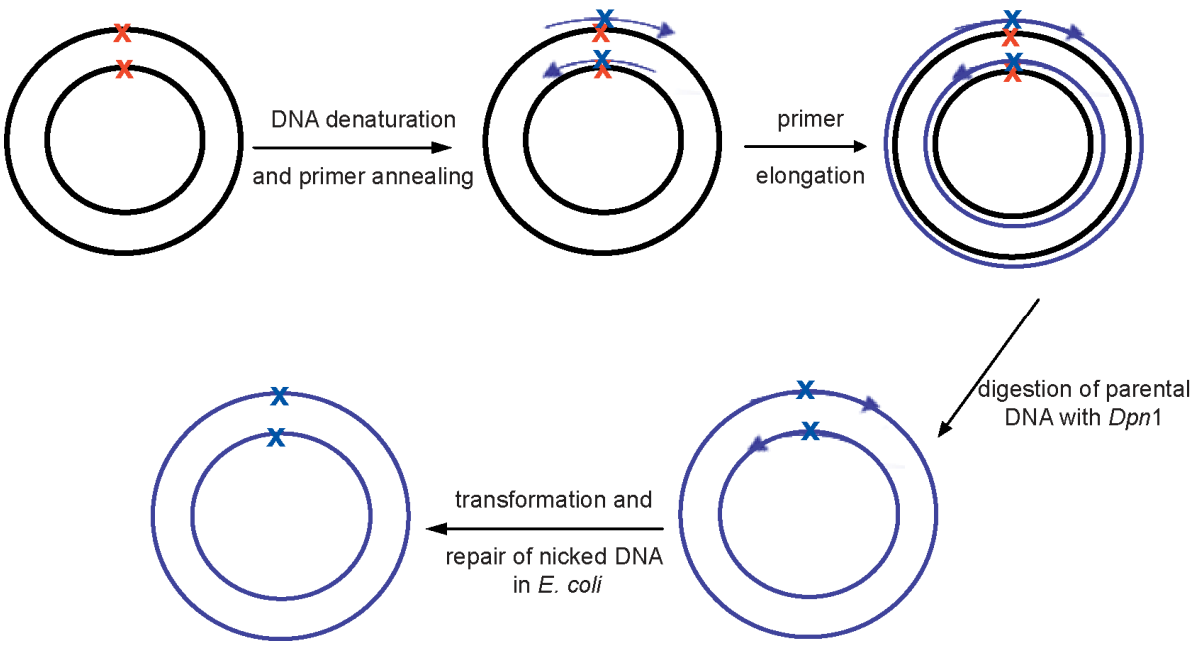

Fig. 11: Outline of the QuikChange Procedure.
Overview of the QuikChange Site-Directed Mutagenesis method (modified from Stratagene Instruction Manual, 1998). — parental DNA, — mutated DNA, X position of the desired mutation, → mutagenic primer, X introduced mutation. A detailed description is given in the text.

PCR reactions with the QuikChange Site-Directed Mutagenesis Kit were carried out according to manufacturer's instructions. Mutated plasmids were transformed into chemocompetent *E. coli* DH10b cells. Oligonucleotide primers listed in Tab. 5 and nucleotides exchanged in comparison to the wild type sequence are underlined. All mutated genes were subjected to DNA sequence determination.

Tab. 5: Oligonucleotide primers used for site-directed mutagenesis of tobacco protoporphyrinogen IX oxidase.

Only oligonucleotide primers in forward orientation are listed. The second oligonucleotide (reverse) always corresponds to the reverse complementary sequence.

Mutant designation	Sequence of oligonucleotide primer (forward) (5´→ 3´)
R98A	CCACTTTCACAAAACAAGGCCTACATTGCCAGAAATGG
R98K	CCACTTTCACAAAACAAGAAGTACATTGCCAGAAATGG
R98E	CCACTTTCACAAAACAAGGAGTACATTGCCAGAAATGG
L356N	GGGCTTTGGGGTTAATGTACCTTCCAAGGAGC
L356V	GGGCTTTGGGGTTGTTGTACCTTCCAAGGAGC
L372N	GACACTAGGCACCAACTTCTCTTCTATGATGTTTCC
L372V	GACACTAGGCACCGTCTTCTCTTCTATGATGTTTCC
F392H	CTCTATACTACTCATGTTGGTGGAAGCC
F392E	CTCTATACTACTGAGGTTGGTGGAAGCC
N67R	GGGATGAAGGGGCACGTACTATGACTG
N67W	GGGATGAAGGGGCATGGACTATGACTG
S374D	GACACTAGGCACCCTCTTCGATTCTATGATGTTTCC

2.5.6 Amplification of DNA Fragments by PCR

2.5.6.1 Design and Synthesis of Oligonucleotide Primers

Oligonucleotide primers for the amplification of the gene *hemB* from *M. barkeri* with the aim of subsequent cloning vector pET32a were designed. Recognition sequences for restriction endonucleases were inserted *via* these primers at both ends of the genes. Oligonucleotide primers are listed in Tab. 6. Recognition sequences of restriction endonucleases are underlined.

Tab. 6: Oligonucleotide primers used for the amplification of DNA fragments.

"Fwd" refers to forward primer and "rev" to reverse primer.

Primer designation	Sequence of oligonucleotide primer (5´→ 3´)	Additional information
MbhemB-fwd	CCGGAATTCCGGATGTTTCCAGATGTCAGGTTAAG	*Eco*RI restriction site
MbhemB-rev	CCGCTCGAGCGGTTACTTCAACATGCGGGCAGC	*Xho*I restriction site

For subsequent cloning into the vector pET32a *M. barkeri hemB* (975 bp) was amplified using primers MbhemB-fwd and MbhemB-rev.

2.5.6.2 PCR Conditions

Taq DNA polymerase (Qiagen) was used for all reactions. After an initial DNA denaturation step, a cycle consisting of the three steps denaturation, primer annealing and primer elongation was completed 30 times and the reaction terminated by a final elongation step. The denaturation temperature of 95°C and the elongation temperature of 72°C remained unchanged. The annealing temperature depended on oligonucleotide length and G+C content and was furthermore influenced by the insertion of mismatches. The T_m was calculated as following:

T_m [°C] = 69.3 + 0.41 (% G+C) - 650/*n*

% G+C represented the G+C content of the primer in % and *n* represented the number of nucleotides.

The duration of the elongation step was chosen according to the length of the DNA fragment to be amplified according to manufacturer's instructions.

Standard thermocycler program	95 ° C	5 min	
	95 ° C	1 min	
	50-60 ° C	30 s	30 x
	71 ° C	1-4 min	
	71 ° C	5-10 min	
	4 ° C	∞	

2.5.6.3 Purification of PCR Products

For quality controls of the amplified DNA, an aliquot of the reaction mixture was analyzed by agarose gel electrophoresis. By detection of one PCR product only, the entire sample was subjected to purification with the QIAquick PCR Purification Kit. If additional PCR products were detected, the entire reaction mixture was electrophoretically separated. The DNA fragment of interest was then excised from the gel and purified using the QIAquick Gel Extraction Kit. All kits were used according to the manufacturer's instructions.

2.5.7 Enzymatic Modification of DNA

2.5.7.1 Restriction of DNA with Restriction Endonucleases

Restriction of DNA (vectors and PCR products) was carried out using restriction endonucleases purchased from New England BioLabs. Reaction buffers, concentrations of enzymes and DNA as well as incubation temperatures were chosen according to the

manufacturer's instructions. The digestion was allowed to proceed for 2 - 3 h and was, if possible, followed by heat inactivation of the restriction endonucleases (20 min at 65°C or 80°C, depending on the enzyme).

2.5.7.2 Ligation

In order to avoid re-circularization of digested vector DNA, the 5'-phosphate groups of linearized vectors were removed prior to the ligation reaction. This was achieved by adding antarctic alkaline phosphatase (New England BioLabs) to the sample immediately after restriction (1 U /µg DNA) and incubation at 37°C for 30 min, followed by heat inactivation (15 min at 65°C). Ligation of DNA was carried out using T4 DNA ligase (MBI Fermentas) in a reaction buffer supplied by the manufacturer. An amount of 25 - 50 ng vector DNA was mixed with insert DNA in excess (insert to vector ratio with regard to molar concentrations ≈ 5:1). 1 - 2 U of T4 DNA ligase were added.

2.5.7.3 DNA Sequencing

DNA sequences were obtained with an Abi Prism^{TM} 310 Genetic Analyzer in our laboratory. The required preparatory PCR with fluorescence-labeled ddNTPs and purification of the PCR product were carried out as described by the manufacturer.

2.6 Protein Biochemical Methods

2.6.1 Production and Purification of *Pseudomonas aeruginosa* Porphobilinogen Synthase

2.6.1.1 Cell Growth for Protein Production

10 x 500 mL vapor sterilized LB medium containing 100 µg/mL ampicillin and 34 µg/mL chloramphenicol in 1 L Erlenmeyer flasks were each inoculated with 5 mL of an overnight culture of *E. coli* BL21(DE3)RIL carrying pGEXPahemB. Cultures were grown at 37°C and 200 rpm to an OD_{578} of 0.6 and expression of *hemB* was induced by addition of IPTG to a final concentration of 500 µM. Incubation was continued overnight at 25°C and 150 rpm. Cells were harvested by centrifugation for 15 min at 4,000 x *g* and 4°C.

2.6.1.2 Cell Disruption

The cell sediment was suspended in 10 mL PBS buffer containing 1 mM phenylmethanesulfonyl fluoride (PMSF). Cells were disrupted by a single passage through a

French Press at 1,500 p.s.i. Cell debris and insoluble protein fraction were removed by centrifugation for 45 min at 4°C and 25,000 x *g*. The resulting supernatant was loaded onto a glutathione sepharose column. All steps were performed at 4°C, protein solutions were stored on ice.

2.6.1.3 First Affinity Chromatography Using Glutathione Sepharose

The purification protocol for PaPBGS was established by Nicole Frankenberg in our laboratory (Frankenberg *et al.*, 1999). A 12 mL glutathione sepharose column was equilibrated with 5 column volumes of PBS buffer containing 1 mM PMSF. After loading the supernatant, the column was washed with 10 column volumes of PBS containing 1 mM PMSF to remove unbound proteins (flow rate 1 mL/min). The PaPBGS-GST fusion protein was then eluted with elution buffer at a flow rate of 1 mL/min. The eluate was collected in 1 mL fractions. Fractions containing PaPBGS-GST were identified by SDS polyacrylamide gel electrophoresis (SDS-PAGE), pooled and concentrated by ultrafiltration. Concentrated protein solutions were dialyzed overnight at 4°C against PreScission protease buffer.

PBS buffer	NaCl	140.0 mM
	KCl	2.7 mM
	Na_2HPO_4	10.0 mM
	KH_2PO_4	1.8 mM
	PMSF	1.0 mM
	in H_2O_{dest}; pH 7.4	
Elution buffer	Tris-HCl	50.0 mM
	glutathione	10.0 mM
	NaCl	150.0 mM
	in H_2O_{dest}; pH 7.4	
PreScission protease buffer	Tris-HCl	50.0 mM
	NaCl	150.0 mM
	EDTA	1.0 mM
	dithiothreitol	1.0 mM
	in H_2O_{dest}; pH 7.0	

2.6.1.4 PreScission™ Protease Cleavage and Second Affinity Chromatography

PreScission™ Protease cleaves site-specifically at its recognition sequence between the GST domain and the target protein. 70 U of PreScission™ Protease were added to the pooled and concentrated protein solution with the subsequent cleavage reaction proceeding in PreScission™ protease buffer at 4°C overnight. A second affinity chromatography with glutathione sepharose was then performed to remove the separated GST-tag, uncleaved PaPBGS-GST fusion protein and the PreScission™ protease, which is also a fusion with

GST. The 12 mL glutathione sepharose column was again equilibrated with 5 column volumes of PBS buffer and the protein solution was loaded onto the column. The column was washed with PBS buffer and PaPBGS was collected with the flow through. In a final step the column was treated with elution buffer, thereby eluting the GST-tag, uncleaved fusion protein and PreScission™ Protease. All steps were monitored by SDS-PAGE-analysis. Fractions containing PaPBGS were again pooled and concentrated by ultrafiltration.

2.6.2 Production and Purification of *Methanosarcina barkeri* Porphobilinogen Synthase

2.6.2.1 Cell Growth for Protein Production

Recombinant *M. barkeri* PBGS (MbPBGS) was produced using *E. coli* strain BL21(DE3)RIL. 10 x 500 mL vapor sterilized LB medium containing 100 µg/mL ampicillin and 34 µg/mL chloramphenicol in 1 L Erlenmeyer flasks were each inoculated with 5 mL of an overnight culture of *E. coli* BL21(DE3)RIL carrying pIH45. Cells were grown in LB medium at 37°C and 200 rpm until cultures reached an OD_{578} of 0.6. Gene expression was induced by the addition IPTG to a final concentration of 150 µM. Cells were further cultivated overnight at 17°C, 150 rpm and subsequently harvested.

2.6.2.2 Cell Disruption

The cell sediment obtained by centrifugation was washed with buffer B and suspended in a minimal volume of buffer B. Cells were disrupted by sonication (Bandelin HD 2070, 0.5 s sound, 0.5 s paused, MS73 tip, 70 % amplitude) and the cell debris was removed by centrifugation at 50,000 x *g* for 45 min. The resulting supernatant was loaded onto Ni-IDA chromatography.

Buffer B	Tris-HCl	50 mM
	NaCl	300 mM
	$ZnCl_2$	10 µM
	in H_2O_{dest}; pH 8.5	

2.6.2.3 Affinity Chromatography Using Ni-IDA Sepharose

Recombinant MbPBGS was purified in a first step by Ni-IDA affinity chromatography using a 5 mL column equilibrated with 10 volumes of buffer B. All steps were carried out at RT, proteins were stored on ice. After loading the cell free extract at a flow rate of

500 µL/min, the column was washed with 10 volumes of buffer B to remove unbound proteins. Bound proteins including His-tagged MbPBGS were eluted using a linear gradient of 0 – 1 M imidazole in buffer B at a flow rate of 1 mL/min. Eluate fractions of 1 mL were collected, fractions containing recombinant MbPBGS were identified by SDS-PAGE, combined and concentrated by ultrafiltration.

2.6.2.4 Ion Exchange Chromatography Using DEAE Sepharose

Anion exchange chromatography using DEAE sepharose was performed at RT. Pooled fractions containing recombinant MbPBGS were applied at a flow rate of 1 mL/min to a 3 mL DEAE Sepharose column equilibrated with buffer B. To remove unbound proteins the column was washed with 7 column volumes of buffer B. Bound proteins including recombinant MbPBGS were eluted with 300 mM NaCl in buffer B. Fractions containing recombinant MbPBGS were identified *via* SDS-PAGE-analysis, combined and concentrated by ultrafiltration.

2.6.2.5 Gel Permeation Chromatography

The last step of MbPBGS purification was performed by gel permeation chromatography at RT using a 30 mL Superdex 200 HR 10/30 equilibrated with buffer B. Combined fractions containing recombinant MbPBGS were chromatographed with a flow rate of 0.5 mL/min. Recombinant MbPBGS was identified by enzyme activity testing, SDS-PAGE analysis and Western Blotting.

2.6.3 Production and Purification of *Arabidopsis thaliana* Uroporphyrinogen III Synthase

2.6.3.1 Cell Growth for Protein Production

Six times 500 mL of vapor sterilized LB media containing 100 µg/mL ampicillin and 34 µg/mL chloramphenicol in 1 L Erlenmeyer flasks were each inoculated with an overnight culture of *E. coli* BL21(DE3) RIL carrying either $pUROS_{full}$ or $pUROS_{mat}$. Cultures were grown at 37°C and 200 rpm to an OD_{578} of 0.7 and expression of *hemD* was induced by the addition of IPTG to a final concentration of 100 µM. Further incubation followed overnight at 25°C and 150 rpm. Cells were subsequently harvested by centrifugation (15 min at 4,000 x *g* and 4°C)

2.6.3.2 Cell Disruption

Cells were washed with buffer D and suspended in a minimal volume of buffer D. Bacteria were disrupted *via* sonication (Bandelin HD 2070, 0.5 s sound, 0.5 s paused, MS73 tip, 70 % amplitude) and the cell free extract cleared from insoluble protein and cell debris by centrifugation at 150,000 x *g* for 45 min. The resulting supernatant was loaded on to Ni-NTA chromatography.

Buffer D	Hepes	20.0	mM
	$MgCl_2$	5.0	mM
	Triton X-100	0.01	% (v/v)
	in H_2O_{dest}; pH 7.5		

2.6.3.3 First Affinity Chromatography Using Ni-NTA Sepharose

Recombinant AtUROS was purified in a first step by Ni-chelating sepharose Fast Flow affinity chromatography using a 5 mL column equilibrated with 10 volumes of buffer D. After loading the supernatant at a flow rate of 0.7 mL/min, the column was washed with 10 volumes of buffer D to remove unbound proteins. Bound proteins including His-tagged AtUROS were eluted using a linear gradient of 0 – 1 M imidazole in buffer D at a flow rate of 1 mL/min. Eluate fractions of 1 mL were collected, fractions containing recombinant AtUROS were identified by SDS-PAGE-analysis, combined and concentrated by ultrafiltration.

2.6.3.4 Ion Exchange Chromatography Using DEAE Sepharose

Anion exchange chromatography using DEAE sepharose was performed at RT. Pooled fractions containing recombinant AtUROS were applied at a flow rate of 1 mL/min to a 3 mL DEAE Sepharose column equilibrated with buffer D. To remove unbound proteins the column was washed with 7 column volumes of buffer D. Bound proteins including recombinant AtUROS were eluted with 200 mM NaCl in buffer D. Fractions containing recombinant AtUROS were identified *via* SDS-PAGE-analysis, combined and concentrated by ultrafiltration.

2.6.3.5 Gel permeation chromatography

The last step of AtUROS purification was performed by gel permeation chromatography at RT using a 30 mL Superdex 200 HR 10/30 equilibrated with buffer D. The column was calibrated using bovine carbonic anhydrase (M_r = 29,000), bovine serum albumin (M_r = 66,000), yeast alcohol dehydrogenase (M_r = 150,000), and amylase (M_r = 200,000) as marker proteins. Combined fractions containing recombinant AtUROS were

chromatographed under identical conditions at a flow rate of 0.5 mL/min. Recombinant AtUROS was identified by enzyme activity testing, SDS-PAGE analysis and Western Blotting.

2.6.4 Production and Purification Tobacco Protoporphyrinogen IX Oxidase

2.6.4.1 Cell Growth for Protein Production

Recombinant proteins were produced using *E. coli* BL21(DE3)RIL containing the plasmids encoding wildtype or mutant NtPPO2. For each variant five times 500 mL vapor sterilized LB medium containing 100 µg/mL ampicillin and 34 µg/mL chloramphenicol in 1 L Erlenmeyer flasks were each inoculated with 5 mL of an overnight culture. Cultures were grown at 37°C and 200 rpm to an OD_{578} of 0.7 and expression of *hemY* was induced by addition of IPTG to a final concentration of 250 µM. Incubation was continued overnight at 25°C and 150 rpm. Cells were harvested by centrifugation for 15 min at 4,000 x *g* and 4°C.

2.6.4.2 Cell Disruption

The cell sediment obtained by centrifugation was washed with buffer Y and suspended in a minimal volume of buffer Y. Cells were broken by sonication (Bandelin HD 2070, 0.5 s sound, 0.5 s paused, MS73 tip, 70 % amplitude) and the cell free extract cleared by centrifugation at 75,000 x *g* for 45 min. The resulting supernatant was loaded on Ni-IDA chromatography.

Buffer Y	Tris-HCl	10.0	mM
	NaCl	300.0	mM
	$MgCl_2$	10.0	mM
	Triton X-100	0.01	% (w/v)
	in H_2O_{dest}; pH 8.0		

2.6.4.3 Affinity Chromatography Using Ni-IDA Sepharose

Recombinant wildtype and mutant NtPPO2 were purified by Ni-IDA affinity chromatography using a 5 mL column equilibrated with 10 volumes of buffer Y. After loading the supernatant at a flow rate of 0.5 mL/min, the column was washed with 10 volumes of buffer Y to remove unbound proteins. Bound proteins including His-tagged wildtype or mutant NtPPO2 were eluted using a linear gradient of 0 – 1 M imidazole in buffer Y at a flow rate of 1 mL/min. Eluate fractions of 1 mL were collected, fractions

containing recombinant wildtype or mutant NtPPO2 were identified by SDS-PAGE-analysis, combined and concentrated by ultrafiltration.

2.6.5 Concentrating Protein Solutions

Protein solutions were concentrated in a 50 mL or in a 10 mL stirred ultrafiltration cell with a YM30 membrane at 3 x 10^5 Pa until a protein concentrations of 2 - 20 mg/mL was reached. All recombinant concentrated proteins were stored at 4°C.

2.6.6 Determination of Protein Concentration

2.6.6.1 Bicinchoninic Acid Protein Assay

Concentrations of protein solutions were determined using the Micro BCA Protein Assay Kit® according to manufacturer's instructions. The Bicinchoninic Acid 8BCA9 Protein Assay combines the reduction of Cu^{2+} to Cu^{1+} by protein in an alkaline medium with the highly sensitive and selective colorimetric detection of the cuprous cation (Cu^{1+}) by bicinchoninic acid. The intensity of the color produced is proportional to the number of peptide bonds participating in the reaction. Bovine serum albumin was used as a standard.

2.6.6.2 Photometric Determination of Protein Concentration

An optical density technique for measuring protein concentration was applied for highly purified recombinant proteins. The extinction coefficient indicates how much light a protein absorbs at a certain wavelength. From the OD_{280} of a homogeneous protein solution its concentration was calculated using the 280 nm extinction coefficient which is specific for a given amino acid sequence (Gill and von Hippel, 1989).

2.6.6.3 Determination of Protein Concentrations *via* S•Tag Rapid Assay Kit

Concentrations of proteins carrying a S•Tag were determined *via* S•Tag Rapid Assay Kit according to manufacturer's instructions.

2.6.7 Determination of FAD Content

2.6.7.1 UV/VIS-Photometric Determination of the FAD Content

To analyze the potential effects of the mutations on FAD binding by NtPPO2, UV/VIS spectra were recorded from 250 to 550 nm for both wild type and mutants under identical conditions in buffer Y (see page 43) at room temperature according to the method described by Maneli and coworkers (Maneli *et al.*, 2003). The FAD content was then obtained by

measuring absorption at the maximum wavelength (450 nm). With an appropriate calibration curve with commercially obtained FAD the content was calculated and expressed as FAD/monomer.

2.6.7.2 Fluorimetric Determination of the FAD Content

As second method for the determination of the FAD content of wildtype and mutant NtPPO2 the fluorescence of FAD was determined as described by Ohno and coworkers (Ohno *et al.*, 1986). Purified enzymes were immersed in boiling water for five minutes and cooled rapidly in melting ice water to extract non-covalently bound FAD. Denatured proteins were removed by centrifugation (10 min at 15,000 x *g* and 4°C). The fluorescence of the samples was measured with the excitation wavelength of 450 nm and the emission wavelength of 535 nm, using a Perkin-Elmer PA LS50B fluorescence spectrophotometer. Thereafter, the pH of the solutions was lowered to a value of 2.6 with 1 N HCI, and the fluorescence was determined again. Standard curves for commercially obtained FAD at pH 8 and pH 2.6 were determined and the FAD content of the recombinant proteins calculated. The FAD content is expressed as FAD/monomer.

2.6.8 Discontinuous SDS-PAGE

Proteins were analyzed by SDS-PAGE as described by Laemmli (Laemmli, 1970) with modifications by Righetti (Righetti, 1990) for discontinuous SDS-PAGE. Protein samples were denatured by heating to 95°C for 10 min in SDS loading dye. Samples were loaded onto the gel which was run at 40 mA. During electrophoresis, proteins were first focused in the stacking gel and subsequently separated according to their relative molecular mass in the running gel. The size standard employed was Protein Molecular Weight Marker. Gels were stained with staining solution and destained with destaining solution until the protein bands were clearly visible.

SDS gel

	running gel [12 % (v/v)]	stacking gel [6 % (v/v)]
acrylamide stock solution	2.0 mL	500.0 µL
buffer for running gel	1.25 mL	-
buffer for stacking gel	-	625.0 µL
H_2O_{dest}	1.75 mL	1.375 mL
APS solution	5.0 µL	3.0 µL
tetramethylen diamine (TEMED)	50.0 µL	30.0 µL

acrylamide stock solution Rotiphorese® Gel 30 (37.5:1) (Roth)

APS solution Ammonium peroxodisulfate in H_2O_{dest} 10.0 % (w/v)

buffer for running gel	Tris-HCl	1.5	M
	SDS	0.4	% (w/v)
	in H_2O_{dest}; pH 8.8		
buffer for stacking gel	Tris-HCl	500.0	mM
	SDS	0.4	% (w/v)
	in H_2O_{dest}; pH 6.8		
Electrophoresis buffer	Tris-HCl	14.5	mM
	glycine	1.441	% (w/v)
	SDS	1.0	% (w/v)
	in H_2O_{dest}; pH 8.4		
SDS loading dye	Tris-HCl	100.0	mM
	glycerol	40.0	% (v/v)
	β-mercaptoethanol	10.0	% (v/v)
	SDS	3.2	% (w/v)
	bromphenol blue	0.2	% (w/v)
	in H_2O_{dest}; pH 6.8		
Staining solution	ethanol	30.0	% (v/v)
	acetic acid	10.0	% (v/v)
	Coomassie Brilliant Blue G-250	0.25	% (w/v)
	in H_2O_{dest}		
Destaining solution	ethanol	30.0	% (v/v)
	acetic acid	10.0	% (v/v)
	in H_2O_{dest}		

Protein Molecular Weight Marker (MBI Fermentas)
(indicated are approximate relative molecular weights)

β-galacosidase, *E. coli*	116,000
albumin, bovine	66,200
albumin, egg	45,000
lactate dehydrogenase, porcine muscle	35,000
restriction endonuclease *Bsp*98I, *E. coli*	25,000
β -lactoglobulin, bovine milk	18,400
lysozyme, egg	14,400

2.6.9 Western Blotting and Immunodetection of Immobilized Proteins

For further analysis proteins separated during SDS-PAGE were transferred in a semi-dry process onto a polyvinylidenfluorid (PVDF)-membrane, which binds the proteins by polar interactions. PVDF-membranes were incubated in methanol for 10 min and similarly to the SDS-gel and blotting paper incubated in transfer-buffer and assembled in the following order on the blotting apparatus: Cathode, blotting paper, PVDF-membrane, SDS-gel, blotting paper, anode. A current of 0.8 mA/cm^2 was applied for 30 min at 10 V. Non-specific binding sites of the membrane were saturated overnight in blocking solution at 4°C and slight shaking. Proteins immobilized on a PVDF-membrane were specifically detected by antibodies. Primary antibodies were directed against GST or His-tag, secondary antibodies were directed against the primary antibody and were coupled to an alkaline

phosphatase. Incubation with the primary antibody was carried out in blocking solution for 1 h (RT) and slight shaking. Next, membranes were washed three times for 10 min with washing-buffer and incubated for 45 min with the secondary antibody. After four additional washing steps with PBS/Tween buffer for 10 min, membranes were incubated for 5 min in alkaline phosphatase buffer and exposed to staining solution until bands became visible. During exposure alkaline phosphatase, the enzyme bound to the antibody, catalyzes the reaction of 5-brom-4-chloro-3-indolylphosphate (BCIP) with nitroblue-tetrazolium (NBT).

Transfer buffer	Tris-HCl	25.0	mM
	glycine	192.0	mM
	methanol	20.0	% (v/v)
	in H_2O_{dest}; pH 8.5		
Blocking solution	skim milk powder	5.0	% (w/v)
	Tween 20	0.1	% (v/v)
	PBS	10.0	% (v/v)
	in H_2O_{dest}		
Washing solution	skim milk powder	0.5	% (w/v)
	Tween 20	0.1	% (v/v)
	PBS	10.0	% (v/v)
	in H_2O_{dest};		
PBS/Tween-buffer	Tween 20	0.1	% (v/v)
	PBS	10.0	% (v/v)
	in H_2O_{dest}		
Alkaline phosphatase buffer	Tris-HCl	100.0	mM
	NaCl	100.0	mM
	$MgCl_2$	5.0	mM
	in H_2O_{dest}; pH 9.5		
Staining solution	NBT solution	0.33	% (v/v)
	BCIP solution	0.33	% (v/v)
	in alkaline phosphatase buffer		
NBT solution	nitroblue-tetrazolium	10.0	% (w/v)
	dimethylenformamide (DMF)	70.0	% (v/v)
	in H_2O_{dest}		
BCIP solution	5-brom-4-chloro-3-indolylphosphate	5.0	% (w/v)
	DMF		

2.7 Enzyme Activity Assays

2.7.1 Determination of Porphobilinogen Synthase Activity

2.7.1.1 Preparation of Bacterial Cell Free Extracts for Porphobilinogen Synthase Activity Testing

Cell-free extracts of several bacterial strains, *i.e. E. coli*, *E. coli* CSA, *B. subtilis*, *B. megaterium*, *S. aureus*, *P. aeruginosa*, *S. avermitilis*, *S. coelicolor* and *S. sp*. A012304,

were required to investigate PBGS activity. To prepare the cell-free extracts, 1 L of the respective strain were grown for 24 h in complex medium at 37°C or for the *Streptomyces* strains at 25°C. Cells were harvested by centrifugation (15 min at 4,000 x *g* and 4°C) and washed with buffer C. Bacteria were disrupted *via* sonication (Bandelin HD 2070, 0.5 s sound, 0.5 s paused, MS73 tip, 70 % amplitude) and the cell free extracts cleared from insoluble protein and cell debris by centrifugation at 150,000 x *g* for 45 min at 4°C. The protein concentrations in cell free extracts were determined by BCA Protein Assay, adjusted to approximately 10 mg/mL and immediately used for the determination of PBGS activity. For background control, proteins from cell free extracts were heat inactivated for 10 minutes at 95°C. Furthermore, reactions without ALA-addition were determined to evaluate the contribution of cellular porphobilinogen.

Buffer C	Tris-HCl	50 mM
	$MgCl_2$	5 mM
	$ZnCl_2$	5 µM
	in H_2O_{dest}; pH 7.0	

2.7.1.2 Porphobilinogen Synthase Activity Assay

The activity of PBGS was determined using a modified Ehrlich's test which is based on the reaction between the product porphobilinogen and 4-(dimethylamino)-benzaldehyde (DMBA). In the first reaction step between porphobilinogen and DMBA a pink reaction product with an absorbance maximum at 555 nm is formed, which reacts with a second porphobilinogen molecule to form colorless dipyrrolphenylmethane (see Fig. 12). Since the second reaction proceeds very slowly, porphobilinogen concentrations can be quantified *via* the Beer-Lambert law and the molar extinction coefficient of the colored intermediate of $\varepsilon(\text{complex}) = 60{,}200\ M^{-1}cm^{-1}$.

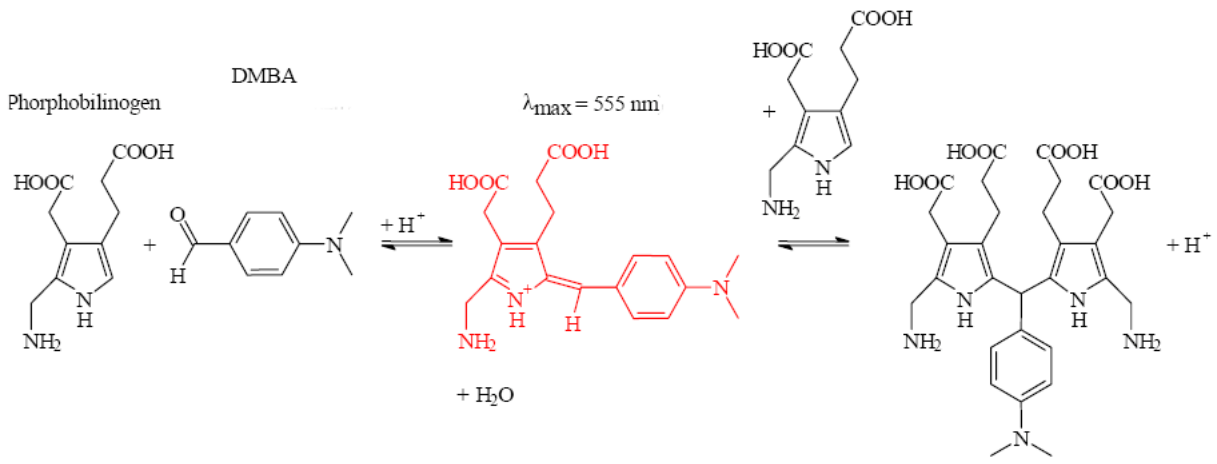

Fig. 12: Colorimetric detection of porphobilinogen.
Porphobilinogen forms a coloured complex with DMBA which can be detected at OD_{555}. This complex slowly reacts with a second porphobilinogen molecule to form colorless dipyrrolphenylmethane.

The Beer-Lambert law is as following:

$$c = \frac{A}{d * \varepsilon}$$

c = *concentration of porphobilinogen [M]*

A = *absorption*

d = *cell diameter [cm]*

ε = *molar extinction coefficient of the colored intermediate* $[M^{-1}cm^{-1}]$

2.7.1.3 Determination of Kinetic Parameters of Porphobilinogen Synthase

A typical assay contained a final concentration of PaPBGS of 2 µg/mL, the concentrations of MbPBGS and HsPBGS were 25 µg/mL. The substrate ALA was dissolved to a concentration of 40 mM in kinetic buffer K1 with either 10 mM $MgCl_2$ for PaPBGS or 10 µM $ZnCl_2$ for MbPBGS, respectively. For HsPBGS kinetic buffer K2 was applied. Kinetic buffers were chosen according to published data (Bhosale *et al.*, 1995, Frankenberg *et al.*, 1999, Jaffe *et al.*, 2000). Stock solutions of protein, buffer and water were mixed and incubated at 37°C for 5 min. To start the reaction, substrate was added to a final concentration of 0 - 10 mM. The PBGS-catalyzed reaction was stopped at different time points (1 - 60 min) by adding equal amounts of ice cold stop reagent to the reaction mixture. Following centrifugation (3 min at 5,000 x *g* at RT), the supernatant was treated with an equal amount of Ehrlich reagent. After 15 min at RT, the amount of product was determined by measuring the OD_{555} and porphobilinogen formation was calculated using the Beer-Lambert law as described above. The Michaelis Menten constant (K_M), the maximal velocity v_{max} and the catalytic constant k_{cat} were determined from substrate velocity plots by measuring the constant velocity formation of porphobilinogen over a substrate range from 0 - 10 mM ALA. Values were determined by computerized Lineweaver Burke iterative curve fitting using SigmaPlot 8.0 Enzyme Kinetics v1.1. For the calculation of the catalytic efficiency k_{cat}, the maximal velocity v_{max} was divided by the corresponding enzyme concentration.

Buffer K1	bis-tris-propane	100 mM
	in H_2O_{dest}; pH 8.5	
Buffer K2	KH_2PO_4	100 mM
	β-mercaptoethanol	10 mM
	$ZnCl_2$	10 µM
	in H_2O_{dest}; pH 7.0	
Stop reagent	trichloroacetic acid	50 % (w/v)
	$HgCl_2$	100 mM
	in H_2O_{dest}	

Ehrlich reagent	DMBA	2 % (w/v)
	acetic acid	50 % (v/v)
	perchloric acid	50 % (v/v)

2.7.1.4 Determination of IC_{50} Values and Inhibition Constants for Porphobilinogen Synthase with Alaremycin

To approximate the inhibitory potency of alaremycin, inhibitor concentrations reducing enzyme activity of PaPBGS, MbPBGS and HsPBGS to 50 % (IC_{50} values) were determined. For the determination of the IC_{50} for the human, *M. barkeri* and *P. aeruginosa* PBGS, enzyme velocity was evaluated at a single concentration of substrate with varying concentrations of the competitive inhibitor. For this purpose, alaremycin was dissolved to a concentration of 40 mM in the respective kinetic buffers. Reactions were carried out in the respective kinetic buffer with a final ALA concentration of 1 mM and alaremycin concentrations from 0 – 10 mM. PBGS and alaremycin were incubated at 37°C for 30 min prior to ALA addition. All further steps were carried out as described above. Results were plotted in a dose-response curve and IC_{50} values were deduced. Time dependency of inhibition was determined by pre-incubating the inhibitor with a fixed concentration of PBGS and ALA in kinetic buffer between 30 s and 30 min. The PBGS activity was determined as described above.

2.7.2 Determination of Uroporphyrinogen III Activity *via* a Coupled Enzyme Activity Assay

AtUROS activity was determined using a coupled enzyme activity assay as outlined in Fig. 13. Recombinant PaPBGS was purified as described before. Purified recombinant *B. megaterium* PBGD was kindly provided by Claudia Schulz from our laboratory.

A standard assay mixture contained 25 µg of purified recombinant AtUROS, 0.2 mM ALA, 10 µg PaPBGS and 10 µg PBGD in a total volume of 800 µL in buffer D. The reaction mixture was incubated for up to 120 min at 37°C in the dark. The reaction was stopped by addition of 300 µL KI/I_2 solution and formed uroporphyrinogen III was oxidized to uroporphyrin III. $Na_2S_2O_5$ solution was added to oxidize residual I_2. Proteins were precipitated by the addition of 100 µL TCA solution and subsequent centrifugation (5 min at 15,000 x *g* and 4°C).

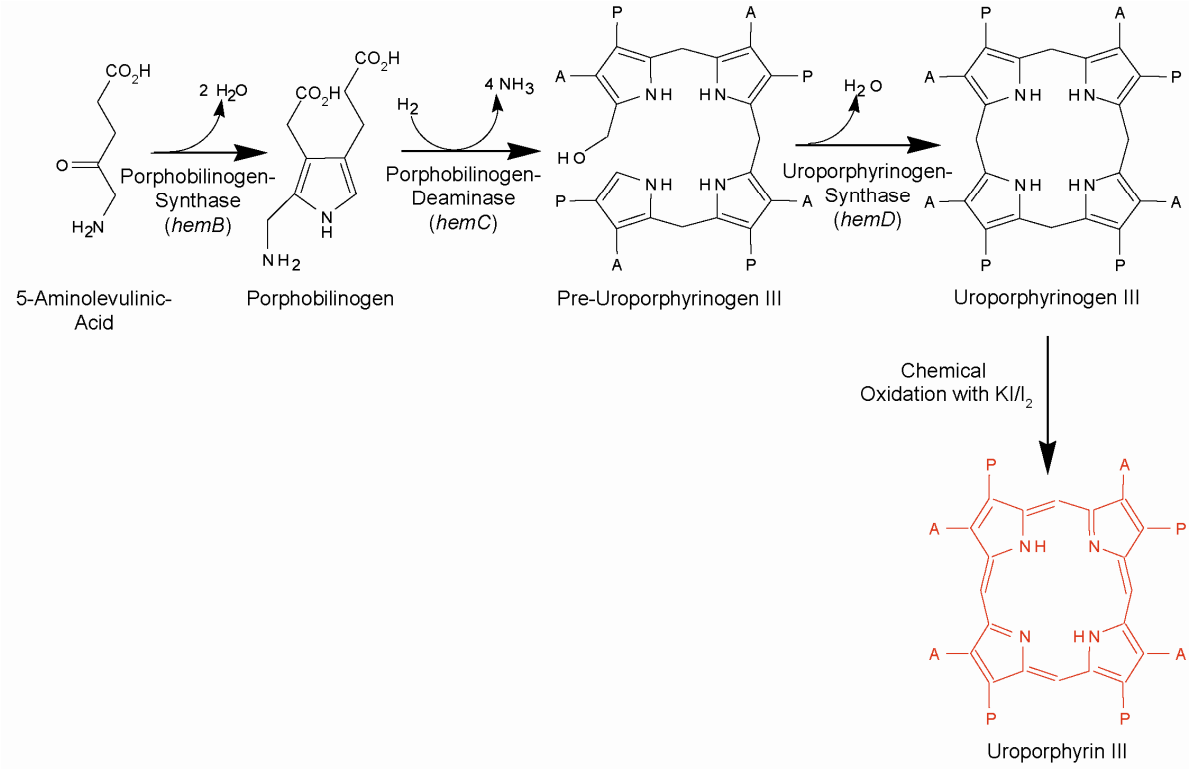

Fig. 13: Coupled enzyme activity assay for uroporphyrinogen III synthase.
UROS activity was monitored using a coupled enzyme activity assay with the photometric and fluorimetric detection of the oxidized reaction product uroporphyrin III.

The amount of enzymatically formed uroporphyrinogen III was determined by fluorimetric detection of uroporphyrin III using a PE LS50B luminescence spectrometer with an excitation wavelength of 400 nm, an emission scan range of 500 - 700 nm, a scan speed of 200 nm/min and a slit widths of 5 nm for emission and excitation. Furthermore, uroporphyrin III was detected by measuring the absorbance at 408 nm. Chemical cyclization of pre-uroporphyrinogen to uroporphyrin I, which reveals similar spectroscopic and fluorimetric properties as uroporphyrin III, was ruled out by control experiments in an enzymatic test without AtUROS addition and in the presence of heat inactivated AtUROS.

KI/I_2 solution	KI	0.5	% (w/v)
	I_2	1.0	% (w/v)
	in H_2O_{dest}		
$Na_2S_2O_5$ solution	$Na_2S_2O_5$	1.0	% (w/v)
	in H_2O_{dest}		
TCA-solution	trichloroacetic acid	50.0	% (w/v)
	in H_2O_{dest}		

2.7.3 Determination of Protoporphyrinogen IX Oxidase Activity

2.7.3.1 Preparation of the Substrate Protoporphyrinogen IX

The oxygen-dependent PPO activity assay was developed by Labbe and coworkers (Labbe *et al.*, 1985). The substrate protoporphyrinogen IX is converted into protoporphyrin IX by PPO in the presence of molecular oxygen as electron acceptor. Excitation of the product at a wavelength of 409 nm results in an emission at 633 nm which was detected fluorimetrically and is therefore clearly distinguishable from the substrate as this reveals no fluorescence spectroscopic properties. The substrate protoporphyrinogen IX was obtained through the reduction of commercially obtained protoporphyrin IX according to modified instructions of Sano and Granick (Sano and Granick, 1961). For this purpose, 500 µmol protoporphyrin IX were dissolved in 3 mL buffer P under N_2 exposure and reduced with 6 g of 3 % sodium-amalgam. After 2 min incubation at 80°C the solution became colorless, indicating the reduction of protoporphyrin IX. Next, the solution was filtered through glass wool, 50 mM DTT was added and the pH was adjusted to 7-8 with 20 % (v/v) phosphoric acid. The protoporphyrinogen IX solution was aliquoted and stored anaerobically in the dark at - 20°C to avoid autooxidation of the substrate by oxygen or light.

Buffer P	KOH	10 mM
	ethanol in H_2O_{dest}	20 % (v/v)

2.7.3.2 Determination of Kinetic Parameters of Tobacco Protoporphyrinogen IX by Fluorescence Stopped Flow Spectrometry

NtPPO2 activity was monitored using a continuous assay *via* the detection of protoporphyrin IX fluorescence. Stopped-flow kinetic experiments were performed under aerobic conditions using a Jasco 810 stopped-flow spectrometer and obtained data were analyzed with Biokine Acquire Kinetics. Averages of three to five individual transients were analyzed. Protoporphyrinogen IX was dissolved in kinetic buffer P. Protoporphyrinogen IX solution and NtPPO2 preparations were mixed in a six to one ratio in a total volume of 300 µL and fluorescence resulting from protoporphyrin IX formation was continuously recorded *via* an excitation at 409 nm and emission measurement above 450 nm. Approximately 8000 measurement points per assay were recorded. Protoporphyrin IX concentrations were calculated using an appropriate calibration curve. The Michaelis Menten constant (K_M), the maximal velocity v_{max} and the catalytic constant k_{cat} were determined from substrate velocity plots by measuring the constant velocity formation of

protoporphyrin IX from protoporphyrinogen IX over a substrate range from 1 - 25 µM and a time course of up to 2 hours at 20°C. The initial reaction rates were linear and values were determined by the computerized Lineweaver Burke iterative curve fitting using SigmaPlot 8.0 Enzyme Kinetics v1.1. For the calculation of the catalytic efficiency k_{cat}, the maximal velocity v_{max} was divided by the corresponding enzyme concentration.

Kinetic buffer P	MES	50 mM
	Triton X-100	1 % (v/v)
	in H_2O_{dest}; pH 6.0	

2.8 Crystallization of *Pseudomonas aeruginosa* Porphobilinogen Synthase

2.8.1 Identification of Crystallization Conditions

For the crystallization of purified PaPBGS the vapor diffusion method was applied, allowing a slow and controlled growth of protein crystals. Since it is difficult to predict conditions for nucleation and growth of well-ordered crystals, conditions were identified empirically using a variety of buffers, precipitants and salts. PaPBGS solutions containing alaremycin were generated by mixing aliquots of protein solution and alaremycin solution. Crystallization lead conditions were identified using Crystal Screen and Crystal Screen 2 in 96-well sitting-drop CrystalClear strip racks with 100 µL of reservoir solution and drops of 3 µL of reservoir and 3 µL of protein solution. Crystallization was attempted at 4°C and 17°C, respectively. Prior to X-ray data collection, crystals were washed in cryoprotective solution for 5 s and flash-frozen in liquid N_2.

Protein solution	Tris-HCL	100 mM
	$MgCl_2$	10 mM
	PaPBGS	20 mg/mL
	in H_2O_{dest}; pH 7.5	
Alaremycin solution	Tris-HCL	100 mM
	$MgCl_2$	10 mM
	alaremycin	5 mM
	in H_2O_{dest}; pH 7.5	
Cryoprotective solution	PEG 400	20 % (v/v)
	reservoir solution	80 % (v/v)

2.8.1.1 Structure Determination

Data collection was performed under cryogenic conditions using synchrotron radiation at beamLine BL1 (BESSYII, Berlin, Germany). Data analysis was kindly performed by

Wolf-Dieter Schubert from the group of Dirk Heinz, Helmholtz Centre for Infection Research, Braunschweig.

2.8.1.2 Molecular Depictions

Molecular depictions were prepared using PyMOL (Delano Scientific LLC, USA).

2.9 Metabolite Extraction and Preparation

2.9.1 Cofactor Extraction from *Methanosarcina barkeri*

2.9.1.1 Heme Extraction

Non-covalently bound heme was extracted from *M. barkeri* by a modification of a previously described method (Weinstein and Beale, 1983). An amount of 1 g of frozen cells were ground under liquid nitrogen, transferred to a test tube and suspended in 10 mL of icecold solution M. The mixture was allowed to stand 10 min on ice and 10 min at room temperature with occasional mixing followed by centrifugation in sealed steel beakers at 10,000 x g for 30 min at 4°C. Four mL of peroxide-free diethyl ether were added to the supernatant. After mixing, 12.5 mL of cold H_2O_{dest} were added with further mixing. The heme-containing upper ether phase was transferred to a rotary evaporator flask and evaporated to dryness. For MALDI-TOF-MS analysis the dried fraction was suspended in 100 µL solution T.

<u>*Solution M*</u>	acetone	90 % (v/v)
	Hal	5 % (v/v)
	in H_2O	
<u>*Solution T*</u>	acetonitrile	20 % (v/v)
	trifluoric acid	1 % (v/v)
	in H_2O	

2.9.1.2 F_{430} and Vitamin B_{12} Extraction

Coenzyme F_{430} is known to contain two methyl groups and vitamin B_{12} seven methyl groups all derived from *S*-adenosyl-*L*-methionine (Jaenchen *et al.*, 1981, Warren *et al.*, 2002). These cofactors were analyzed as controls as following. One mL of grown *M. barkeri* culture was centrifuged for 5 min and cells suspended in solution T. After sonication for 3 min the extract was centrifuged (5 min at 15,000 x g and 4°C) and the resulting supernatant was analyzed by MALDI-TOF-MS.

2.9.1.3 Feeding on Radioactively Labeled Substrate

The archaeon *M. barkeri* was cultivated anaerobically at 37°C with 250 mM methanol as sole carbon and energy source in low salt medium. For the quantification of the uptake of SAM and methionine by *M. barkeri*, 5 mL cell culture was fed on 0.1 µCi *L*-[*methyl*-^{14}C]methionine or *S*-Adenosyl-*L*-[*methyl*-^{14}C]methionine, respectively at 37°C for 48 hours. Cells were harvested and amounts of [^{14}C]-SAM and [^{14}C]-methionine in cell sediment and medium were determined using a Liquid Scintillation Analyzer. The scintillation cocktail employed was OptiPhase HiSafe 2. To determine the origin of the methyl groups of heme, *M. barkeri* was grown in 200 mL low salt medium supplemented with *L*-[*methyl*-D_3]methionine (98 atom % D) added to the autoclaved medium to a final concentration of either 2 mM, 5 mM or 10 mM from a sterile stock solution. Growth was initiated with a 10 % inoculum (grown in absence of methionine) and followed photometrically at 578 nm. At the end of the exponential growth phase, cells were harvested anaerobically by centrifugation at 10,000 x *g* for 30 min at 4°C and stored under H_2 saturated atmosphere at - 20°C. Per 200 mL culture approximately 1 g cells (wet mass) were obtained.

2.9.1.4 Identification of Cofactors *via* MALDI-TOF

The mass spectra were kindly collected by Jörg Kahnt from the group of Rolf Thauer, Max-Planck Institute for Terrestrial Microbiology, Marburg in the reflector positive ion mode. Samples were measured after an appropriate dilution of the sample with saturated α-cyano-4-hydroxy cinnamic acid in solution F on a steel target. The spectra were determined with an Ultraflex from Bruker and commercially obtained hemin was used as standard. The natural isotopic distribution of protoheme, F_{430} and vitamin B_{12} were calculated aided by the isotope pattern calculator provided by the University of Sheffield at the ChemPuter site (http://winter.group.shef.ac.uk/chemputer/isotopes.html). The fraction of protoheme, F_{430} or vitamin B_{12} labeled with methyl-D_3 was determined by solving the binomial equation (a+b)n for n = 2 (protoheme or F_{430}) and n = 7 (B_{12}) using the "Solver" facilities provided by Excel 97 as described by (Selmer *et al.*, 2000).

Solution F	acetonitrile	70	% (v/v)
	trifluoric acid in H_2O_{dest}	0.1	% (v/v)

2.9.2 Preparation of Precorrin-2

2.9.2.1 Combined Production of Porphobilinogen Synthase, Porphobilinogen Deaminase, Uroporphyrinogen III Synthase and Uroporphyrinogen III Methyltransferase

Two times 500 mL vapor sterilized LB medium containing 100 µg/mL ampicillin and 34 µg/mL chloramphenicol in 1 L Erlenmeyer flasks were each inoculated with 5 mL of an overnight culture of *E. coli* BL21(DE3)RIL carrying the pETcoco2 derivative vector pIH41 encoding *M. barkeri cobA*, *M. thermoautotrophicum hemB* and *B. megaterium hemC* and *hemD*. Cultures were grown at 37°C and 200 rpm to an OD_{578} of 0.4 and the vector copy number was shifted from low copy to high copy state by addition of *L*-arabinose to a final concentration of 0.02 % (w/v). After 1 h incubation at 37°C and 200 rpm expression of the respective genes was induced by addition of IPTG to final concentration of 400 µM. Incubation was continued overnight at 25°C and 150 rpm. Cells were harvested by centrifugation for 15 min at 4,000 x *g* and 4°C.

2.9.2.2 Cell Disruption

The cell sediment obtained by centrifugation was washed with buffer R1 and suspended in a minimal volume of buffer R1. Cells were disrupted by sonication (Bandelin HD 2070, 0.5 s sound, 0.5 s paused, MS73 tip, 70 % amplitude) and the cell debris was removed by centrifugation at 50,000 x *g* for 45 min. The resulting supernatant was loaded on Ni-IDA chromatography column.

Buffer R1	Hepes	20 mM
	NaCl	300 mM
	$MgCl_2$	5 mM
	in H_2O_{dest}; pH 7.5	

2.9.2.3 Affinity Chromatography Using Ni-IDA Sepharose

Recombinant proteins were purified by Ni-IDA affinity chromatography using a 3 mL gravity flow column equilibrated with 10 volumes of buffer R1. After loading the cell free extract, the column was washed with 10 volumes of buffer R1 to remove unbound proteins. Bound proteins were eluted with 1 M imidazole in buffer R1. Eluate fractions of 1 mL were collected and fractions containing recombinant proteins were identified by SDS-PAGE, combined and concentrated by ultrafiltration.

All further steps were carried out under anaerobic conditions in an anaerobic chamber. For desalting, combined fractions containing recombinant proteins were applied to a PD-10

column equilibrated with buffer R2. Flowthrough was collected in 1 mL fractions and fractions containing recombinant proteins were identified by SDS PAGE and employed for precorrin-2 production.

Buffer R2	Tris-HCl	50 mM
	NaCl	100 mM
	in H_2O_{dest}; pH 8.0	

2.9.2.4 Preparation of Precorrin-2

For the production of precorrin-2, 200 µL protein solution (approx. 5 mg/mL) containing purified recombinant CobA, PBGS, PBGD and UROS, 1 mg ALA and 2 mg SAM were combined in a total volume of 1 mL buffer R2 under anaerobic conditions in the dark overnight. To separate recombinant proteins from synthesized precorrin-2, the solution was anaerobically applied to a 3 mL Ni-IDA gravity flow column equilibrated with 10 volumes of buffer R2 the and flowthrough containing precorrin-2 was collected.

2.9.3 Preparation of Alaremycin from Culture Broth of *Streptomyces sp.* A012304

2.9.3.1 Conditions for Alaremycin Production

Alaremycin production was performed with a slight modification of the method described before (Awa *et al.*, 2005). The major difference to the published method is the preparation of production medium. Dextrin was autoclaved separately and the pH of the medium was not adjusted to pH 7.0 but to pH 8.5. *S. sp.* A012304 was grown in 200 mL of seed medium inoculated with a single colony for four days at 25°C and 250 rpm. Once the growing seed culture altered the color of the medium to dark brown, indicating secondary metabolite expression (Matseliukh, 2006), production of the antibiotic was initiated by inoculation of 400 mL production medium with 20 mL of seed culture and cells were allowed to grow for 5 days at 25°C and 250 rpm. Cultures were subjected to centrifugation for 45 min, 4,000 x *g* at 4°C and culture supernatant was used for alaremycin preparation.

2.9.3.2 Alaremycin Preparation

Alaremycin was extracted from the culture broth by a slight modification of the method described by Awa and coworkers (Awa *et al.*, 2005). Culture supernatant was sterile filtrated to remove residual cells and applied to Diaion HP-20 hydrophobic interaction chromatography. The flowthrough was adjusted to pH 2.0 with 1 N HCl and extracted with

freshly purchased ethyl acetate. The organic layer was further extracted with water pH 9.0 and applied to a cation exchange column using a gravity flow column with fibrious cation exchange resign (Whatman). The flowthrough was carefully adjusted to pH 2 with 1 N HCl and extracted with ethyl acetate. The organic layer was evaporated to dryness and alaremycin was stored at - 20°C.

2.10 Comparative Genome Analysis

Comparative genome analysis was employed for the identification of open reading frames (ORF) potentially involved in archaeal heme biosynthesis. This computational approach is based on the assumption that a second ancient heme biosynthesis pathway with conserved proteins solely exists in a certain group of organisms. If so, these proteins should be found exclusively in these organisms but not in those which synthesize heme *via* the common pathway or in such that do not produce heme at all. This potential feature was evaluated using a specific BLAST analysis. The BLAST analyses were performed using NCBI BLAST version 2.2.14-x64 (Altschul *et al.*, 1997). In order to evaluate and control the BLAST analyses a Java (version 1.5) based software running on a 64 bit dual processor computer was implemented. All analyzed amino acid sequences were downloaded from the Integr8 database release 44 (Kersey *et al.*, 2005). Two proteins were assigned as homolog once the e-value of the BLAST hit was less than 10^{-10}. The corresponding bioinformatic tool was developed by Karsten Hiller from our institute.

Several organisms of which the complete genome sequence has been determined were examined for their ability to synthesize heme by intensive literature research. If so, the deduced proteomes were screened for the occurrence of common heme biosynthesis protein homologs and organized into three groups. The first group consisted of organisms which synthesize heme *via* the ancient pathway, *i.e*. they are capable of synthesizing heme but do not possess the proteins operating in the common pathway. Therefore, the proteomes of *M. barkeri*, *M. acetivorans*, *M. mazei*, *Archaeoglobus fulgidus*, *Sulfolobus solfataricus*, *Sulfolobus tokodaii*, *Halobacterium salinarium*, *Pyrobaculum aerophilum* and *Aeropyrum pernix* were included in this group. The second group comprised organisms that are not capable of synthesizing heme: *Caenorhabditis elegans*, *Lactococcus lactis*, *M. thermoautotrophicum*, *Mycoplasma genitalium*, *Mycoplasma pneumoniae*, *Mycoplasma pulmonis*, *Pyrococcus abyssi*, *Pyrococcus horikoshii*, *Thermotoga maritima*, *Treponema pallidum*, *Streptococcus pneumoniae*, *Streptococcus pyogenes*, *Borellia burgdorferi* and

Ureaplasma urealyticum. Finally, the third group consisted of organisms that synthesize heme *via* the common pathway, *i.e*. they possess the corresponding proteins: *Drosophila melanogaster*, *Homo sapiens sapiens*, *Saccharomyces cerevisiae*, *Plasmodium falciparum*, *B. subtilis*, *Schizosaccharomyces pombe*, *E. coli* and *P. aeruginosa*.

The comparative genome analysis was performed in three steps, which are visualized in Fig. 34: Firstly, the set of all proteins that are common for all organisms belonging to group one was determined. Therefore, each protein of the first group was blasted against the proteomes of all organisms of this group and collected only those proteins that yielded in significant BLAST hits in all organisms of this group. Secondly, all proteins from this "intersection" that feature homologs in any of the organisms of group two were removed. Finally, all sequences that have homologs in group three were removed from the set of collected proteins.

3 RESULTS AND DISCUSSION

This thesis investigated several different steps of heme biosynthesis in archaea, bacteria and plants.

3.1 The Molecular Function of Alaremycin

The function of a newly discovered antibiotic, named alaremycin due to its structural similarity to ALA, was investigated at the cellular, enzymatic and finally at the atomic level. The novel antibiotic was purified, tested on various bacteria, on purified PBGS from different sources and was finally co-crystallized with one of the target enzymes.

3.1.1 Purification of Alaremycin Produced by *Streptomyces sp.* A012304

The original purification scheme was provided by Masaaki Wachi and coworkers from the Tokyo Institute of Technology, Japan (Awa *et al.*, 2005). M. Wachi kindly provided us with the corresponding *Streptomyces* strain and we tried to reproduce the published purification procedure which employs several steps of organic and inorganic extraction. Alaremycin is negatively charged at pH 9 due to the abstraction of a proton from its carboxyl group at a basic pH. In contrast, at a pH 2, the antibiotic is uncharged and thus soluble in organic solvents. This chemical feature was employed for the extraction of alaremycin from the culture broth. The extraction procedure was carried out as described under MATERIALS AND METHODS.

We realized that also the pH value of the producing culture was crucial for alaremycin biosynthesis and excretion. In the published protocol the pH of the production medium had been adjusted to pH 7. However, no alaremycin was recovered from the culture broth at this condition. Finally, adjustment of the production medium to a pH of 8.5 yielded amounts of alaremycin between 5 mg/L and 50 mg/L. Interestingly, the producer strain *S. sp*. A012304 possesses at least three different phenotypes in liquid and on solid LB media (see Fig. 14). The “white” and “yellow” phenotypes shared the same coccoid multicellular organization, whereas in “brown” colonies the cells were aligned in chains (see Fig. 14 C and D). It was referred to as the “brown” phenotype due to the secretion of a brownish substance into the medium after an incubation exceeding four days, which is most likely a secondary metabolite (Matseliukh, 2006). The “brown” phenotype produced white spores (see Fig. 14 B), whereas the yellow and white phenotype did not show spore formation. In production medium, *S. sp*. A012304 possesses a phenotype similar to the described

"yellow" one. In order to find the most efficient alaremycin producer, cells from the various phenotypes were tested as source for liquid preliminary cultures. Highest alaremycin yields were obtained with "yellow" *S. sp.* A012304 (50 mg/L compared to 5 mg/L for the "white" and 10 mg/L for the "brown" phenotype, respectively).

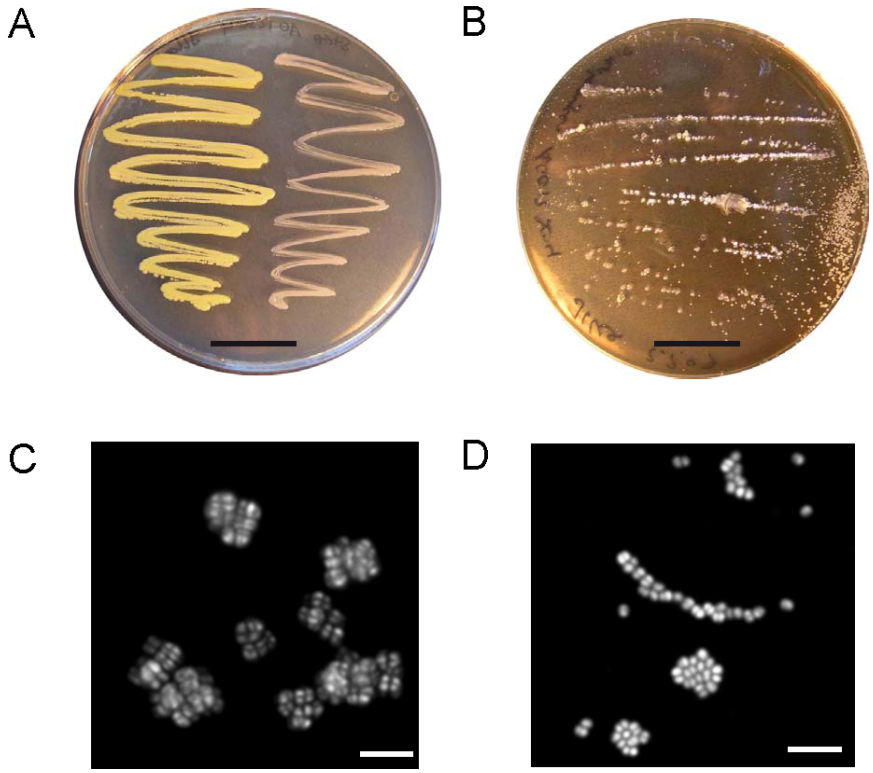

Fig. 14: Different phenotypes of *Streptomyces sp.* A012304 on LB media.
(A+B) LB Agar Plates. *S. sp.* A012304 cells were grown at 30°C for 3 days. Scale bar = 2 cm. **(A)** Left the "yellow" and right handed the "white" phenotype are shown. **(B)** The "brown" phenotype with white spores is visible. **(C+D)** Confocal micrographs of fixed cells, stained with SYBR Green II. Scale bar = 5 µm. **(C)** The "yellow" phenotype formed coccoid packs of 4 and multiples of 4 cells. **(D)** The "brown" phenotype formed cell chains and unordered clusters. Confocal micrographs were kindly made by Sebastian Hannemann from the group of Oliver Fackler, Hygiene Institute University Hospital Heidelberg.

3.1.2 Antimicrobial Activity of Alaremycin on Various Organisms

One interesting feature of many antibiotics is their capability to affect the growth of a broad range of different bacteria. However, the antimicrobial capacity of the lately discovered antibiotic alaremycin was solely investigated on *E. coli*. Consequently, MICs for several Gram positive and Gram negative bacterial species including the pathogens *P. aeruginosa* and *S. aureus* were determined. Alaremycin exhibited minimal inhibitory concentrations values of 4 mM to 18 mM, detailed values are given in Tab. 7. Antibiotic activity was lower in defined media compared to complex media, *i.e.* for example 4 mM and 10 mM for *E. coli*, respectively. This feature is probably due to the differences in growth rates between the two tested conditions. In complex medium bacteria usually develop a significantly faster

growth compared to minimal media. Therefore, in complex medium growth inhibitory effects are more profound and require lower amounts of antibiotics. Since *S. aureus* did not reveal growth with any of the used minimal media, no inhibition parameters for this condition could be deduced. Even though all tested bacterial strains showed inhibition of growth by the antibiotic at varying concentrations, the producer strains *S. sp*. A012304 was not affected by alaremycin concentrations up to 20 mM. In contrast, the two *Streptomyces* species, *i.e. S. coelicolor* and *S. avermitilis* showed growth inhibition in complex and minimal media at 8 mM and 14 mM, respectively, indicating that *Streptomyces* strains are not tolerant to alaremycin *per se*. Thus, *S. sp.* A012304 must have developed a resistance against its own antibiotic which is effective at even high concentrations.

Tab. 7: Minimal inhibitory concentrations of alaremycin for various Gram negative and positive bacteria.

MICs were determined as described in MATERIALS AND METHODS. The standard deviation of the shown results was between 10 and 15 %. The MIC for *S. aureus* on minimal media could not be determined since *S. aureus* failed to grow on any of the employed media.

	Complex media	Minimal media
E. coli	4 mM	10 mM
P. aeruginosa	12 mM	18 mM
B. subtilis	14 mM	18 mM
B. megaterium	4 mM	10 mM
S. coelicolor	8 mM	14 mM
S. avermitilis	8 mM	14 mM
S. aureus	14 mM	/
S. sp. A012304	> 20 mM	> 20 mM

The evaluated MICs revealed that alaremycin is a broad range antibiotic which exhibits antimicrobial activity against several Gram positive and Gram negative bacterial species, including human pathogens such as *S. aureus* and *P. aeruginosa*.

3.1.3 Bacterial Heme Biosynthesis is the Target of Alaremycin Activity

The overall structure of alaremycin is similar to ALA. Consequently, we tested its activity on heme biosynthesis of *E. coli*. For this purpose the heme auxotrophic and heme permeable *E. coli* strain *E. coli* CSA (*hemA*$^-$, *env*) was used. The usually employed *E. coli* laboratory strains have lost their capability to transport heme through the outer membrane. However, the generation of a strain permeable to heme through chemical mutagenesis has been

described before (McConville and Charles, 1979). For the generation of such an *E. coli* strain, the *hemA* deficient *E. coli* EV61 was employed. This strain lacks active glutamyl-tRNA reductase and cannot synthesize heme *de novo*. It thus grows as very small dwarf colonies on LB media after two days. Due to chemical mutagenesis of *E. coli* EV61 a strain was recovered that is capable to utilize external heme sources and forms normal sized colonies if grown on heme containing LB media. This strain was designated *E. coli* CSA and was kindly provided by Claudia Schulz from our laboratory.

Since heme was fed to this strain, its growth was independent of intrinsic heme biosynthesis. Consequently, if alaremycin is inhibiting heme biosynthesis, this *E. coli* strain should show normal growth in the presence of heme and alaremycin. However, *E. coli* CSA showed inhibition of growth at alaremycin concentrations of 10 mM and 18 mM for complex and minimal media with heme, respectively. Clearly, the cells showed significantly reduced growth inhibition compared to common *E. coli* strains, which were inhibited at 4 mM and 10 mM for complex and minimal media, respectively. This indicates that heme biosynthesis was indeed the target of alaremycin. For the residual inhibition of *E. coli* CSA growth due to alaremycin treatment, it has to be taken into account that *E. coli* is not solely heme dependent but also requires other tetrapyrroles such as siroheme (Zeghouf *et al.*, 2000). The inhibition of the biosynthesis of these compounds by alaremycin as well may account for the observed growth defect at high alaremycin concentrations. However, we cannot exclude that alaremycin has additional toxic side effects and antibacterial activity of alaremycin may not be restricted to heme biosynthesis alone. Nevertheless, one may surely conclude that heme biosynthesis is the main target of alaremycin antibacterial activity.

3.1.4 Alaremycin Inhibits Various Porphobilinogen Synthases

As outlined before, alaremycin carries typical features of ALA. Since ALA is the substrate for PBGS, this enzyme is the obvious target for alaremycin. Therefore, we tested the impact of alaremycin on PBGS activity in cell free extracts of various bacteria. PBGS activities of *S. coelicolor*, *S. avermitilis*, *S. sp.* A012304, *E. coli*, *B. megaterium*, *B. subtilis*, *P. aeruginosa*, *E. coli* and *E. coli* CSA were determined with a standard activity test with the addition of none, 5 mM and 10 mM alaremycin. In all cell free extracts comparable PBGS activity was detected and set to 100 % for the respective strain. Completely different responses of the various tested bacterial PBGS towards alaremycin treatment were observed and are presented in Tab. 8. *E. coli* and *E. coli* CSA cell free extract PBGS activities were similar and disappeared after addition of 10 mM alaremycin, whereas *P. aeruginosa* (25 %)

and *B. subtilis* (30 %) cell free extracts showed residual PBGS activity at this concentration. At 5 mM, all *Streptomyces* cell free extracts revealed 68 - 90 % residual activity, whereas at 10 mM alaremycin *S. coelicolor* PBGS activity was abolished. In contrast, *S. sp.* A012304 revealed 78 % residual activity at 10 mM alaremycin.

Tab. 8: Inhibition of porphobilinogen synthase activity in cell free extracts from various Gram negative and positive bacteria by the addition of alaremycin.

PBGS activity was measured as described under MATERIALS AND METHODS. Activity in cell free extracts without alaremycin addition was referred to as 100 % for the corresponding strain. Alaremycin was added to final concentrations of 5 mM and 10 mM. PBGS synthase activity in cell free extracts is given in % PBGS activity. The standard deviation of the shown results was between 10 and 15 %.

	5 mM alaremycin	**10 mM alaremycin**
E. coli	30 %	< 1 %
P. aeruginosa	92 %	25 %
B. subtilis	61 %	30 %
B. megaterium	3 %	< 1 %
S. coelicolor	77 %	22 %
S. avermitilis	68 %	< 1 %
E. coli CSA	36 %	< 1 %
S. sp. A012304	90 %	79 %

The obtained results are in line with the assumption that alaremycin exhibits its mode of action *via* inhibition of PBGS. All tested cell free extracts responded to alaremycin addition and showed reduction in PBGS activity. Most interestingly, PBGS activity of the producer strain *S. sp.* A012304 seemed to possess a certain immunity against the alaremycin antibiotic action. With more than three quarters of residual activity at a concentration of 10 mM inhibitor in cell free extracts, it seemed improbable that this feature is solely explained by differences in PBGS concentrations between the various assayed extracts. It implies a modified PBGS active site, which may have evolved in parallel to the capability of alaremycin production. In summary, one may conclude that the target of alaremycin is indeed PBGS.

3.1.5 Cloning, Purification and Characterization of Recombinant Porphobilinogen Synthases

The obtained results for PBGS activity in cell free extracts indicated that alaremycin exhibits its mode of action *via* the inhibition of PBGS activity. To further investigate this feature, magnesium dependent PBGS from *P. aeruginosa* was recombinantly produced,

purified and tested for its response to alaremycin. In order to determine if alaremycin mode of action is restricted to bacterial PBGS, an archaeal, zinc-dependent enzyme from *M. barkeri* and the human zinc-dependent protein were employed for activity and inhibition testing as well.

3.1.5.1 Recombinant Porphobilinogen Synthase from *Pseudomonas aeruginosa*

The production and purification of recombinant *P. aeruginosa* PBGS (PaPBGS) has been established by Nicole Frankenberg in our laboratory. PaPBGS was produced in *E. coli* BL21(DE3)RIL and purified to apparent homogeneity using glutathione-S-sepharose. In a first chromatographic step, the fusion protein consisting of PaPBGS and the N-terminal GST-tag was isolated. After PreScission™ Protease cleavage of the GST-PBGS fusion protein, recombinant PaPBGS was separated from the released GST-tag and the GST-tagged protease by a second affinity chromatography. Fig. 15 provides documentation of the purification procedure.

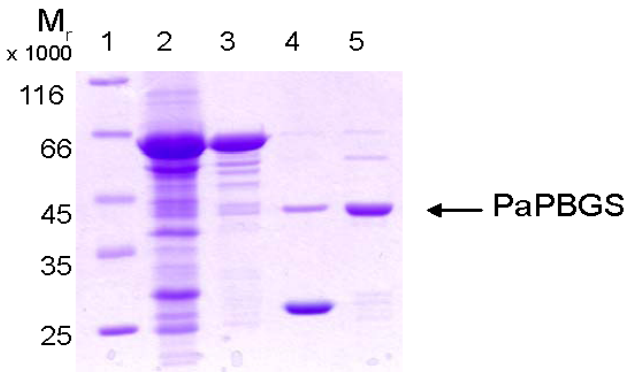

Fig. 15: Production, purification and processing of recombinant *P. aeruginosa* porphobilinogen synthase produced in *E. coli*.
Proteins were separated by 12 % SDS-PAGE and visualized by staining with Coomassie Brilliant Blue. Lane 1: molecular weight marker; lane 2: total cellular extract after overnight induction of gene expression with 250 µM IPTG; lane 4: eluate from the glutathione sepharose column; lane 5: protein solution after digestion with prescission protease lane 6: purified MbPBGS after removal of the GST-tag with a second glutathione sepharose column.

SDS PAGE analysis of the purified protein (lane 8 in Fig. 15) revealed a single band corresponding to a protein with a relative molecular mass of about 38,000, which is in good agreement with the calculated molecular mass of 36,831 Da. About 5 mg of purified recombinant PaPBGS were obtained per liter cell culture.

Kinetic parameters for PaPBGS were evaluated in a standard activity test with a final concentration of 2 µg/mL recombinant PaPBGS. Different substrate concentrations were employed in the activity test, *i.e.* 0 mM, 0.1 mM, 0.2 mM, 0.5 mM, 1 mM, 2 mM, 5 mM and 10 mM ALA, respectively. As displayed in Fig. 16, product formation was increased over time in a substrate concentration dependent manner. In order to determine kinetic parameters of PaPBGS time dependent porphobilinogen formation was recorded and kinetic parameters computed using Sigma Plot 8.0 Enzyme Kinetics module v1.1. For PaPBGS the

K_M was 0.32 mM, the k_{cat} 16.1 s^{-1} and k_{cat}/K_M 50.3 $mM^{-1}s^{-1}$, respectively. All kinetic parameters are listed in Tab. 9. These kinetic properties of PaPBGS resembled previously described results for the same enzyme (Frankenberg *et al.*, 1999).

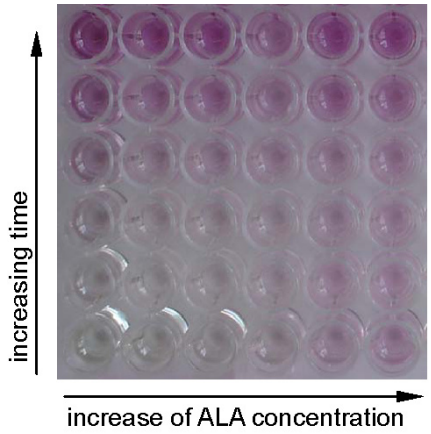

Fig. 16: Outline of porphobilinogen synthase activity assay in microtitre plates.
Using a modified Ehrlich´s test, porphobilinogen formation was evident from the resulting color formation which is recorded at A_{550} nm. From left to right substrate concentrations were raised. Time was increased from bottom to top. Product formation is dependent on substrate concentration and time.

3.1.5.2 Recombinant Porphobilinogen Synthase from *Methanosarcina barkeri*

The cloning of *M. barkeri hemB* was accomplished by PCR using primers based upon the sequence of Maeder and coworkers. (Maeder *et al.*, 2006) (Genbank accession CP000099.1; locus tag Mbar_A1463) and genomic *M. barkeri* DNA as template. The obtained sequence for the cloned *hemB* gene was similar to the published one. Recombinant *M. barkeri* PBGS (MbPBGS) was produced in *E. coli* BL21(DE3)RIL and the resulting His-fusion protein was purified *via* Ni-NTA affinity chromatography. Recombinant MbPBGS eluted with 500 mM imidazole (Fig. 17, lane 4). Fractions containing MbPBGS were combined and applied to a DEAE Sepharose column at a concentration of 0.7 mg/mL column volume. Recombinant protein was eluted with 300 mM NaCl. Fractions containing MbPBGS were combined (Fig. 17, lane 5), concentrated and purified *via* gel permeation chromatography to apparent homogeneity. SDS-PAGE analysis of the purified protein (Fig. 17, lane 6) revealed a predominant protein band corresponding to a protein with a relative molecular mass of about 62,000. This is in good agreement with the calculated molecular mass of the fusion protein of 63,444 Da. An amount of 9 mg recombinant MbPBGS per liter cell culture were yielded. Purified MbPBGS did not show any detectable degradation at 4°C for more than two months.

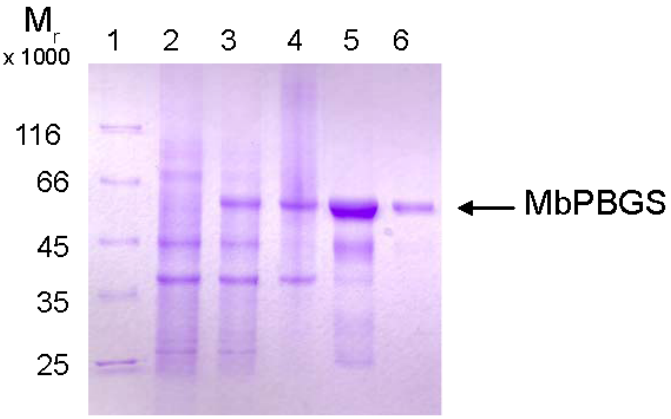

Fig. 17: Production and purification of recombinant *M. barkeri* porphobilinogen synthase produced in *E. coli*.
Proteins were separated by 12 % SDS-PAGE and visualized by staining with Coomassie Brilliant Blue. Lane 1: molecular weight marker; lane 2: total cellular extract without induction of gene expression; lane 3: total cellular extract after overnight induction of gene expression with 250 µM IPTG; lane 4: eluate from the Ni-NTA column with 500 mM imidazole; lane 5: eluate from DEAE sepharose column; lane 6: purified MbPBGS after gel filtration.

Purified recombinant MbPBGS was tested for activity under standard assay conditions with 25 µg/mL MbPBGS referred to the native enzyme without fused tags. For MbPBGS the K_M was 0.07 mM, the k_{cat} 0.012 s^{-1} and k_{cat}/K_M 0.17 $mM^{-1}s^{-1}$, respectively. All kinetic parameters are listed in Tab. 9. Features of MbPBGS have previously been described for the native purified enzyme, which possesses a specific activity of 0.39 µmol $min^{-1}mg^{-1}$ (Bhosale *et al.*, 1995). The recombinant enzyme thus revealed a high substrate affinity and showed, compared to the native protein a comparable specific activity of 0.61 µmol $min^{-1}mg^{-1}$.

3.1.5.3 Recombinant Human Porphobilinogen Synthase

Recombinant purified human PBGS variant N59/C162A (HsPBGS) was kindly provided by Eileen Jaffe, Fox Chase Cancer Center, Philadelphia, USA. The enzyme was stable at -80°C for at least two month. For determination of kinetic parameters the protein concentration was adjusted to a final concentration of 25 µg/mL with substrate concentrations as described above. For HsPBGS at pH 7.0 the K_M was 1.0 mM, the k_{cat} = 0.049 s^{-1} and k_{cat}/K_M = 0.049 $mM^{-1}s^{-1}$, respectively. Formerly obtained results from Tang and coworkers showed a K_M of 0.25 mM and a v_{max} of 55 µmol h^{-1} mg^{-1} (Tang *et al.*, 2005). In this study a v_{max} of 8.8 µmol $h^{-1}mg^{-1}$ was obtained. Obviously, substrate affinity and turnover were reduced. Since the purified enzyme was shipped, these slight differences might be due to loss of activity during transportation.

3.1.6 Single Enzyme Inhibition Studies with Recombinant Porphobilinogen Synthase

The so far obtained results for the mode of action of alaremycin indicated that the antibiotic activity is exhibited by inhibition of PBGS and thus *via* blocking of the biosynthesis of essential tetrapyrroles. However, this has not been directly experimentally proven by testing of purified PBGS enzymes so far. Now, PBGS from three sources, bacterial, archaeal and

eukaryotic, were purified and showed catalytic activity. To evaluate the inhibitory potency of alaremycin on recombinant PBGS, activity tests were performed in the presence and absence of the antibiotic in various concentrations. Inhibitor concentrations reducing enzyme activity by 50 % (IC_{50}) were determined using various protein concentrations as described above and ALA concentrations of 1 mM. Different amounts from 1 – 10 mM of alaremycin were added to the activity tests. Dose response curves were obtained for all three recombinant proteins and IC_{50} values were deduced (Tab. 9).

Tab. 9: Kinetic parameters and IC_{50} values for alaremycin for *P. aeruginosa*, *M. barkeri* and human porphobilinogen synthase.

The Michaelis Menten constant K_M, the k_{cat} and the k_{cat}/K_M values for the various PBGS were determined from substrate velocity plots by measuring the constant velocity formation of porphobilinogen from ALA over a substrate range from 1 - 10 mM. Values were determined by the computerized Lineveaver Burk iterative curve fitting (SigmaPlot 8.0 Enzyme Kinetics v1.1). For inhibition studies 0 - 10 mM alaremycin was added to the enzyme activity test at an ALA concentration of 1 mM.

	PaPBGS		MbPBGS		HsPBGS	
K_M	0.32±0.04	mM	0.07±0.012	mM	1.009±0.11	mM
k_{cat}	16.11±1.25	s^{-1}	0.012±0.001	s^{-1}	0.049±0.002	s^{-1}
k_{cat}/K_M	50.3±0.15	$mM^{-1}s^{-1}$	0.17±0.032	$mM^{-1}s^{-1}$	0.049±0.0057	$mM^{-1}s^{-1}$
IC_{50}	2.1±0.4	mM	2.2±0.5	mM	4.1±0.9	mM

All three recombinant enzymes showed inhibition by alaremycin at concentrations from 2 - 4 mM, with the human enzyme showing a slightly higher tolerance compared to the archaeal and bacterial PBGS. When measuring the IC_{50} values, time-dependence of inhibition was detected. The obtained IC_{50} values are within the range of earlier tested inhibitors for PaPBGS (Frere *et al.*, 2006, Gacond *et al.*, 2007). The inhibitory effect of alaremycin is slightly more effective than for levulinic acid at an IC_{50} = 10 mM (Frere *et al.*, 2002). Possibly, the inhibitory effect of alaremycin is only on an average level compared to formerly tested inhibitors due to its bulky nature, since large PBGS inhibitors have been shown to reveal reduced inhibition capacities compared to smaller ones (Gacond *et al.*, 2007). Nevertheless, alaremycin may serve as a lead structure for chemically engineering of more effective derivatives. Furthermore, the inhibition capacity of alaremycin on enzymes is not restricted to the bacterial variants. The archaeal PBGS from *M. barkeri* revealed similar inhibition behavior as the *P. aeruginosa* enzyme. The human enzyme was inhibited by alaremycin in slightly higher concentrations. In summary, the obtained results revealed that PBGS is indeed the molecular target of alaremycin. The antibiotic reduced PBGS activity and thus disturbed tetrapyrrole biosynthesis, which consequently lead to significantly reduced bacterial growth.

3.1.7 Co-Crystallization of *Pseudomonas aeruginosa* Porphobilinogen Synthase with Alaremycin

Since alaremycin selectively inhibits PBGS activity, it was of high interest to determine the exact molecular mode of alaremycin inhibition at the atomic level. Knowledge of the alaremycin coordination chemistry is one basis for further rational drug design. In previous co-crystallographic studies it has been shown that chemically synthesized inhibitors of PBGS are usually located in the active site of the enzyme and interact with one or both catalytic lysines. Consequently, the crystallization of PaPBGS in complex with the natural antibiotic alaremycin was attempted.

The crystal structure of wildtype PaPBGS has been previously solved by Nicole Frankenberg in our laboratory in cooperation with the group of Dirk Heinz at the Helmholtz Centre for Infection Research, Braunschweig (Frankenberg *et al.*, 1999). To obtain protein crystals in the presence of alaremycin similar conditions were employed using Crystal Screen I and II with a protein concentration of 10 mg/mL and alaremycin concentrations from 1 - 5 mM. Finally, crystallization was achieved by the sitting drop vapor diffusion method and crystals grew within two to three days. Most homogeneous crystals (see Fig. 18 A) were obtained with 10 mg/mL PaPBGS and 5 mM alaremycin in 100 mM Hepes pH 7.5, 200 mM $MgCl_2$ and 30 % PEG400 at 17°C. Data collection was performed under cryogenic conditions using synchrotron radiation at beamline BL1 (BESSYII, Berlin, Germany) yielding a data set with diffraction up to 1.75 Å (Fig. 18 B + C). The following data analysis and manipulations were performed by Wolf-Dieter Schubert from the group of Dirk Heinz, Helmholtz Centre for Infection Research, Braunschweig. Data were indexed, integrated and scaled using HKL2000 (Otwinowski and Minor, 1997). All further manipulations were performed using the CCP4 suite of programs (Collaborative Computational Project Number 4, 1994). Data statistics are listed in Tab. 10. The structure of PaPBGS in complex with alaremycin was determined by molecular replacement using Phaser (McCoy *et al.*, 2005) and the A-chain of a previous crystal structure of the same protein (PDB code 1B4K, Frankenberg *et al.*, 1999) as a structural search model. The structure was refined using simulated annealing techniques (Brunger *et al.*, 1998), followed by restrained refinement with TLS-protocols (Murshudov *et al.*, 1997). For manual adjustments and quality control the graphics program Coot was used (Emsley and Cowtan, 2004).

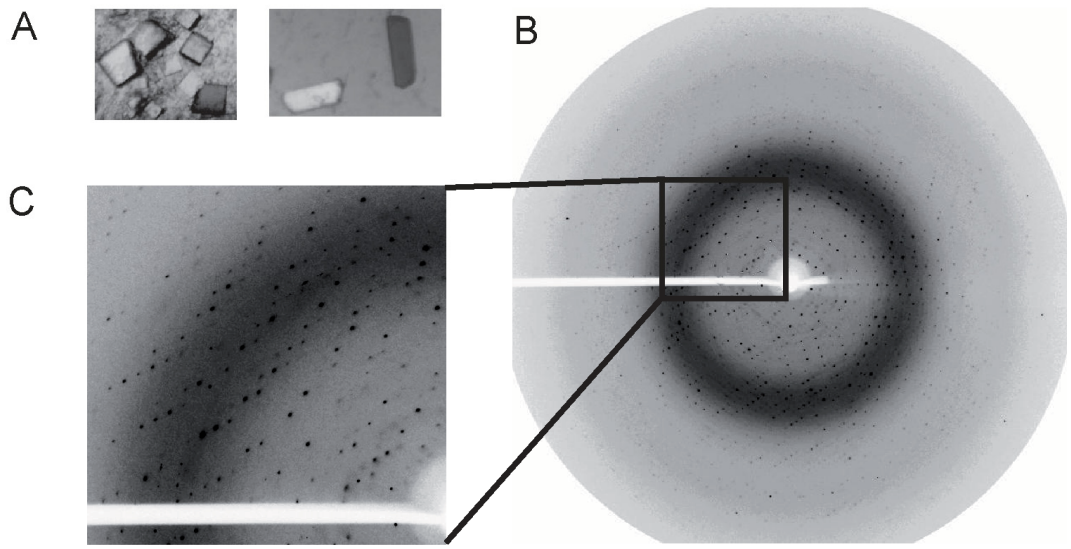

Fig. 18: Crystallization of *P. aeruginosa* porphobilinogen synthase and data collection.
(A) Crystals obtained with 20 mg/mL PaPBGS and 5 mM Alaremycin in 100 mM Hepes pH 7.5, 200 mM $MgCl_2$ and 30 % PEG400 at 17°C. **(B)** Diffraction pattern of PaPBGS in complex with alaremycin. Crystals diffracted up to 1.75 Å **(C)** Magnification of the diffraction pattern reveals ordered scattering.

Tab. 10: Data collection and refinement statistics for the *P. aeruginosa* porphobilinogen synthase - alaremycin co-crystals

[a] >1σ; [b] value for shell of highest resolution in parentheses; [c] $R_{merge} = 100\left(\sum_{h,i}\left|I_{h,i} - I_h\right| \div \sum_{h,i} I_{h,i}\right)$ where summation is over all observations $I_{h,i}$ contributing to the reflection intensities I_h.; [e] 5 % of data were omitted from refinement. [f] determined using Coot; [g] Calculated using Refmac.

Crystallographic data	
Space group	I422
Cell dimensions: a;b;c (Å)	84.4; 84.4; 158.5
Total reflections (>1σ)	401 885
Unique reflections	29 316
Resolution range (Å)[b]	28–1.75 (1.78-1.75)
Completeness (%)[b]	100 (99.9)
Redundancy[b]	13.7 (8.6)
R_{merge}[c]	6.9 (50.4)
I/σ_I[b]	46.0 (5.3)
Temperature factor (Å^2)	18.7
Refinement	
Resolution range (Å)	27.9–1.75
Reflections[a]	27 8236
Non-H protein atoms/monomer	2 646
Solvent molecules/monomer	195
Ions/monomer: Na^+; Mg^{2+}	2; 1
Average B-factor (Å^2)	16.2
R-factor (%); R_{free} (%)[e]	14.2; 18.2
R.m.s. deviation from idealist: bond lengths (Å); bond angles (deg.)[g]	0.018; 1.54
Estimate overall coordinate error, based on maximum likelihood (Å)	0.11

3.1.8 Co-Crystal Structure of Porphobilinogen Synthase with Alaremycin

The high-resolution structure of PaPBGS at 1.75 Å in complex with a single alaremycin gives an ambiguous picture of the inhibitor's binding. PaPBGS is a homooctameric protein composed of four dimers arranged around a central four-fold axis (Frankenberg *et al.*, 1999, Frere *et al.*, 2002). The extended N-terminal arm of each monomer closely wraps around its dimeric partner. The PaPBGS monomer is a classic TIM-barrel (see Fig. 19). The PBGS monomer is a single domain protein showing $(\beta\alpha)_8$-barrel-fold where eight parallel β-strands form a circular and closed β-barrel that is surrounded by α-helices linking neighboring β-strands. In the crystal, however, there is no ordered electron density for the nine amino acid residues attached to the N-terminus derived from the site-specific cleavage of the GST-tag and the first five native amino acids. This is in agreement with earlier findings (Frankenberg *et al.*, 1999). As in all known $(\beta\alpha)_8$-barrel-containing enzymes, the active site of PBGS is located at the C-terminal side of the β-barrel, where extended loops and additional secondary structure elements restrict the opening. The entrance to the active site in PaPBGS is shielded from the surrounding solvent by a "lid" constituted by two short α-helices. The opening of the active site has previously been shown to possess two different conformations, an "open" and a "closed" form. However, in contrast to the previously described crystal structures from PaPBGS in complex with various inhibitors (Frankenberg *et al.*, 1999, Frere *et al.*, 2006), the dimer in the obtained structure is not asymmetric (see below). A single alaremycin is located in the active site (Fig. 19).

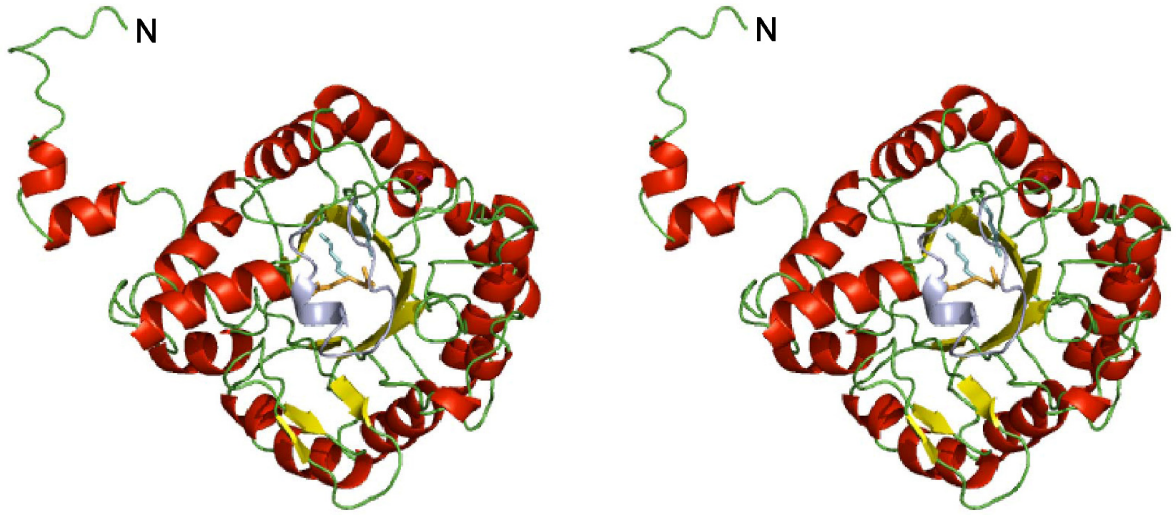

Fig. 19: Stereo ribbon diagram showing the fold of *P. aeruginosa* porphobilinogen synthase monomer A in complex with alaremycin.

The N-terminus is labeled. β-strands are shown in yellow, α-helices in red and loops in green. The unordered lid covering the active site is colored in grey. The side chains of the two active site lysines Lys260 and Lys205 are also shown in light blue. Alaremycin (orange) is covalently attached to Lys260 *via* a Schiff base.

The overall structure was unaffected by inhibitor binding which is in agreement with earlier studies (Frere *et al.*, 2006). In summary, the crystal structure is very similar to the ones previously obtained in our laboratory and co-crystallization of alaremycin in complex with PaPBGS was successful.

3.1.8.1 A Monovalent Cation in the Active Site

The crystal structure of PaPBGS in complex with alaremycin showed a monovalent cation in the active site which has been observed previously (Frere *et al.*, 2002). As depicted in Fig. 20, the monovalent sodium ion was located in the active site in a position where in a single case a divalent magnesium ion has been described (Frere *et al.*, 2006). Sodium is coordinated by three aspartates, Asp131, Asp139 and Asp176. Asp131 and Asp139 have been postulated to participate in the coordination of Mg^{2+} in the active site of Mg^{2+} dependent PBGS (Frankenberg *et al.*, 1999). Additionally, Asp139 has previously been shown to play an important role in the formation of a "closed" lid conformation shielding the active site from the surrounding medium (Frankenberg *et al.*, 1999, Frere *et al.*, 2002). The lid which covers the active site had, as mentioned previously, two different conformations in former studies: An ordered "closed" form including two α-helices in monomer A as well as a more unordered "open" form in monomer B. The importance of the lid region for the enzyme's catalytic function is reflected by the high degree of amino acid conservation for this part of the region in all known PBGSs (Frankenberg *et al.*, 1999). Surprisingly, this structure of PaPBGS in complex with alaremycin revealed an intermediate conformation for both monomers with a partly unordered lid in the region Ser220 – Asn227 resembling the situation in monomer B. The conformation of Asp139 pointing towards the active site resembles the one usually found in monomer A with the ordered lid (see Fig. 20). The adjacent loop regions (residues 134-149) are as well alike to monomer A.

The obtained results indicate that alaremycin binding to both monomers of the dimer fixes them in an intermediate state and prevents the formation for a completely closed conformation, however letting Asn139 already adopt a closed monomer conformation. Consequently, part of the lid which prevents solvent exposure during catalysis, remains in a partly unordered position, not fully developing the short α-helical structure typical for the ordered closed lid conformation (α-helix 8).

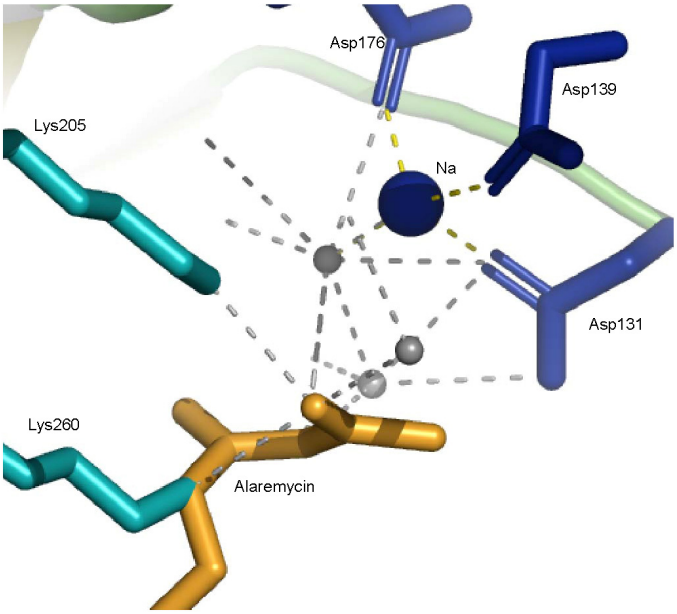

Fig. 20: Sodium binding site in the active centre of *P. aeruginosa* porphobilinogen synthase in complex with alaremycin.
Sodium (dark blue) is coordinated by three aspartates, Asp131, Asp139 and Asp176, depicted in blue. Alaremycin is depicted in orange, active site lysines in cyan. Waters are colored in grey. Ionic interactions of Na^+ are indicated in yellow, all other ionic interactions are shown in grey.

3.1.8.2 Binding of Alaremycin

In the obtained crystal structure, a single alaremycin was found to be located within the active site. This is in line with earlier findings for PBGS inhibitors co-crystallized in the active site cavity of PaPBGS (Frere *et al.*, 2006, Frere *et al.*, 2002). In these studies synthetic inhibitors were designed to investigate the enzymatic mechanism converting the two ALA substrates to porphobilinogen. Most of these inhibitors were found to bind to the active lysines *via* Schiff base formation.

Alaremycin is as well coordinated by the two active lysines (Lys205 and Lys260) in the active site, which usually coordinate the two ALA *via* Schiff base formation. Similarly, a Schiff base is formed between the amino group of the P-site lysine (Lys260) and C_4 of alaremycin. This coordination resembles the binding of the substrate ALA and is comparable to the conformation of the inhibitors levulinic acid and 5-fluorolevulinic acid in the active site cavity (Frankenberg *et al.*, 1999, Frere *et al.*, 2002). Due to a double bond within the inhibitor molecule, its conformation is rigid and stable in the active site (Fig. 21). Furthermore, this conformation is stabilized by two hydrogen bonds of the carboxyl-group of the antibiotic with Ser286. The same has previously been reported for a 5-hydroxylevulinic acid (5-OH-LA) molecule, a substrate analog, in the P-site of PaPBGS (Frere *et al.*, 2006). This indicates that alaremycin imitates the substrate ALA in the P-site rather than the product porphobilinogen. The second Schiff-base of the inhibitor with Lys205 in the A-site is not present. Instead a hydrogen-bridge is formed between the amino group of A-site lysine (Lys205) and the keto group of C_7 of alaremycin. This conformation is stabilized by hydrophilic interactions of the inhibitor with water molecules which in turn

interact with polar amino acids and the sodium ion, respectively. The part of the antibiotic which blocks the A-site of the active site reveals a similar conformation as previously observed for inhibitors mimicking the intermediate of the condensation reaction (Frere *et al.*, 2006).

Due to the crystal structure of PaPBGS in complex with alaremycin it is unambiguous that PaPBGS is indeed the molecular target of the antibiotic. The active site is efficiently blocked by an inhibitor in a rigid and stable conformation. Alaremycin displays the first natural antibiotic to be crystallized within the active site cavity of PBGS.

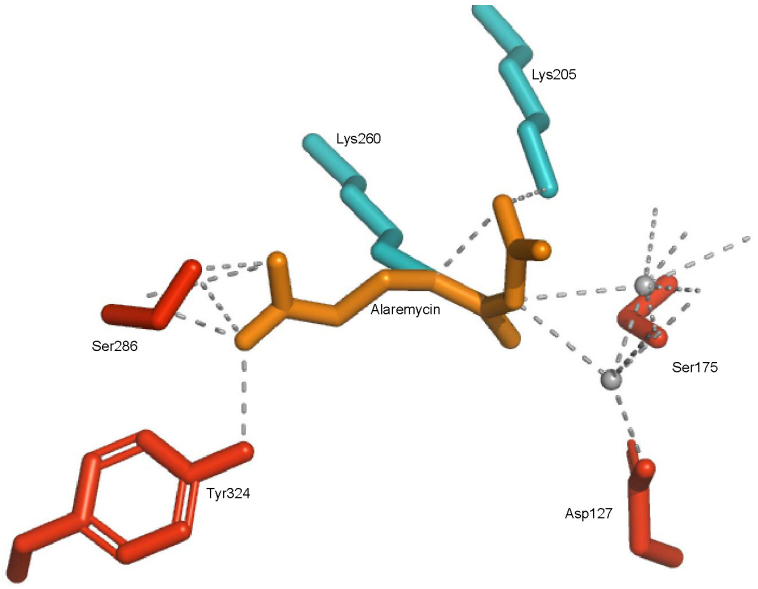

Fig. 21: The active site of *P. aeruginosa* porphobilinogen synthase in complex with alaremycin.
Labels are according to PaPBGS numbering. Lys205 and Lys260 are colored in cyan, alaremycin is colored in orange. Water molecules are depicted in grey. Surrounding residues are colored in red. Alaremycin is bound to Lys205 (A-site) and Lys260 *via* a hydrogen bond and a Schiff base, respectively. Ionic interactions are marked as grey dots.

3.1.9 Alaremycin Induces "Small Colony Variants" of *Staphylococcus aureus*

S. aureus strains deficient in heme biosynthesis have been isolated from persistent infections in humans. They revealed a significantly higher tolerance towards antibiotics and a reduced growth phenotype. So called "small colony variants" (SCV) lack a functional PBGS due to a mutation in the *hemB* gene or its promoter (von Eiff *et al.*, 2006). *S. aureus* strains with a genomic knockout of *hemB* have been chosen as model organism for genomic and proteomic investigations of SCV.

If alaremycin inhibits PBGS from *S. aureus* as seen for PBGS in cell free extracts, the induction of a SCV has to be expected. Therefore, investigations of growth phenotypes of *S. aureus* on solid media were carried out at 0 mM, 5 mM and at 10 mM alaremycin on LB-Agar media. *S. aureus* formed dwarf colonies (see Fig. 22) with 5 mM alaremycin and showed no growth at 10 mM alaremycin on solid media. The obtained results imply that alaremycin gives rise to an inducible *S. aureus* SCV phenotype. This observation may be suitable for a wide range of applications in *S. aureus* infection research. Currently, research is done with an irrevocable genomic *hemB* knockout. Nevertheless, further studies of

alaremycin antimicrobial activity, employing different *S. aureus* strains including the mentioned *S. aureus hemB*$^-$ strain and clinical isolates will give further insight into this feature.

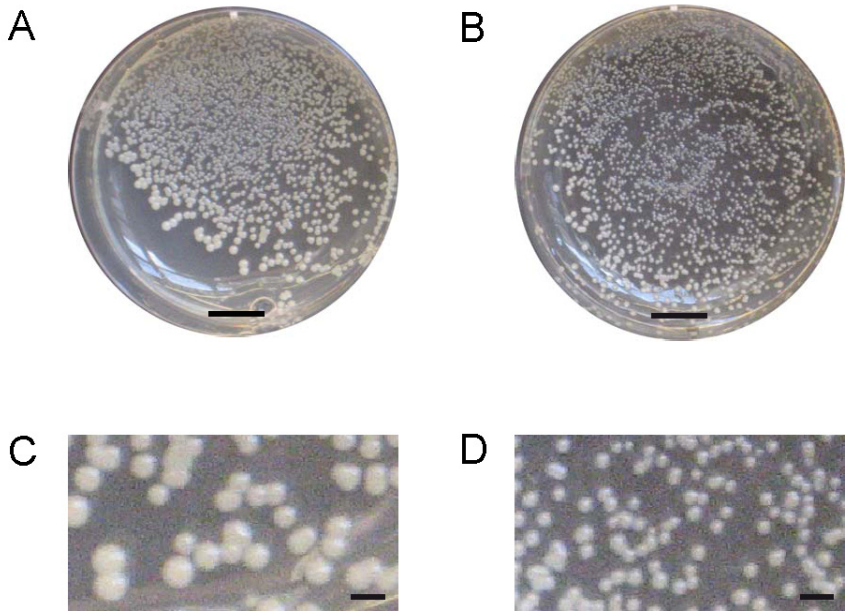

Fig. 22: *S. aureus* phenotypes with and without alaremycin treatment.
S. aureus was grown on solid LB-Agar for 20 h at 37°C and subjected to no (**A+C**) or 5 mM **(B+D)** alaremycin. At 5 mM of the antibiotic, the cells grew as dwarf colonies indistinguishable to the *S. aureus* SCV. **(A+B)** Scale bar = 1 cm; **(C+D)** Scale bar = 1 mm.

3.1.10 Conclusions from the Investigation of the Molecular Target of Alaremycin

It was shown in the framework of this thesis, that alaremycin, produced by *S. sp*. A012304, is a potent, broad spectrum antibiotic which exhibits its function *via* selective PBGS inactivation. The antibiotic was an inhibitor of recombinant purified PBGS from the bacterium *P. aeruginosa*, the archaeon *M. barkeri* and in higher concentrations also of the human enzyme.

Since the human enzyme also responded to alaremycin, it is most likely that alaremycin will not serve as a therapeutically relevant antibiotic. Furthermore, first experiments revealed cytotoxic effects on human cells at the alaremycin concentrations employed in this study (Masaaki Wachi, personal communication). Nevertheless, there are further possible applications for this natural inhibitor of heme biosynthesis. Even though alaremycin concentrations needed to be in a molar ratio, it may serve as a potent lead structure for the development of novel antibiotics targeted on heme biosynthesis. Furthermore, there is the perspective to identify a resistant PBGS from the producer strain *S. sp*. A012304. Since the *M. barkeri* enzyme was also inhibited, alaremycin may serve as a selective agent applicable in archaeal genetic systems. Today, there are only a few antibiotics available which are

appropriate as a selection marker in archaea. Another interesting feature of this antibiotic was the creation of inducible *S. aureus* SCV, which may lead to further applications in infection biology research. Until now, *S. aureus* strains carrying a permanent genomic knockout of *hemB* serve as model organism to mimic the highly infective SCV. An inducible SCV model may simplify research since it prevents problems associated with the slow growth of *S. aureus* SCV at early stages of an experiment.

3.2 Plant Uroporphyrinogen III Synthase

Enzymes of the tetrapyrrole biosynthesis pathways have been intensively studied over the past decades. Yet, the identity of the plant enzyme catalyzing the conversion of pre-uroporphyrinogen to uroporphyrinogen III has not been established *via* simple database miming. Therefore, the laboratory of Alison Smith, Cambridge, UK sought to identify the gene encoding *A. thaliana* UROS (AtUROS) *via* an approach using functional complementation of a corresponding yeast mutant (S150-2B::ΔHEM4) (Tan *et al.*, unpublished data). They identified an ORF encoding 321 amino acids which was furthermore able to complement an *E. coli hemD* mutant defective in UROS. The amino acid sequence of the ORF was used to query all GenBank, EMBL, DDBJ and PDB sequences in the databases with BLAST (Altschul *et al.*, 1997) on the NCBI server. This did not identify UROS genes described from other organisms. Comparison of the sequence of AtUROS with that of the human enzyme revealed conservation of the seven invariant residues identified for UROS, including three shown to be important for enzyme activity. Furthermore, a structure-based homology search of the protein data base with AtUROS identified the human crystal structure.

An N-terminal extension of about 81 residues was identified as a chloroplast targeting sequence with the precursor protein of M_r = 34,000 being targeted to the chloroplasts and processed to the mature size of 30,000 *in vivo*. For a final identification, it was essential to determine the enzymatic function for the recombinant protein. Therefore, the AtUROS was recombinantly produced, purified and tested for activity.

3.2.1 Purification of Putative *Arabidopsis thaliana* Uroporphyrinogen III Synthase

In the laboratory of Alison Smith genes for two protein variants of AtUROS have been constructed. Full length AtUROS was encoded by $pUROS_{full}$ and the mature form lacking

the 81 amino acid signal peptide was encoded by $pUROS_{mat}$, respectively. Recombinant full length and mature UROS were produced in *E. coli* BL21(DE3)RIL carrying the respective plasmids. The recombinant production of full length protein resulted in solely insoluble protein. Therefore, the truncated version was chosen for further studies. Recombinant putative mature *A. thaliana* UROS was produced in *E. coli* BL21(DE3)RIL and the resulting fusion protein was purified *via* Ni-NTA affinity chromatography. Recombinant protein eluted with 300 mM imidazole (Fig. 23, lane 4) and fractions containing recombinant AtUROS were combined and applied to a DEAE sepharose column at a concentration of 0.5 mg per mL column volume.

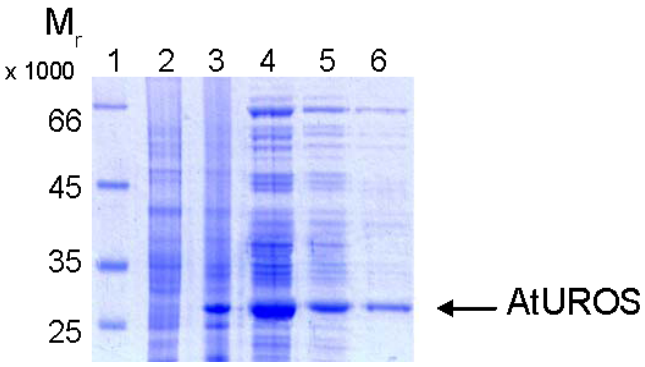

Fig. 23: Production and purification of recombinant *A. thaliana* uroporphyrinogen III synthase.

Proteins were separated by 12 % SDS -PAGE and visualized by staining with Coomassie Brilliant Blue. Lane 1: molecular weight marker; lane 2: total cellular extract without induction; lane 3: total cellular extract after overnight induction of gene expression with 100 µM IPTG; lane 4: eluate from the Ni-NTA column with imidazole; lane 5: eluate from DEAE sepharose column; lane 6: purified AtUROS after gel filtration.

Recombinant AtUROS was eluted with 200 mM NaCl and fractions were combined (Fig. 23, lane 5), concentrated and purified by gel permeation chromatography to apparent homogeneity. SDS-PAGE analysis of the purified protein (Fig. 23, lane 6) revealed a predominant protein band which corresponded to a protein with a relative molecular mass of about 30,000. Approximately one mg recombinant AtUROS per liter cell culture was obtained.

3.2.2 Determination of *Arabidopsis thaliana* Uroporphyrinogen III Synthase Activity

To determine enzymatic activity of AtUROS *in vitro*, a coupled enzyme activity test had to be established. The linear pre-uroporphyrinogen substrate of UROS is highly instable and spontaneously cyclizes to uroporphyrinogen I. Therefore, it is not commercially available. Consequently, pre-uroporphyrinogen was formed enzymatically from ALA using purified recombinant PaPBGS and *B. megaterium* PBGD. PaPBGS was purified as described before, purified *B. megaterium* PBGD was kindly provided by Claudia Schulz from our laboratory. Purified recombinant putative AtUROS was tested for UROS activity under assay conditions described in MATERIALS AND METHODS, using two different systems for

the detection of uroporphyrinogen III formation. Recombinant AtUROS was able to convert pre-uroporphyrinogen into uroporphyrinogen III as demonstrated by both fluorimetric and spectroscopic detection of the oxidized product uroporphyrin III in a coupled enzyme assay. Due to enzymatic conversion of ALA to uroporphyrinogen III, the absorbance at 408 nm for the oxidized reaction product uroporphyrin III increased over time (5 to 120 minutes) from 0.03 to 0.87. Furthermore, the amount of enzymatically formed uroporphyrinogen III was determined *via* fluorimetric detection of uroporphyrin III with fluorescence maxima at 600 nm and 620 nm (Fig. 24 A). Both applied methods revealed that the ORF identified by the laboratory of Alison Smith indeed encoded active *A. thaliana* UROS.

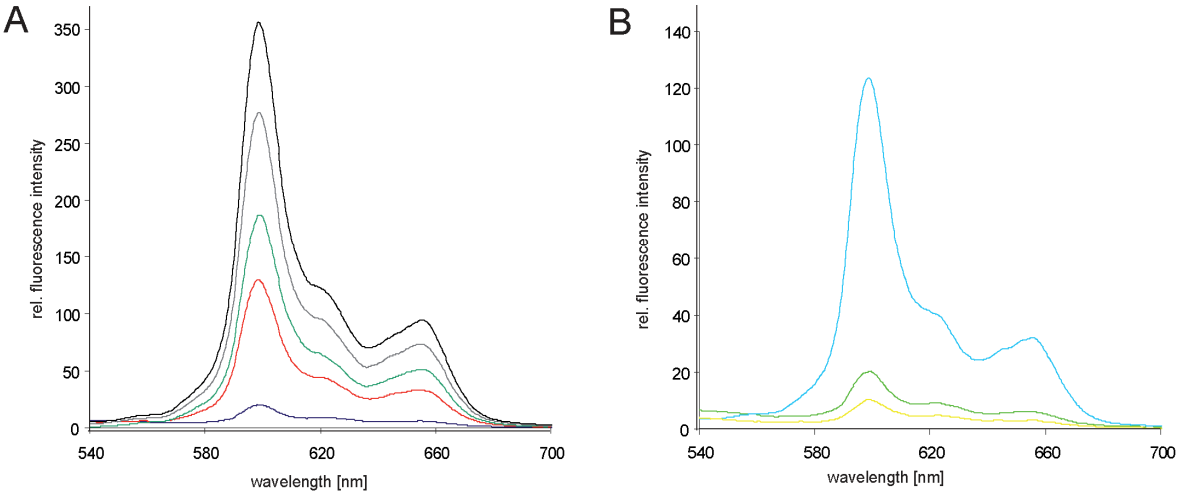

Fig. 24: Uroporphyrinogen III synthase activity assay for the recombinant purified *A. thaliana* enzyme. Assays were carried out as described in MATERIALS AND METHODS. The enzymatic activity of recombinant AtUROS was measured in a coupled enzyme activity assay with PBGS and PBGD, thus the conversion of ALA to uroporphyrinogen III. The amount of enzymatically formed uroporphyrinogen III was determined *via* fluorimetric detection of its oxidized form uroporphyrin III which has fluorescence maxima at 600 nm and 620 nm. Presented are the emission spectra from 540 to 700 nm with an excitation wavelength of 400 nm. **(A)** A standard enzyme activity assay was used, the reaction was carried out for 5 (—), 30 (—), 60 (—), 90 (—) and 120 (—) minutes at 37°C. Uroporphyrin III formation was increased over time. **(B)** A spectrum of commercially available uroporphyrin III (—) is depicted. A standard assay without (—) or with heat inactivated AtUROS (—) revealed no detectable uroporphyrin III formation.

Since all previously studied UROS were sensitive to heat denaturation, enzyme activity was evaluated after 2 minutes incubation at 60°C as described for the *E. coli* enzyme (Alwan *et al.*, 1989). The in this way treated purified recombinant enzyme revealed no residual activity as shown in Fig. 24 B. Heat-instability is also known from UROS human erythrocytes (Tsai *et al.*, 1987) which possesses almost identical properties. At room temperature AtUROS lost approximately 30 % of its activity over two hours, but was relatively stable at 4°C (60 - 80 % residual activity over night). Nevertheless, this feature in combination with the instability of the substrate pre-uroporphyrinogen and the resulting

necessity to employ a coupled enzyme activity assay complicated the determination of reliable kinetic parameters.

3.2.3 Subunit Structure of *Arabidopsis thaliana* Uroporphyrinogen III Synthase

During the purification of AtUROS, the last step involved gel filtration chromatography. By reference to the elution of molecular mass standards, the AtUROS was estimated to have a relative molecular mass of 62,000 ± 5,000, compared to the predicted mass of 29,994 Da for the monomeric protein with an N-terminal His_6-tag. All other analyzed UROSs from spinach, rat liver, *Euglena gracilis*, human erythrocytes and *E. coli* were found to be monomers (Shoolingin-Jordan, 1995). It is unlikely that the plant enzyme should behave differently. Rather, the unusual asymmetric shape of the protein, as seen in the crystal structure of the human enzyme (Mathews *et al.*, 2001), may well interfere with the gel filtration process.

3.2.4 Conclusions from Investigations of *Arabidopsis thaliana* Uroporphyrinogen III Synthase

Most of the genes encoding tetrapyrrole biosynthetic enzymes can be easily identified through amino acid sequence similarity searches using a known homolog. Many of the ubiquitous enzymes of heme synthesis have been identified this way (Hansson *et al.*, 1991). However, contrary to almost all the other enzymes of the pathway, UROS has very little sequence conservation between unrelated organisms. The complexity of the reaction performed by the UROS is not reflected in the primary structure of the enzyme. It is possible that the enzymatic conformation of UROS may require the conservation of only a few residues, while the rest are under little or no selection pressure, leading to the primary sequence divergence of homologs found in different organisms. Hence, for this unique enzyme, a conserved tertiary structure may play a more important role for its catalytic properties.

With the obtained results it was now possible to confirm the identity of *A. thaliana* UROS which led to identification of further putative plant UROS encoding ORFs from rice, wheat and the green algae *Ostreococcus lucimarinus* and *Ostreococcus tauri via* BLAST searching. These proteins were all very similar to one another (about 50 % identity) suggesting that they have diverged from the UROSs found in other kingdoms early on in evolution. The plant enzymes shared 26 % identity with that from cyanobacteria. In summary, with the obtained results it was possible to clearly identify the first gene encoding

a plant UROS, which is the first step towards a closer biochemical and structural investigation.

3.3 Investigation of the Substrate Binding Site of Tobacco Protoporphyrinogen IX Oxidase

The penultimate step of heme biosynthesis is the conversion of protoporphyrinogen IX to protoporphyrin IX. This six electron oxidation is catalyzed by PPO which in eukaryotes is a flavin-containing, oxygen-dependent protein. A mutation in the corresponding gene in humans may result in defective PPO, which leads to a disease commonly known as variegate porphyria (VP). Manifestations of VP may include cutaneous photosensitivity and systemic symptoms arising from neurologic dysfunction. In contrast, the inhibition of PPO is deliberately induced in plant treatment by substrate analogs such as diphenylether herbicides.

The crystal structure of tobacco enzyme was solved in 2004 by Koch and coworkers (Koch *et al.*, 2004) and represented the first structural information available for proto-porphyrinogen IX oxidases. This raised the possibility to determine the structural basis for substrate binding, herbicidal mode of action and the human disease VP. The NtPPO2 structure in complex with the inhibitor 4-bromo-3-(50-carboxy-40-chloro-20-fluoro-phenyl)-1-methyl-5-trifluoro-methyl-pyrazol revealed that its active site is located between the FAD- and the substrate-binding domain. The inhibitor represents ring A and B of the tetrapyrrole substrate. In Fig. 25 the modeling of the substrate protoporphyrinogen IX into the active site is depicted. Modeling was kindly performed by Michael Koch, Laboratoire de Biologie et de Génomique Structurales, Cedex, France. The substrate-binding site beneath the FAD is a flat cavity that is formed by a number of aromatic and aliphatic amino acids as well as by Asn67 and Arg98 (Koch *et al.*, 2004). Based on a model that was calculated from the solved crystal structure of NtPPO2, it was deduced *in silico* that amino acid residues Arg98, Leu356, Leu372 and Phe392 play a central role in substrate coordination.

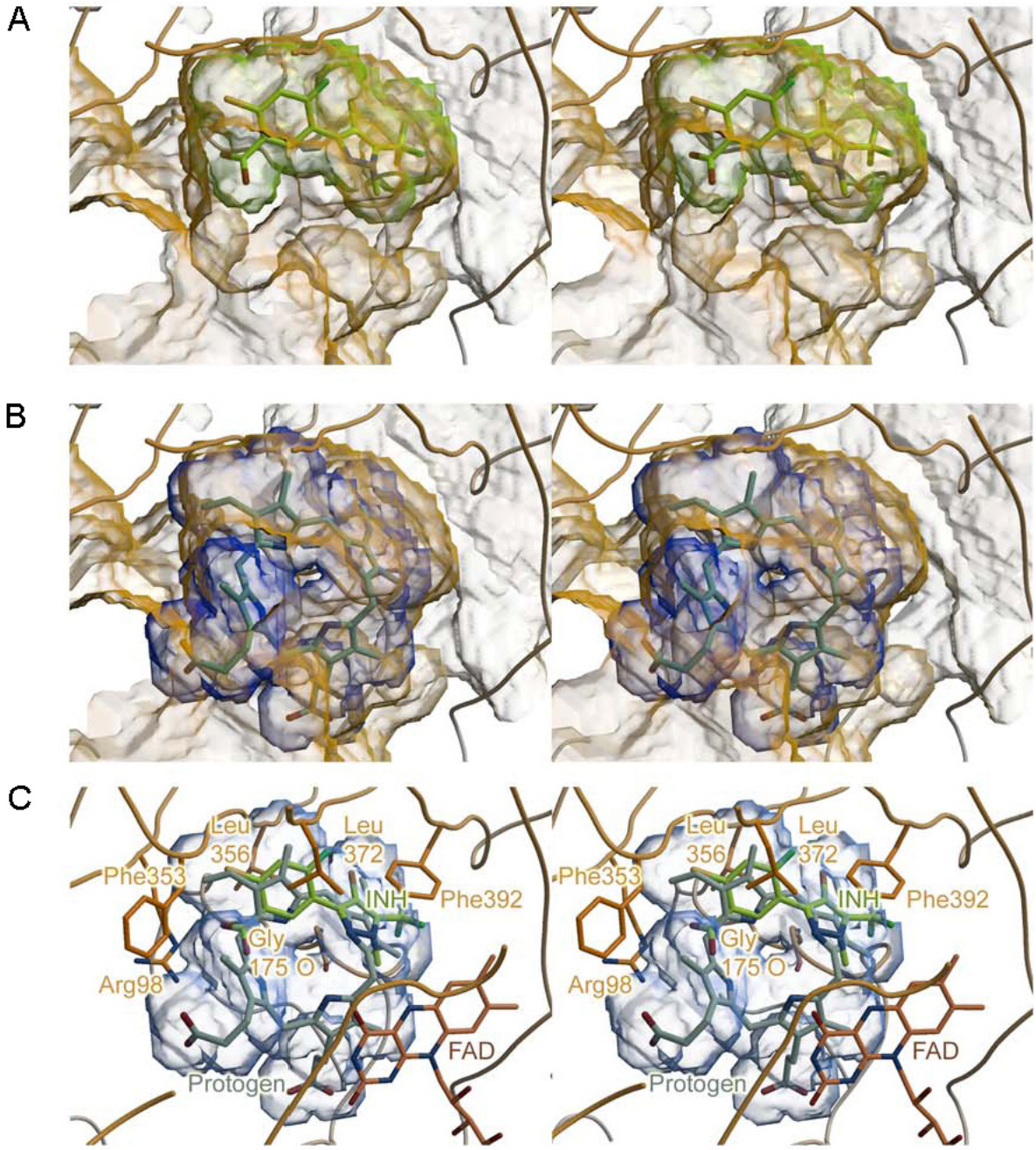

Fig. 25: Modeling of the substrate protoporphyrinogen IX into the binding pocket of tobacco mitochondrial protoporphyrinogen IX oxidase.

(A) The inhibitor (green) is shown surrounded by its molecular surface (green) in the active site of NtPPO2 (surface of NtPPO2 depicted in orange). **(B)** The position of the substrate protoporphyrinogen IX (grey) shown inside its molecular surface (blue) is illustrated in its good fitting into the active site cavity of NtPPO2 (orange). **(C)** The active site residues and the FAD of NtPPO2 are depicted around the bound inhibitor (green) and the modeled substrate, protoporphyrinogen IX (grey) in the shape of the substrate surface (blue).

In animal PPOs including human PPO, the conserved Arg59 plays an important catalytic role. In 94 % of the cases in South Africa, the human disease VP is caused by a single mutation of Arg59 to tryptophan. In the structure of NtPPO2, Ser374 that is conserved between various plant species is in a position opposite to Asn67. The corresponding residue

in animal PPOs is the conserved Asp349 that is likely to form a salt bridge with Arg59. The disruption of this salt bridge may play a central role in the human disease. Nevertheless, none of these assumptions deduced from the crystal structure have been proven experimentally so far. To further investigate these features of NtPPO2, the enzyme and respective mutants were recombinantly produced, purified and kinetically characterized.

3.3.1 Purification and Biochemical Characterization of Tobacco Protoporphyrinogen IX Oxidase

Recombinant NtPPO2 was produced using *E. coli* strain BL21(DE3)RIL as outlined in MATERIALS AND METHODS. The resulting fusion protein was purified *via* affinity chromatography on a Ni-IDA resin. Recombinant NtPPO2 eluted with 500 mM imidazole (Fig. 26, lane 4). SDS-PAGE analysis of the purified protein revealed a predominant protein band which corresponded to a protein with a relative molecular mass of about 68,000, which is in good agreement with the calculated molecular mass of the fusion protein of 70,670 Da. Only about 0.5 mg recombinant NtPPO2 per liter cell culture were obtained. Most of the recombinant protein was found insoluble.

The PPO activity assay was carried out under standard conditions *via* detection of the fluorescence of the reaction product protoporphyrin IX. The enzymatic reaction was, as expected, oxygen-dependent.

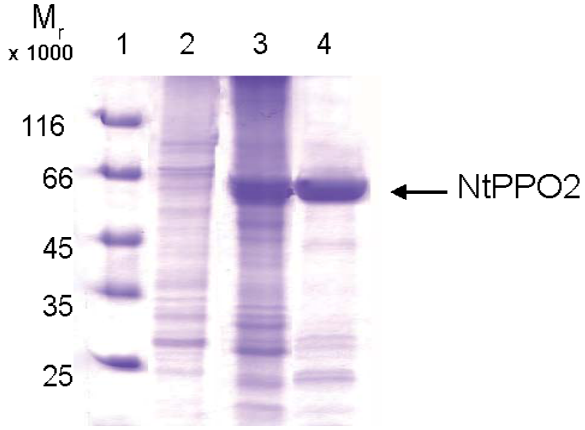

Fig. 26: Recombinant production and affinity chromatography purification of *N. tabacum* protoporphyrinogen IX oxidase.
Proteins were separated by 12 % SDS-PAGE as described in MATERIALS AND METHODS and visualized by staining with Coomassie Brilliant Blue. Lane 1: molecular weight marker; lane 2: total cell extract made from culture without induction of gene expression; lane 3: total cell extract after overnight induction of gene expression with 250 µM IPTG; lane 4: eluate from the Ni-IDA resin with 500 mM imidazole.

Under anaerobic conditions no noteworthy amount of protoporphyrin IX was formed (data not shown). The Michaelis Menten constant (K_M), the maximal velocity v_{max} and the catalytic constant k_{cat} were determined from substrate velocity plots by measuring the constant velocity formation of protoporphyrin IX from protoporphyrinogen IX over a substrate range from 1 - 25 µM and a time course of up to 2 hours at 20°C. Values were determined by the computerized Lineveaver Burk iterative curve fitting (SigmaPlot 8.0, Enzyme Kinetics modulev1.1). The FAD content of wildtype and mutant NtPPO2 were

determined spectroscopically. The apparent K_M value of purified wildtype NtPPO2 protein for its substrate was 1.17 µM with a k_{cat} value of 6.0 s^{-1}. The determined kinetic parameters were within the range of values measured for PPOs from other organisms, *e.g.* K_M = 1.0 µM, k_{cat} = 0.0031 s^{-1} for *B. subtilis* (Corrigall *et al.*, 1998), K_M = 0.1 µM for *S. cerevisiae* (Camadro *et al.*, 1994), K_M = 2.8 µM for *A. aeolicus*, (Wang *et al.*, 2001) and K_M = 0.85 µM and for *H. sapiens* either a k_{cat} = 0.175 s^{-1} (Dailey and Dailey, 1996) or a k_{cat} = 5.95 s^{-1} (Maneli *et al.*, 2003), respectively. The FAD content of wildtype NtPPO2 was measured as described in MATERIALS AND METHODS and was 0.63 moles FAD/subunit NtPPO2. The incomplete saturation of NtPPO2 with FAD was in agreement with earlier findings of Dailey and coworkers who determined 0.4 - 0.5 FAD/subunit in *M. xanthus* (Dailey and Dailey, 1996).

3.3.2 Functional Investigation of the Substrate Binding Site of Protoporphyrinogen IX Oxidase

The crystal structure of NtPPO2 revealed a close insight into the three-dimensional structure of the enzyme. The substrate protoporphyrinogen IX was modeled into the active site and is outlined in Fig. 27. Residues Arg98, Phe392, Leu372 and Leu356 coordinate the inhibitor 4-bromo-3-(50-carboxy-40-chloro-20-fluoro-phenyl)-1-methyl-5-trifluoromethyl-pyrazol, which was co-crystallized within the active site of NtPPO2. These four amino acid residues were found highly conserved throughout the PPO family of proteins. Ring A is coordinated *via* aromatic stacking with Phe392 (Fig. 27) (Koch *et al.*, 2004).

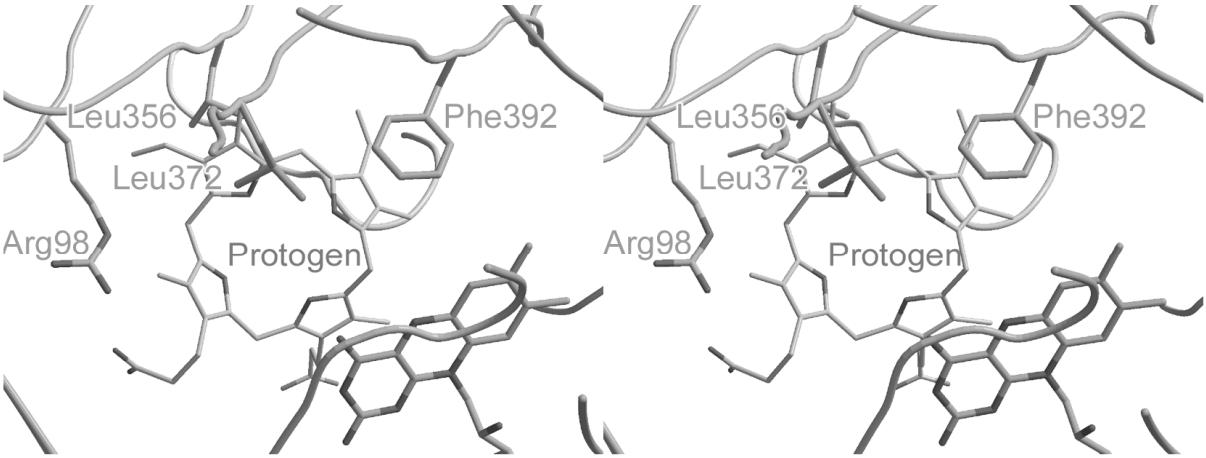

Fig 27: Active site of tobacco PPO2 with the modeled substrate protoporphyrinogen IX.
Depicted are the investigated amino acid residues Arg98, Leu356, Leu372 and Phe392. Phe392 is shown to coordinate ring A of the protoporphyrinogen IX. Leu356 and Leu372 stack protoporphyrinogen IX ring B from the "back" and the "front", Arg98 is supposed to coordinate the propionate carboxylate group of the protoporphyrinogen IX ring C, respectively (Heinemann *et al.*, 2007).

The side chains of Leu356 and Leu372 interact hydrophobically with ring B. The side chain of residue Arg98 forms a salt bridge to the propionate carboxyl group of ring C, which additionally might be stabilized by flipping and subsequent stacking of the conserved residue Phe392. The dome conformation of the substrate is probably stabilized by the carbonyl oxygen of the highly conserved Gly175.

3.3.2.1 Mutagenesis of the Amino Acid Residues Arg98, Leu356, Leu372 and Phe392

According to the crystal structure of NtPPO2 and the deduced model for substrate binding, the highly conserved residues Arg98, Leu356, Leu372 and Phe392 are suspected to be involved in substrate coordination. In order to evaluate their chemical contribution to substrate binding and catalysis, a strategy of introducing conservative and non-conservative amino acid exchanges for these residues was applied and single amino acid exchanges were conducted. Phe392 is involved in the coordination of substrate ring A and was replaced by histidine and glutamate, respectively. Residues Leu356 and Leu372, which coordinate substrate ring B *via* hydrophobic interactions, were replaced by valine and asparagine, respectively. Residue Arg98 forms a salt bridge to the propionate carboxyl group of ring C and was replaced by alanine, lysine and glutamate, respectively. The mutated enzyme variants were produced in *E. coli* BL21(DE3)RIL and purified to apparent homogeneity under conditions identical to those established for the wild type enzyme. All mutant proteins were analyzed for their FAD content and their overall PPO activity.

3.3.2.2 Catalytic Activity and FAD Content of Active Site Mutants from Tobacco Protoporphyrinogen IX Oxidase

For all recombinant mutant proteins kinetic parameters and the FAD content were determined as described for the wildtype enzyme and are listed in Tab. 11.

Ring A. The crystal structure and the respective modeling revealed that ring A of the substrate is kept in position by aromatic stacking with residue Phe392, which stabilizes the electron transfer over the ring during the reaction. An amino acid exchange to Glu392 in the variant F392E was tolerated within the active site cavity and resulted in inferior binding of the substrate protoporphyrinogen IX (K_M = 11.2 µM). However, once the substrate was bound, its conversion was catalyzed sufficiently (k_{cat} = 11 s^{-1}).

Tab. 11: Kinetic parameters of wildtype tobacco protoporphyrinogen IX Oxidase and corresponding active site mutants.

The Michaelis Menten constant K_M, the k_{cat} and the k_{cat}/K_M values for wildtype and mutant NtPPO2 were determined from substrate velocity plots by measuring the constant velocity formation of protoporphyrin IX from protoporphyrinogen IX over a substrate range from 1-25 µM. The FAD content was calculated using commercially obtained FAD. The standard deviation of the shown results was between 5 and 10 %.

Protein variant	K_M [µM]	k_{cat} [s^{-1}]	k_{cat}/K_M [$\mu M^{-1}s^{-1}$]	FAD content [mol/subunit]
Wildtype	1.17	6	5.1	0.63
Substrate binding ring A				
F392H	n.d.	n.d.	n.d.	0.58
F392E	11.2	11	1.0	0.60
Substrate binding ring B				
L356N	11	38	3.4	0.55
L356V	7.3	300	41.1	0.62
L372N	16.4	7	0.4	0.60
L372V	103	597	5.8	0.53
Substrate binding ring C				
R98K	2.6	37	14.4	0.50
R98E	12.5	34	2.7	0.51
R98A	8.3	365	44	0.57

n.d. not detectable

The tetrapyrrole ring is made positive by the hydride abstraction at the N_5 atom of FAD. Thus the negative charge of the introduced glutamate might stabilize the ring and catalysis may proceed equally fast. In this case only the stabilization of the substrate by aromaticity is lowered and as a result its binding is weaker. Additionally, the NtPPO2 variant F392H was found to be virtually inactive. Determination of reliable kinetic parameters was not possible. Histidine at a pH below its p_K at 6.1 is positively charged. Here at pH 6.0, this held true for most histidine molecules of NtPPO2. The positive charge of the histidine ring at this position lead to repulsion and obstructed substrate binding, consequently reaction kinetics collapsed. Detailed kinetic parameters of the mutant proteins are listed in Tab. 11.

Ring B. In the model for substrate binding deduced from the NtPPO2-inhibitor crystal structure, ring B of protoporphyrinogen IX is sandwiched between the conserved residues Leu356 and Leu372. Both amino acid residues were exchanged to either valine or asparagine, respectively. In both cases the conservative amino acid exchange to valine enhanced catalysis up to 100-fold (k_{cat} = 300 s^{-1} and k_{cat} = 597 s^{-1}, respectively). However, by exchange of the amino acid Leu372 to valine, binding of the substrate protoporphyrinogen IX was reduced 100-fold (K_M = 103 µM). In contrast, the NtPPO2 variants L356N and L372N showed a slightly inferior binding capacity, only, compared to

the wildtype and revealed comparable catalytic activities (see Tab. 11). Valine possesses comparable hydrophobic features to leucine. However, the carbon backbone of the side chain is shorter than that of leucine. Probably the appropriate location of the hydrophobic residue in relation to the coordinated substrate ring is essential, explaining the increasing K_M values of L356V and especially L372V. Once the substrate was bound, catalysis was found enhanced for both mutants. Most likely the smaller side chain of valine better accommodated the necessary complex arrangement of the substrate during catalysis. On the other hand, asparagine obviously provided the necessary side-chain length and chemical character to supplement for leucine in both positions.

Ring C. The next investigated amino acid residue potentially involved in substrate binding was Arg98. It was deduced from the NtPPO2 crystal structure that Arg98 provides the counter charge for the carboxylate group of the inhibitor which most likely mimics the propionate group of ring C of protoporphyrinogen IX. The NtPPO2 variants R98K, R98E and R98A were chosen to evaluate the contribution of this positively charged amino acid. While the conservative exchange R98K improved enzyme activity (k_{cat} = 37 s^{-1}), the non-conservative exchange R98E resulted in inferior substrate binding (K_M = 12.5 μM). Thus, the introduced negative charge could prohibit the ionic interaction necessary for the stabilization of ring C. In agreement with this assumption, the replacement of Arg98 with the non polar amino acid alanine resulted in an enzyme variant (R98A) with an eight-fold increased K_M value. Interestingly, all three variants in position 98 showed an increased k_{cat} value, especially variant R98A (k_{cat} = 309 s^{-1}), indicating improved turnover in the absence of ionic interactions between enzyme and substrate. Nevertheless, the overall response of NtPPO2 towards the introduced amino acid exchanges in position 98 was nicely reflected by the k_{cat} and K_M values.

The FAD content of all mutant enzymes was quite similar and thus the introduced amino acid exchanges do not seem to have an impact on FAD binding.

3.3.2.3 Conclusions from the Active Site Mutagenesis Studies

The obtained results for mutants of amino acids residues from NtPPO2 located close to the modeled substrate strongly implied that the well conserved amino acid residues Arg98, Phe392, Leu356 and Leu372 were indeed functionally involved in substrate coordination within the active site. Most likely all four rings of the protoporphyrinogen IX substrate of NtPPO2 were coordinated during substrate binding by NtPPO2. Ring A was stacked by Phe392, ring B was sandwiched in between Leu356 and Leu372 and the propionate

carboxylate of ring C was bound to Arg98. Moreover, ring D might have been stacked against the A ring of the isoalloxazine moiety of the FAD. Most of the generated NtPPO2 variants were characterized by an increase in K_M and k_{cat} values. Nevertheless, it was surprising to find that some amino acid exchanges even enhanced catalysis, even though most mutations resulted in a decrease of substrate affinity. Furthermore, a misplaced substrate did not have a prominent effect on FAD binding, since the FAD content was rather unaffected. One may conclude that NtPPO2 was optimized during evolution rather towards a stringent substrate recognition and discrimination than towards catalytic turnover.

3.3.3 Investigation of Amino Acid Residues Involved in Variegate Porphyria

The dominantly inherited genetic disorder VP in humans results from impaired PPO activity as a consequence of an amino acid residue exchange. In more than 94 % of the VP cases in South Africa, Arg59 is mutated to tryptophan (Meissner *et al.*, 1996). The corresponding residue to human Arg59 in the NtPPO2 is Asn67. It is positioned on a long loop between a β-strand and an α-helix between the FAD binding and substrate-binding sites (Fig. 28). The residue is conserved in all known mitochondrial and plastidic plant PPO amino acid sequences. However, in the NtPPO2 crystal structure Ser374 is the residue opposite to Asn67. The corresponding residue in human PPO is Asp349 conserved in all known animal PPOs as well. Asp349 is likely to form a salt bridge with Arg59, which would sterically fit in this area of the protein (Koch *et al.*, 2004).

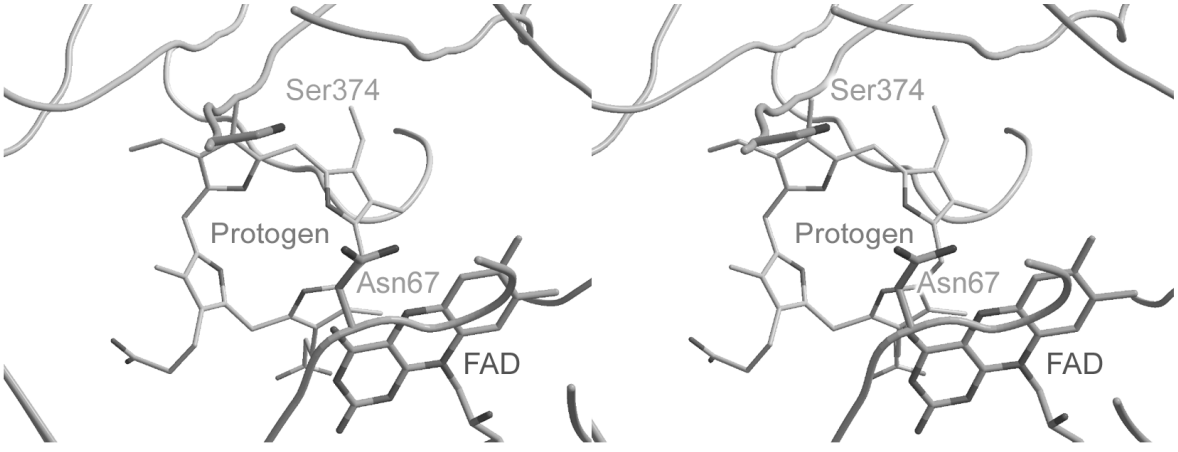

Fig. 28: Residues involved in human variegate porphyria assigned to tobacco protoporphyrinogen IX oxidase.

In the human enzyme a mutation of Arg59 to tryptophan is the main cause for VP. The corresponding amino acid residue in the tobacco enzyme is Asn67, which forms a salt bridge to Ser374. Depicted amino acid residues Asn67 and Ser374 are located in close proximity to the modeled substrate protoporphyrinogen IX (Heinemann *et al.*, 2007).

3.3.3.1 Mutagenesis of the Residues Asn67 and Ser374

Since the corresponding residue to Arg59 in the human enzyme is Asn67 in the tobacco enzyme, the protein was first mutated to resemble the human variant and further adapted to the disease causing situation. Furthermore, the tobacco enzyme was adapted towards its human counterpart by the introduction of a salt bridge to Ser374. The mutant enzymes were produced in *E. coli* BL21(DE3)RIL and purified to apparent homogeneity under conditions identical to those established for the wildtype enzyme (see MATERIALS AND METHODS).

3.3.3.2 Catalytic Activity and FAD Content of Variegate Porphyria Mutants from Tobacco Protoporphyrinogen IX Oxidase

All mutant proteins were analyzed for their FAD content and their overall PPO activity. Obtained results are listed in Tab. 12. In order to mimic the human enzymes situation on the basis of the related NtPPO2 crystal structure, Asn67 was mutated to arginine. The obtained mutant N67R was found to be reasonably active. Even though the mutation resulted in inferior substrate binding, the catalytic efficiency was acceptable (see Tab. 12 for detailed kinetic parameters). This observation was in agreement with the findings of Maneli and coworkers (Maneli *et al.*, 2003) who underlined the importance of a hydrophilic, favorably positively charged amino acid at position Arg59 in the human enzyme. Replacing Asn67 by tryptophan abolished enzyme activity. The bulky nature of an aromatic tryptophan in position Asn67 resulted in impaired enzyme activity. Thus, the enzymatic defect responsible for most VP cases in humans can be transferred onto NtPPO2 and the spatial structure of NtPPO2 can be used as a model for human PPO.

In order to further adapt NtPPO2 towards the human counterpart, Ser374 was mutated to aspartate. The S374D single mutant showed reduced substrate binding capacity with a significantly increased k_{cat} value (k_{cat} = 208 s^{-1}). Subsequently, Asn67 of protein variant S374D was mutated to arginine to reconstruct the assumed salt bridge Asp374/Arg67 in the human enzyme for our tobacco VP model. The resulting N67R/S374D double mutant showed an almost wildtype level K_M value (K_M =1.4 µM). Thus, this NtPPO2 variant had almost wildtype like substrate recognition and even improved catalytic properties (k_{cat} = 111 s^{-1}) caused by a reconstruction of the salt bridge in the tobacco enzyme. These results argue for the existence of a salt bridge linking Arg59 and Asp349 in the human enzyme as well.

Tab. 12: Kinetic parameters and FAD content of tobacco protoporphyrinogen IX oxidase mutant enzymes reflecting the variegate porphyria genotype.

The Michaelis Menten constant K_M, the k_{cat} and the k_{cat}/K_M values for wildtype and mutant NtPPO2 were determined from substrate velocity plots by measuring the constant velocity formation of protoporphyrin IX from protoporphyrinogen IX over a substrate range from 1 - 25 µM. Values were determined by the computerized Lineveaver Burk iterative curve fitting (SigmaPlot 8.0 Enzyme Kinetics module v1.1). The FAD content of wildtype and mutant NtPPO2 was determined spectroscopically. The FAD content was calculated using commercially obtained FAD. The standard deviation of the shown results was between 5 and 10 %.

Protein variant	K_M [µM]	k_{cat} [s^{-1}]	k_{cat}/K_M [$\mu M^{-1}s^{-1}$]	FAD content [mol/subunit]
Wildtype	1.17	6	5.1	0.63
S374D	10.9	208	18.5	0.55
N67R	97.0	97	1.0	0.61
N67W	n.d.	n.d.	n.d.	0.48
N67R/S374D ("human PPO")	1.4	111	79.4	0.65
N67W/S374D ("human VP")	21.0	12	0.57	0.38

n.d. not detectable

The double mutation N67W/S374D, mimicking VP in the human enzyme significantly reduced enzyme activity. The K_M value was 20-fold increased while the k_{cat}/K_M value decreased 10-fold. Obviously, the also reduced FAD content of 0.38 moles FAD/subunit for NtPPO2 variant N67W/S473D, representing approximately 60 % of the wildtype enzyme content, did not account for the observed decrease in enzyme activity. Similar observations were made for the human R59W mutant enzyme before (Maneli *et al.*, 2003). In contrast to most other generated mutant enzymes this NtPPO2 variant showed an increased K_M with a parallel decreased k_{cat} compared to the double mutant N67R/S374D. Both amino acids neighboring Asp349 (Ser374 in NtPPO2) in the human enzyme have previously been characterized. A mutation of tryptophan in position 348 of the human enzyme to cysteine resulted in a wildtype-like K_M value and a tenfold reduced k_{cat} (Maneli *et al.*, 2003). A mutation of Ser350 to proline in the human enzyme abolished enzyme activity (Roberts *et al.*, 1998). These observations underscore that the structural integrity of this region is important for enzyme activity.

3.3.3.3 Conclusions from Mutagenesis Studies of Amino Acid Residues Involved in Variegate Porphyria

The results showed that the enzymatic defect responsible for causing VP in humans can be mimicked with the NtPPO2 model. Therefore, NtPPO2 represents a useful model system for the understanding of the structure-function relationship underlying detrimental human enzyme defects.

3.4 Investigation of a Proposed Alternate Heme Biosynthesis Pathway in *Methanosarcina barkeri*

In the majority of prokaryotes not all genes required for heme biosynthesis have been identified. A database search performed in 2002 considered all 69 prokaryotes of which the entire genome had been sequenced at that date (Panek and O'Brian, 2002). This approach revealed that in about two-thirds of the genomes one or several genes of the heme biosynthetic pathway were missing. In the genomes of several heme synthesizing archaea only the genes required for uroporphyrinogen III formation were detected. This raises the possibility of an alternative pathway for the remaining steps. It has been shown earlier that *D. vulgaris* utilizes a pathway for heme biosynthesis which differs from the well investigated one (Ishida *et al.*, 1998). In *D. vulgaris* the pathway for heme biosynthesis branches from the common pathway after uroporphyrinogen III formation, which is converted into precorrin-2 *via* two methylation reactions utilizing SAM. Next, precorrin-2 is converted to 12,18-(didecarboxy)-precorrin-2 which is afterwards deacylated to coproporphyrinogen III. At this point the alternate route for *D. vulgaris* was proposed to reenter the common pathway. However, this last step is improbable to occur in archaea since the genes for the enzymes necessary for the reactions from coproporphyrinogen III to heme have not been found in the respective genomes. A possible alternate route would be the oxidation of coproporphyrinogen III to coproporphyrin III which is than decarboxylated to protoporphyrin IX. Iron chelation may either be the last step in this pathway or may occur at an earlier time point.

Since the late heme biosynthesis genes are missing in the genomes of *M. barkeri, Methanosarcina acetivorans* (Galagan *et al.*, 2002) and *Methanosarcina mazei* (Deppenmeier *et al.*, 2002), we chose *M. barkeri* for further studies. *M. barkeri* is a strictly anaerobic methanogenic archaeon that is able to grow on H_2 and CO_2, acetate, methylamines or methanol as sole carbon and energy sources. It is a member of the order *Methanosarcinales,* which are all known to contain cytochromes *b* and *c* and other proteins with protoheme derived prosthetic groups (Kamlage and Blaut, 1992, Kuhn and Gottschalk, 1983). The organism also contains the nickel tetrapyrrole coenzyme F_{430} (Diekert *et al.*, 1981) and the cobalt tetrapyrrole hydroxybenzimidazolyl cobamide, which is a vitamin B_{12} homolog (Thauer and Sauer, 1999). These tetrapyrroles are involved in different steps of methanogenesis and thus absolutely essential for the organism. *M. barkeri* in low salt media grows in clusters of 8-32 cells (see Fig. 29). If the above outlined pathway applies to archaea, protoheme should similarly be synthesized from precorrin-2 in the heme forming

methanogenic archaeon *M. barkeri* and should involve the SAM-dependent methylation of uroporphyrinogen III. In the common pathway no such methylation step occurs.

Fig. 29: Phenotype of *M. barkeri* in low salt media.
Cells were grown in low salt media under strictly anaerobic conditions at 37°C for 3 days. Scale bar = 5 µm. Micrographs of fixed cells stained with SYBR Green II were kindly taken by Sebastian Hannemann from the group of Oliver Fackler, Hygiene Institute, University Hospital, Heidelberg.

Two different approaches were used in order to identify the possible alternative heme biosynthetic pathway. The in *vivo* approach included the incorporation of labeled precursors such as SAM to follow the possible methylation steps during heme biosynthesis. Furthermore an *in silico* approach was employed using comparative genomics to identify enzymes potentially involved in alternative heme biosynthesis.

3.4.1 First Steps Towards an Alternative Pathway

A first step in the investigation of the unknown pathway in *M. barkeri* was to determine the fate of uroporphyrinogen III. *In vivo* integration of methyl groups from SAM in uroporphyrinogen III with the formation of precorrin-2 and its subsequent conversion into heme was probed. The use of [^{14}C] labeled and deuterated transferable methyl groups should allow for mass spectrometry identification of SAM-derived methyl groups in heme. Isolated heme carrying [^{14}C] labeled or deuterated methyl groups should be identified by the mass increase compared to regular heme.

First experiments revealed that *M. barkeri* was not able to take up radioactively labeled [^{14}C]-SAM from the media in sufficient amounts. Cells were grown in the presence of 0.1 µCi [^{14}C]-SAM per mL cell culture for 2 - 72 hours, harvested and washed twice with media. The ^{14}C-content of the cells was measured with a scintillation counter as described under MATERIALS AND METHODS. Less than 0.5 % of the added radioactivity was recovered from the cells. In contrast, [^{14}C]-methionine uptake was rather efficient, as up to 17.5 % of the deployed ^{14}C was found within the cells after 72 hours at the end of the exponential growth phase. Therefore, the methanogenic archaeon was grown on methanol in the absence and presence of *L*-[*methyl*-D_3]methionine, which is better applicable for MALDI-TOF determination due to its additional mass when incorporated into heme.

Methionine is a precursor of SAM, an incorporation of methyl-groups derived from SAM into protoheme should consequently result in the introduction of labeled methyl-groups. At the end of the exponential growth phase, cells were harvested and non-covalently bound protoheme was extracted from *M. barkeri* as described in MATERIALS AND METHODS. Coenzyme F_{430} is known to contain two methyl groups (Jaenchen *et al.*, 1981) and vitamin B_{12} seven methyl groups, all derived from *S*-adenosyl-*L*-methionine (Warren *et al.*, 2002). These cofactors were analyzed as controls. The mass spectra were collected by Jörg Kahnt and Bärbel Buchenau from the laboratory of Rolf Thauer, Max-Planck-Institute for Terrestrial Microbiology, Marburg. Mass spectra of commercially obtained protoheme, of heme extracted from unlabeled cells and of heme extracted from cells grown in the presence of 2 mM, 5 mM and 10 mM labeled *L*-[*methyl*-D_3]methionine, respectively, are shown in Fig. 30.

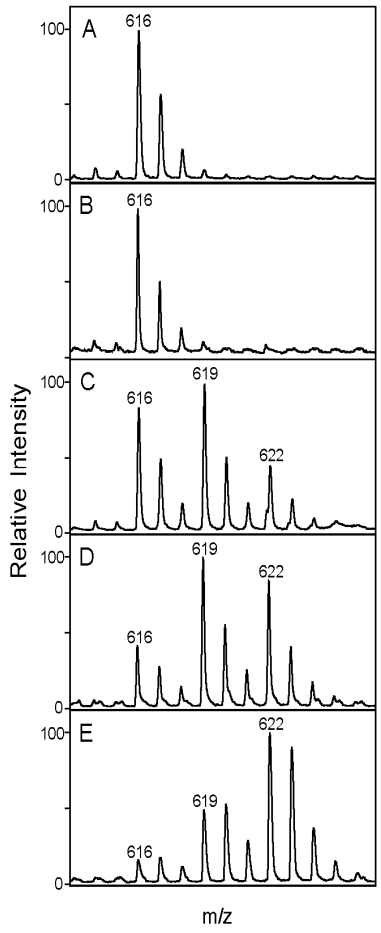

Fig. 30: MALDI-TOF mass spectra of heme extracted from *M. barkeri.*

(A) protoheme, **(B)** heme extracted from *M. barkeri* cells grown in the absence of *L*-[*methyl*-D_3]methionine and **(C)** heme extracted from *M. barkeri* cells grown in the presence of 2 mM, **(D)** 5 mM and **(E)** 10 mM *L*-[*methyl*-D_3]methionine.

The mass spectra of commercially obtained protoheme (Fig. 30 A) and of heme extracted from the unlabeled cells (Fig. 30 B) were found to be almost identical. The highest peak representing a mass of 616 Da corresponds to the mass of protoheme composed of only ^{12}C, ^{14}N and ^{56}Fe. The other peaks with masses of 614, 615, 617, 618, 619 and 620 Da reflect the

natural abundance of ^{13}C (1.1 %), ^{15}N (0.37 %) and ^{54}Fe (5.82 %), ^{56}Fe (91.72 %), ^{57}Fe (2.1 %) and ^{58}Fe (0.3 %), respectively, in this molecule. The relative peak heights agreed well with those calculated for this isotope composition. The mass spectroscopic analysis thus yielded reliable results.

In Fig. 30 C the mass spectrum of heme extracted from *M. barkeri* cells grown in the presence of 2 mM *L*-[*methyl*-D_3]methionine is shown. The spectrum revealed the presence of 37 % unlabeled protoheme (616 Da), 44 % protoheme with a mass of 619 Da and 19 % with a mass of 622 Da. This observation is consistent with one and two methyl groups, of protoheme being derived from the methyl group of methionine. When the *L*-[*methyl*-D_3]methionine concentration in the growth medium was 5 mM the percentage of protoheme with a mass of 622 Da (two methyl groups from methionine) was 33 %. The corresponding percentage of 10 mM was 56 % (Fig. 30 D, E). A similar methionine concentration dependency has been reported for coenzyme F_{430} labeling in *Methanothermobacter marburgensis* (Jaenchen *et al.*, 1981, Selmer *et al.*, 2000).

As an internal control, the incorporation of the methyl group of *L*-[*methyl*-D_3]methionine into F_{430} and B_{12} was determined *via* mass spectrometry in the same experiment. F_{430} contains two methyl groups and vitamin B_{12} seven methyl groups derived from methionine *via* SAM. Labeling efficiency followed the same concentration dependence as found for protoheme (Fig. 31). This clearly indicates that the mass increase of 6 Da observed in the case of protoheme is due to the incorporation of two intact methyl groups derived from *L*-[*methyl*-D_3]methionine during protoheme biosynthesis in *M. barkeri.*

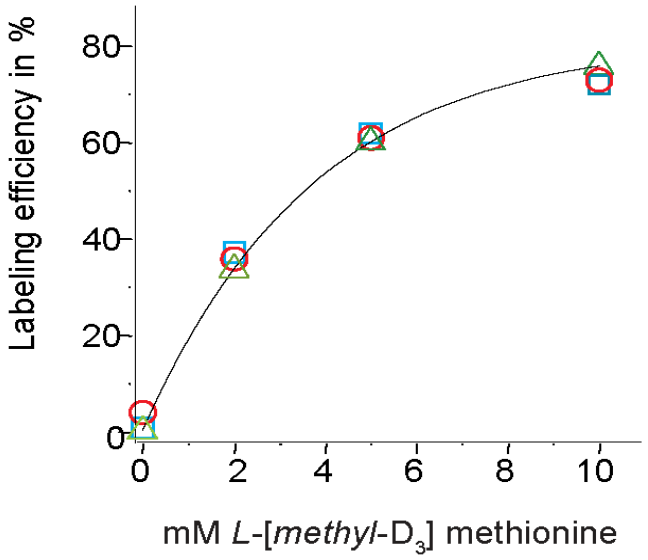

Fig. 31: Incorporation of methyl groups in cofactors of *M. barkeri.*

Methyl group of methionine incorporated into heme (○), F_{430} (△) and B_{12} (□) after growth of *M. barkeri* in the presence of *L*-[*methyl*-D_3]methionine at different concentrations. The labeling efficiency represents the *methyl*-D_3-labeled fraction of the total methyl content of the sample.

3.4.2 The Participation of Precorrin-2 in the Alternative Heme Biosynthesis Pathway

3.4.2.1 Preparation of Precorrin-2

The recombinant production of proteins required to form precorrin-2 from ALA was achieved by coexpression of all the corresponding genes *hemB*, *hemC*, *hemD* and *cobA* from various organisms. The resulting His-tagged fusion proteins were applied to Ni-IDA affinity chromatography, eluted with 1 M imidazole (Fig. 32 A, lane 4) and desalted *via* a gel filtration PD-10 column. Recombinant proteins were employed for precorrin-2 production under anaerobic conditions as described under MATERIALS AND METHODS. Precorrin-2 production was successful with commercially obtained ALA, clearly visible from the lime green color (see Fig. 32 B). However, the production of radioactively labeled precorrin-2 with [^{14}C]-ALA as initial substrate in parallel was unsuccessful (Fig. 32 C). [^{14}C]-ALA is shipped in 1 N HCl. Nevertheless appropriate adjustments of the pH to 8.0 and addition of equal amounts of non-labeled ALA did not improve the formation of precorrin-2.

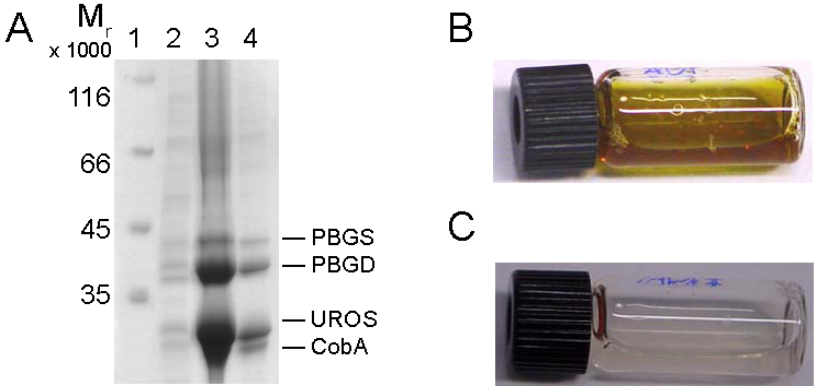

Fig. 32: Preparation of precorrin-2.
(A) Combined production and purification of recombinant *M. barkeri* CobA, *M. thermoautotrophicum* PBGS, *B. megaterium* PBGS and UROS. Proteins were separated by 12 % SDS-PAGE as described in MATERIALS AND METHODS and visualized by staining with Coomassie Brilliant Blue. Lane 1: molecular weight marker; lane 2: total cellular extract without induction; lane 3: total cellular extract after overnight induction of gene expression with 400 µM IPTG; lane 4: Ni-NTA column elution with imidazole. **(B)** Preparation of precorrin-2 with commercially obtained ALA as substrate. Precorrin-2 formation is detected by the lime-green color of precorrin-2. **(C)** Employment of [^{14}C]-ALA did not lead to precorrin-2 formation.

Approximately 100 µg unlabeled precorrin-2 in 100 µL were added to 200 µL crude cell extract or cell free extract under strictly anaerobic conditions. Precorrin-2 turn over was monitored by measuring the absorbance at 500 nm. Unfortunately, no turn over from unlabeled precorrin-2 in either *M. barkeri* crude cell extract or *M. barkeri* cell free extracts was observed. Presumably, cellular enzyme concentrations were too low to be tested in cell free extract as observed for other organisms. Moreover, yet unknown cofactors, co-substrates or metals may be necessary to retrieve precorrin-2 turnover.

3.4.3 Implications from Genomic Arrangements in *Methanosarcina barkeri*

The data shown above make it very likely that the first step of the alternative heme biosynthetic pathway in *M. barkeri* after uroporphyrinogen III formation is the incorporation of the two methyl groups yielding precorrin-2. In all sequenced *Methanosarcina* strains (*i.e. M. barkeri*, *M. acetivorans* and *M. mazei*) and *M. thermoautotrophicum* a gene encoding an uroporphyrinogen III methyltransferase (CobA) is located in an operon structure with UROS (see Fig. 33). The *M. barkeri* CobA protein was employed for precorrin-2 production as shown above and will most probably fulfill the same function *in vivo*. This genomic arrangement further underscores the probability of the methylation step occurring as part of the archaeal heme biosynthesis pathway.

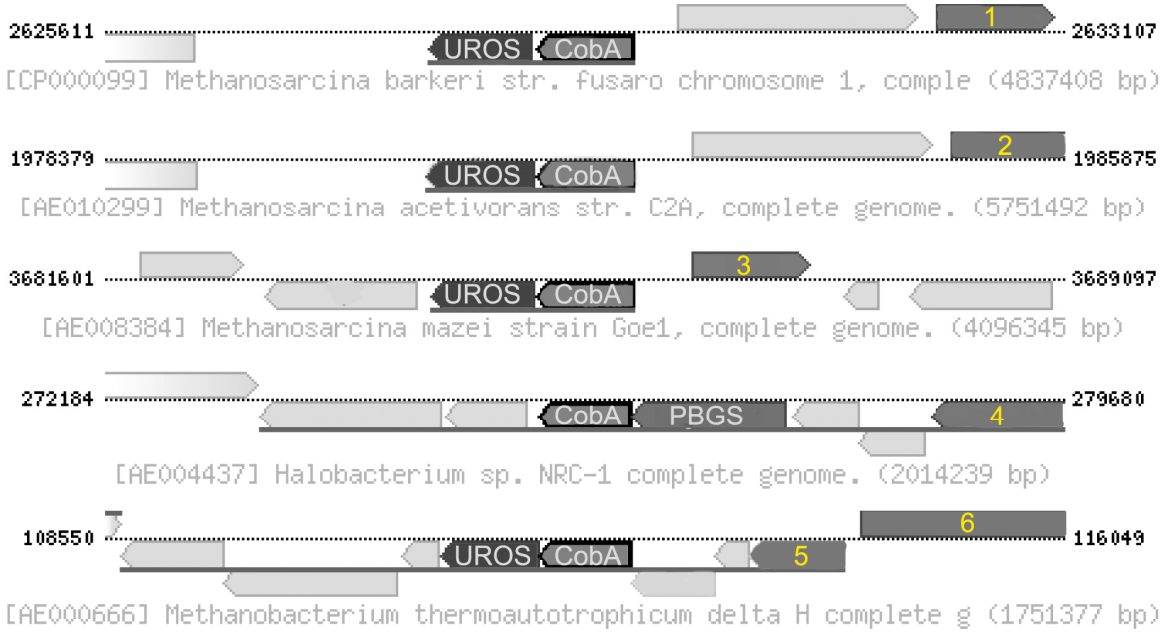

Fig. 33: Operon structures around the *cobA* gene in several archaea retrieved from BRENDA (Schomburg *et al.*, 2004).

In several archaea uroporphyrinogen III methyltransferase (CobA-like protein) is located in an operon structure with the anterior protein of the heme biosynthesis pathway, UROS. In *Halobacterium sp*. NRC-1 a large operon has been postulated which includes PBGS and proteins with unknown function. Open reading frames with unassigned function are depicted in light grey, whereas open reading frames with assigned function are depicted in dark grey with numbering as following. (1, 2, 3) ribonuclease Z; (4) GSAM; (5) phosphoribosyl- amino- imidazole- succino- carboxamide synthase: (6) glutamine- fructose- 6 -phosphate transaminase.

3.4.4 Identification of Enzymes Involved in the Alternate Heme Biosynthesis Pathway *In Silico*

In order to identify candidate proteins possibly participating in the ancient heme biosynthesis pathway, the approach of comparative genome analysis was chosen. Several organisms were chosen and grouped according to their capability to synthesize heme.

The intersection of group one contains proteins which are common to all organisms possessing heme but not the proteins necessary for its synthesis. The intersection of group two contains proteins common to organisms which do not synthesize heme. The intersection of group three consists of proteins in common to organism capable of heme biosynthesis in the well investigated pathway. A scheme of this analysis is depicted in Fig. 34.

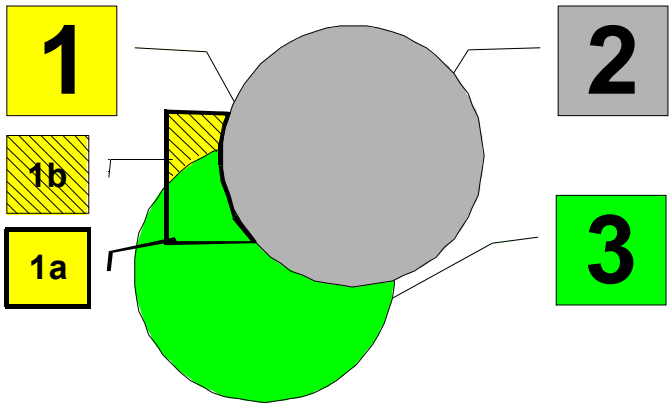

Fig. 34: Comparative genome analysis.
(1) Intersection: Proteins with homologs in organisms synthesizing heme *via* the ancient pathway: *M. barkeri*, *M. acetivorans*, *M. mazei*, *A. fulgidus*, *S. solfataricus*, *S. tokodaii*, *H. salinarium*, *P. aerophilum* and *A. pernix* K1. **(1a)** Proteins present in heme-synthesizing archaea but absent in organisms which do not produce heme. **(1b)** Proteins present in heme-synthesizing archaea but absent in organisms which produce heme *via* the common pathway or not at all. **(2)** Proteomes of organisms which do not synthesize heme: *C. elegans*, *L. lactis*, *M. thermoautotrophicum*, *M. genitalium*, *M. pneumoniae*, *M. pulmonis*, *P. abyssi*, *P. horikoshii*, *T. maritima*, *T. pallidum*, *S. pneumoniae*, *S. pyogenes*, *B. burgdorferi* and *U. urealyticum.* **(3)** Proteomes of organisms synthesizing heme *via* the common pathway: *D. melanogaster*, *H. sapiens*, *S. cerevisiae*, *P. falciparum*, *B. subtilis*, *S. pombe*, *E. coli* and *P. aeruginosa*.

To evaluate whether the chosen method was suitable, the comparative genome analysis was applied in order to find proteins operative in the common heme biosynthesis pathway. Therefore, an intersection of proteins from group two was calculated and proteins which gave significant hits in proteomes of groups one or three were removed. Only proteins which are not operative in organisms either synthesizing heme in the ancient pathway or not synthesizing heme at all should appear as a final result. The computational analysis of genomes of organisms containing or not containing the genes necessary for common heme biosynthesis was performed as described under MATERIALS AND METHODS. Surprisingly, only proteins fulfilling solely one function remained, *i.e.* UROD, a protein functional in the common pathway of heme biosynthesis. All heme biosynthesis proteins

except CPO and PPO were found in the intersection, which is reasonable since *E. coli* lacks a HemY (Panek and O'Brian, 2002), *B. subtilis* a HemF (Hippler *et al.*, 1997) and all eukaryotes a HemN homolog. Due to their function in F_{430} biosynthesis and probably as well in the ancient heme biosynthesis pathway PBGS, PBGD, and UROS were removed because they gave significant hits in group one or three. FC was withdrawn because *S. pneumoniae* possesses a FC homolog. Therefore, the finding of only UROD was congruent with our expectations.

After the method was shown to be suitable, it was applied to determine potential proteins functional in the ancient heme biosynthesis pathway. The intersection of group one consists of 4129 proteins performing about 400 different functions. After the removal of proteins that feature homologs in group two, 541 proteins fulfilling about 100 different functions remained. One third of these proteins function in genetic information processing, whereas another third represents hypothetical proteins. Once having removed all proteins that feature homologs in group three, the final set consisted of ten proteins (see Tab. 13). Since most heme containing archaea synthesize protoheme using the alternate pathway *via* precorrin-2, they should have proteins for this pathway in common and thus be present in all proteomes of organisms listed in the first group. These proteins should not be found in the proteomes of organisms listed in the second or third group. The ten retrieved proteins were classified in four functional groups. The *M. barkeri* homologs are depicted in Tab. 13. A further analysis of these ORFs revealed that three of the four groups are unique to archaea. The only exception is the hypothetical protein Q46CH6 where homologs in many taxonomic groups were identified. These encode for proteins operational in heme d_1 biosynthesis, *i.e.* NirH. The protein Q46E11, assigned to be a putative heat shock protein has homologs in crenarchaeota and euryarchaeota but as well in three bacterial proteomes, *i.e. Pelodictyon*, *Thermoanaerobacter* and *Psychromonas*. The remaining proteins are Q46GA9, a probable SSU ribosomal protein and Q46C74, a probable DNA primase small subunit. Unfortunately, none of these proteins seems to be a suitable candidate for the ancient pathway of heme biosynthesis. It may be the case that either one of the organisms from group one does not posses this pathway or employs non-homolog proteins or that there is more than one alternative to the common heme biosynthesis pathway.

Tab. 13: Results of a comparative genomics analysis.

Functional group	BLAST result (Swissprot ID)	assigned function	organism	*M. barkeri* homolog (Swissprot ID)
1	Q8PXG4	Putative heat shock protein	*M. mazei*	Q46E11
	Q9HSS6	Putative heat shock protein	*H. halobium*	
	Q8PXG3	Putative heat shock protein	*M. frisia*	
	Q8THE4	Hypothetical protein	*M. acetivorans*	
2	Q975Y5	Hypothetical protein	*S. tokadai*	Q46CH6
	Q9YBV2	Hypothetical protein	*A. pernix*	
3	Q8PV36	SSU ribosomal protein S14P	*M. mazei*	Q46GA9
	Q8TRT3	Ribosomal protein S14P	*M. acetivorans*	
4	Q9YEZ8	Probable DNA primase small subunit	*A. pernix*	Q46C74
	Q97Z83	Probable DNA primase small subunit	*S. solfataricus*	

3.4.5 Conclusions from the Investigation of Heme Biosynthesis in *Methanosarcina barkeri*

The obtained results identified the existence of an alternative pathway for heme biosynthesis in *M. barkeri* which has previously exclusively been described for the sulfate-reducing δ-proteobacterium *D. vulgaris*. Tetrapyrrole biosynthesis in *M. barkeri* proceeded *via* the incorporation of two methyl groups from *S*-adenosyl-*L*-methionine into protoheme. Nevertheless, the nature of the of intermediates and enzymes involved in the proceeding steps remained a mystery.

4 SUMMARY

This thesis approached four open questions regarding the pathway for the biosynthesis of heme and involved enzymes in bacteria, archaea and plants.

1. The novel antibiotic alaremycin was shown to inhibit porphobilinogen synthase from various bacterial, archaeal and eukaryotic sources. A co-crystal structure of alaremycin with *Pseudomonas aeruginosa* porphobilinogen synthase was obtained. Thus, the molecular basis of alaremycin function was solved at the atomic level.

2. Bioinformatic approaches failed to detect the uroporphyrinogen III synthase gene in plants. Our cooperation partner Alison Smith at Cambridge University, UK, had genetically isolated a potential open reading frame from *Arabidopsis thaliana.* In this thesis the corresponding protein was recombinantly produced and uroporphyrinogen III synthase activity was demonstrated, providing final proof for the identity of the gene.

3. The recently solved crystal structure of tobacco protoporphyrinogen IX oxidase was used as basis for the functional definition of the corresponding substrate binding site. Furthermore, the structural constellation causing the human disease variegate porphyria was functionally explored. For this purpose 14 enzyme variants were generated, produced, purified and tested for their kinetics and FAD contents. A detailed picture of the various chemical reactions occurring during substrate-enzyme interactions was obtained. The chemical basis for the enzymatic defect responsible for variegate porphyria was elucidated.

4. An alternative pathway for the biosynthesis of hemes in archaea was discovered and initially characterized. It was shown that in the archaeon *Methanosarcina barkeri* heme is synthesized *via* precorrin-2. Therefore, the last four to five steps of archaeal heme biosynthesis are completely different to their bacterial and eukaryotic counterparts.

5 OUTLOOK

Interaction between Porphobilinogen synthase and alaremycin

As outlined above, the results of this work provided insight into the molecular target of alaremycin. The following questions have to be addressed in future experiments.

1) Evaluation of the resistance of the porphobilinogen synthase from the producer strain *Streptomyces sp*. A012304 towards alaremycin.
2) Investigation of the effect of alaremycin on *Staphylococcus aureus hemB*$^{-}$ strains.
3) Determination of the suitability of alaremycin for the generation of inducible *S. aureus* small colony variants.

Plant uroporphyrinogen III synthase

In this study it was possible to confirm the identity of *Arabidopsis thaliana* uroporphyrinogen III synthase. The recombinant protein showed the corresponding enzyme activity. This was the first step towards a characterization of plant uroporphyrinogen III synthase. Further studies have to be carried out to determine its features more closely.

1) Determination of kinetic parameters and pH dependence.
2) Investigations on the oligomeric state of the native protein.
3) Crystallization of plant uroporphyrinogen III synthase.

Alternative heme biosynthesis

In this study evidence for an alternative pathway for heme biosynthesis was obtained. The first step deviating from the common pathway is the methylation of uroporphyrinogen III *via S*-adenosyl-*L*-methionine to form precorrin-2. Nevertheless, it is necessary to perform further investigations to identify intermediates and enzymes participating in the ancient pathway.

1) Genomic knockout of *M. barkeri* uroporphyrinogen III methyltransferase to clarify its participation in the ancient heme biosynthetic pathway.
2) Identification of possible intermediates *via* further labeling experiments.
3) *In vitro* protein purification attempts to isolate involved enzymes.

6 REFERENCES

Akhtar, M. (1991) Mechanism and stereochemistry of the enzymes involved in the conversion of uroporphyrinogen III into haem. Elsevier, Amsterdam.

Akutsu, H., Park, J. S., and Sano, S. (1993) *L*-Methionine methyl is specifically incorporated into C-2 and C-7 positions of the porphyrin in cytochrome c_3 in a strictly anaerobic bacterium, *Desulfovibrio vulgaris*. *J. Am. Chem. Soc.* **115:**12185-12186.

Altschul, S. F., Madden, T. L., Schaffer, A. A., Zhang, J., Zhang, Z., Miller, W., and Lipman, D. J. (1997) Gapped BLAST and PSI-BLAST: a new generation of protein database search programs. *Nucleic Acids Res* **25:**3389-402.

Alwan, A. F., Mgbeje, B. I., and Jordan, P. M. (1989) Purification and properties of uroporphyrinogen III synthase (co-synthase) from an overproducing recombinant strain of *Escherichia coli* K-12. *Biochem J* **264:**397-402.

Arabidopsis Genome Initiative (2000) Analysis of the genome sequence of the flowering plant *Arabidopsis thaliana*. *Nature* **408:**796-815.

Awa, Y., Iwai, N., Ueda, T., Suzuki, K., Asano, S., Yamagishi, J., Nagai, K., and Wachi, M. (2005) Isolation of a new antibiotic, alaremycin, structurally related to 5-aminolevulinic acid from *Streptomyces sp*. A012304. *Biosci Biotechnol Biochem* **69:**1721-5.

Banerjee, R., and Ragsdale, S. W. (2003) The many faces of vitamin B_{12}: catalysis by cobalamin-dependent enzymes. *Annu Rev Biochem* **72:**209-47.

Battersby, A. R., Fookes. C.J.R., Gustafson-Potter, K.E., Matcham, G.W.J. and McDonald. E. (1979) *J. Chem. Soc. Chem. Commun.*316-319.

Beale, S. I. (1999) Enzymes of Chlorophyll biosynthesis. *Photosynthesis Research* **60:**43-73.

Beale, S. I., and Castelfranco, P. A. (1973) ^{14}C incorporation from exogeneous compunds into δ-aminolevulinic acid by green cucumber cotyledons. *Biochem Biophys Res Commun* **52:**143-149.

Berger, S. A., and Edberg, S. C. (1987) Microbial nomenclature: a list of names and origins. *Diagn Microbiol Infect Dis* **6:**343-56.

Bhosale, S., Kshirsagar, D., Pawar, P., Yeole, T., and Ranade, D. (1995) Purification and characterization of 5-aminolevulinic acid dehydratase from *Methanosarcina barkeri*. *FEMS Microbiology letters* **127:**151-155.

Breinig, S., Kervinen, J., Stith, L., Wasson, A. S., Fairman, R., Wlodawer, A., Zdanov, A., and Jaffe, E. K. (2003) Control of tetrapyrrole biosynthesis by alternate quaternary forms of porphobilinogen synthase. *Nat Struct Biol* **10:**757-63.

Brenner, D. A., and Bloomer, J. R. (1980) The enzymatic defect in variegate prophyria. Studies with human cultured skin fibroblasts. *N Engl J Med* **302:**765-9.

Brunger, A. T., Adams, P. D., Clore, G. M., DeLano, W. L., Gros, P., Grosse-Kunstleve, R. W., Jiang, J. S., Kuszewski, J., Nilges, M., Pannu, N. S., Read, R. J., Rice, L. M., Simonson, T., and Warren, G. L. (1998) Crystallography & NMR system: A new software suite for macromolecular structure determination. *Acta Crystallogr D Biol Crystallogr* **54:**905-21.

Burg, R. W., Miller, B. M., Baker, E. E., Birnbaum, J., Currie, S. A., Hartman, R., Kong, Y. L., Monaghan, R. L., Olson, G., Putter, I., Tunac, J. B., Wallick, H., Stapley, E. O., Oiwa, R., and Omura, S. (1979) Avermectins, new family of potent anthelmintic agents: producing organism and fermentation. *Antimicrob Agents Chemother* **15:**361-7.

Camadro, J. M., Thome, F., Brouillet, N., and Labbe, P. (1994) Purification and properties of protoporphyrinogen oxidase from the yeast *Saccharomyces cerevisiae*. Mitochondrial location and evidence for a precursor form of the protein. *J Biol Chem* **269:**32085-91.

Chadwick, D. J., Ackrill, K. (eds.) (1994) The Biosynthesis of Tetrapyrrole Pigments, vol. 180. Wiley and Sons, Chichester, UK.

Cheh, A., and Neilands, J. B. (1973) Zinc, an essential metal ion for beef liver delta-aminolevulinate dehydratase. *Biochem Biophys Res Commun* **55:**1060-3.

Chelstowska, A., Zoladek, T., Garey, J., Kushner, J., Rytka, J., and Labbe-Bois, R. (1992) Identification of amino acid changes affecting yeast uroporphyrinogen decarboxylase activity by sequence analysis of *hem12* mutant alleles. *Biochem J* **288 (Pt 3):**753-7.

Collaborative Computational Project Number 4 (1994) The CCP4 suite: programs for protein crystallography. *Acta Crystallogr D Biol Crystallogr* **50:**760-3.

Corradi, H. R., Corrigall, A. V., Boix, E., Mohan, C. G., Sturrock, E. D., Meissner, P. N., and Acharya, K. R. (2006) Crystal structure of protoporphyrinogen oxidase from *Myxococcus xanthus* and its complex with the inhibitor acifluorfen. *J Biol Chem* **281:**38625-33.

Corrigall, A. V., Siziba, K. B., Maneli, M. H., Shephard, E. G., Ziman, M., Dailey, T. A., Dailey, H. A., Kirsch, R. E., and Meissner, P. N. (1998) Purification of and kinetic studies on a cloned protoporphyrinogen oxidase from the aerobic bacterium *Bacillus subtilis*. *Arch Biochem Biophys* **358:**251-6.

Dailey, H. A. (2002) Terminal steps of haem biosynthesis. *Biochem Soc Trans* **30:**590-5.

Dailey, H. A., and Dailey, T. A. (1996) Protoporphyrinogen oxidase of *Myxococcus xanthus*. Expression, purification, and characterization of the cloned enzyme. *J Biol Chem* **271:**8714-8.

Dailey, H. A., and Karr, S. W. (1987) Purification and characterization of murine protoporphyrinogen oxidase. *Biochemistry* **26:**2697-701.

Dailey, T. A., and Dailey, H. A. (1996) Human protoporphyrinogen oxidase: expression, purification, and characterization of the cloned enzyme. *Protein Sci* **5:**98-105.

Dailey, T. A., and Dailey, H. A. (1998) Identification of an FAD superfamily containing protoporphyrinogen oxidases, monoamine oxidases, and phytoene desaturase. Expression and characterization of phytoene desaturase of *Myxococcus xanthus*. *J Biol Chem* **273:**13658-62.

Dean, G. (1971) Screening tests for porphyria. *Lancet* **1:**86-7.

Deppenmeier, U., Johann, A., Hartsch, T., Merkl, R., Schmitz, R. A., Martinez-Arias, R., Henne, A., Wiezer, A., Baumer, S., Jacobi, C., Bruggemann, H., Lienard, T., Christmann, A., Bomeke, M., Steckel, S., Bhattacharyya, A., Lykidis, A., Overbeek, R., Klenk, H. P., Gunsalus, R. P., Fritz, H. J., and Gottschalk, G. (2002) The genome of *Methanosarcina mazei*: evidence for lateral gene transfer between bacteria and archaea. *J Mol Microbiol Biotechnol* **4:**453-61.

Desnick, R. J., Glass, I. A., Xu, W., Solis, C., and Astrin, K. H. (1998) Molecular genetics of congenital erythropoietic porphyria. *Semin Liver Dis* **18:**77-84.

Deybach, J. C., da Silva, V., Grandchamp, B., and Nordmann, Y. (1985) The mitochondrial location of protoporphyrinogen oxidase. *Eur J Biochem* **149:**431-5.

Diekert, G., Konheiser, U., Piechulla, K., and Thauer, R. K. (1981) Nickel requirement and factor F_{430} content of methanogenic bacteria. *J Bacteriol* **148:**459-64.

Dunn, N. W., and Holloway, B. W. (1971) Pleiotrophy of p-fluorophenylalanine-resistant and antibiotic hypersensitive mutants of *Pseudomonas aeruginosa*. *Genet Res* **18:**185-97.

Emsley, P., and Cowtan, K. (2004) Coot: model-building tools for molecular graphics. *Acta Crystallogr D Biol Crystallogr* **60:**2126-32.

Erskine, P. T., Newbold, R., Roper, J., Coker, A., Warren, M. J., Shoolingin-Jordan, P. M., Wood, S. P., and Cooper, J. B. (1999) The Schiff base complex of yeast 5-aminolaevulinic acid dehydratase with laevulinic acid. *Protein Sci* **8:**1250-6.

Erskine, P. T., Norton, E., Cooper, J. B., Lambert, R., Coker, A., Lewis, G., Spencer, P., Sarwar, M., Wood, S. P., Warren, M. J., and Shoolingin-Jordan, P. M. (1999) X-ray structure of 5-aminolevulinic acid dehydratase from *Escherichia coli* complexed with the inhibitor levulinic acid at 2.0 A resolution. *Biochemistry* **38:**4266-76.

Erskine, P. T., Senior, N., Maignan, S., Cooper, J., Lambert, R., Lewis, G., Spencer, P., Awan, S., Warren, M., Tickle, I. J., Thomas, P., Wood, S. P., and Shoolingin-Jordan, P. M. (1997) Crystallization of 5-aminolaevulinic acid dehydratase from *Escherichia coli* and *Saccharomyces cerevisiae* and preliminary X-ray characterization of the crystals. *Protein Sci* **6:**1774-6.

Frankenberg, N., Erskine, P. T., Cooper, J. B., Shoolingin-Jordan, P. M., Jahn, D., and Heinz, D. W. (1999) High resolution crystal structure of a Mg^{2+}-dependent porphobilinogen synthase. *J Mol Biol* **289:**591-602.

Frankenberg, N., Heinz, D. W., and Jahn, D. (1999) Production, purification, and characterization of a Mg^{2+}-responsive porphobilinogen synthase from *Pseudomonas aeruginosa*. *Biochemistry* **38:**13968-75.

Frankenberg, N., and Lagarias, J. C. (2003) Phycocyanobilin:ferredoxin oxidoreductase of *Anabaena sp*. PCC 7120. Biochemical and spectroscopic. *J Biol Chem* **278:**9219-26.

Frankenberg, N., Moser, J., and Jahn, D. (2003) Bacterial heme biosynthesis and its biotechnological application. *Appl Microbiol Biotechnol* **63:**115-27.

Frere, F., Nentwich, M., Gacond, S., Heinz, D. W., Neier, R., and Frankenberg-Dinkel, N. (2006) Probing the active site of *Pseudomonas aeruginosa* porphobilinogen synthase using newly developed inhibitors. *Biochemistry* **45:**8243-53.

Frere, F., Schubert, W. D., Stauffer, F., Frankenberg, N., Neier, R., Jahn, D., and Heinz, D. W. (2002) Structure of porphobilinogen synthase from *Pseudomonas aeruginosa* in complex with 5-fluorolevulinic acid suggests a double Schiff base mechanism. *J Mol Biol* **320:**237-47.

Friedmann, H. C., and Thauer, R. K. (1987) Non-enzymatic ammonia formation from glutamine under growth conditions for *Methanobacterium thermoautotrophicum*. *FEMS Microbiol Lett* **40:**179-181.

Gacond, S., Frere, F., Nentwich, M., Faurite, J. P., Frankenberg-Dinkel, N., and Neier, R. (2007) Synthesis of bisubstrate inhibitors of porphobilinogen synthase from *Pseudomonas aeruginosa*. *Chem Biodivers* **4:**189-202.

Galagan, J. E., Nusbaum, C., Roy, A., Endrizzi, M. G., Macdonald, P., FitzHugh, W., Calvo, S., Engels, R., Smirnov, S., Atnoor, D., Brown, A., Allen, N., Naylor, J., Stange-Thomann, N., DeArellano, K., Johnson, R., Linton, L., McEwan, P., McKernan, K., Talamas, J., Tirrell, A., Ye, W., Zimmer, A., Barber, R. D., Cann, I., Graham, D. E., Grahame, D. A., Guss, A. M., Hedderich, R., Ingram-Smith, C., Kuettner, H. C., Krzycki, J. A., Leigh, J. A., Li, W., Liu, J., Mukhopadhyay, B., Reeve, J. N., Smith, K., Springer, T. A., Umayam, L. A., White, O., White, R. H., Conway de Macario, E., Ferry, J. G., Jarrell, K. F., Jing, H., Macario, A. J., Paulsen, I., Pritchett, M., Sowers, K. R., Swanson, R. V., Zinder, S. H., Lander, E., Metcalf, W. W., and Birren, B. (2002) The genome of *M. acetivorans* reveals extensive metabolic and physiological diversity. *Genome Res* **12:**532-42.

Gartner, P. (1991) Characterization of a quinole-oxidase activity in crude extracts of *Thermoplasma acidophilum* and isolation of an 18-kDa cytochrome. *Eur J Biochem* **200:**215-22.

Gill, S. C., and von Hippel, P. H. (1989) Calculation of protein extinction coefficients from amino acid sequence data. *Anal Biochem* **182:**319-26.

Goethe, J. W. (1808) Faust. Gotta'sche Buchhandlung Tübingen.

Hansson, M., and Hederstedt, L. (1994) *Bacillus subtilis* HemY is a peripheral membrane protein essential for protoheme IX synthesis which can oxidize coproporphyrinogen III and protoporphyrinogen IX. *J Bacteriol* **176:**5962-70.

Hansson, M., and Hederstedt, L. (1992) Cloning and characterization of the *Bacillus subtilis hemEHY* gene cluster, which encodes protoheme IX biosynthetic enzymes. *J Bacteriol* **174:**8081-93.

Hansson, M., Rutberg, L., Schroder, I., and Hederstedt, L. (1991) The *Bacillus subtilis hemAXCDBL* gene cluster, which encodes enzymes of the biosynthetic pathway from glutamate to uroporphyrinogen III. *J Bacteriol* **173:**2590-9.

Hart, G. J., and Battersby, A. R. (1985) Purification and properties of uroporphyrinogen III synthase (co-synthetase) from *Euglena gracilis*. *Biochem J* **232:**151-60.

Heidelberg, J. F., Seshadri, R., Haveman, S. A., Hemme, C. L., Paulsen, I. T., Kolonay, J. F., Eisen, J. A., Ward, N., Methe, B., Brinkac, L. M., Daugherty, S. C., Deboy, R. T., Dodson, R. J., Durkin, A. S., Madupu, R., Nelson, W. C., Sullivan, S. A., Fouts, D., Haft, D. H., Selengut, J., Peterson, J. D., Davidsen, T. M., Zafar, N., Zhou, L., Radune, D., Dimitrov, G., Hance, M., Tran, K., Khouri, H., Gill, J., Utterback, T. R., Feldblyum, T. V., Wall, J. D., Voordouw, G., and Fraser, C. M. (2004) The genome sequence of the anaerobic, sulfate-reducing bacterium *Desulfovibrio vulgaris* Hildenborough. *Nat Biotechnol* **22:**554-9.

Heinemann, I. U., Diekmann, N., Masoumi, A., Koch, M., Messerschmidt, A., Jahn, M., and Jahn, D. (2007) Functional definition of the tobacco protoporphyrinogen IX oxidase substrate-binding site. *Biochem J* **402:**575-80.

Higuchi, M., and Bogorad, L. (1975) The purification and properties of uroporphyrinogen I synthases and uroporphyrinogen III cosynthase. Interactions between the enzymes. *Ann N Y Acad Sci* **244:**401-18.

Hippler, B., Homuth, G., Hoffmann, T., Hungerer, C., Schumann, W., and Jahn, D. (1997) Characterization of *Bacillus subtilis hemN*. *J Bacteriol* **179:**7181-5.

Hunger, W., and Claus, D. (1981) Taxonomic studies on *Bacillus megaterium* and on agarolytic *Bacillus* strains. Academic Press, London.

Ilag, L. L., and Jahn, D. (1992) Activity and spectroscopic properties of the *Escherichia coli* glutamate 1-semialdehyde aminotransferase and the putative active site mutant K265R. *Biochemistry* **31:**7143-51.

Ishida, T., Yu, L., Akutsu, H., Ozawa, K., Kawanishi, S., Seto, A., Inubushi, T., and Sano, S. (1998) A primitive pathway of porphyrin biosynthesis and enzymology in *Desulfovibrio vulgaris*. *Proc Natl Acad Sci U S A* **95:**4853-8.

Jacobs, J. M., and Jacobs, N. J. (1984) Protoporphyrinogen oxidation, an enzymatic step in heme and chlorophyll synthesis: partial characterization of the reaction in plant organelles and comparison with mammalian and bacterial systems. *Arch Biochem Biophys* **229:**312-9.

Jaenchen, R., Diekert, G., and Thauer, R. K. (1981) Incorporation of methionine-derived methyl groups into factor F_{430} by *Methanobacterium thermoautotrophicum*. *FEBS Lett* **130:**133-136.

Jaffe, E. K. (2000) The porphobilinogen synthase family of metalloenzymes. *Acta Crystallogr D Biol Crystallogr* **56:**115-28.

Jaffe, E. K., Abrams, W. R., Kaempfen, H. X., and Harris, K. A., Jr. (1992) 5-Chlorolevulinate modification of porphobilinogen synthase identifies a potential role for the catalytic zinc. *Biochemistry* **31:**2113-23.

Jaffe, E. K., Volin, M., Bronson-Mullins, C. R., Dunbrack, R. L., Jr., Kervinen, J., Martins, J., Quinlan, J. F., Jr., Sazinsky, M. H., Steinhouse, E. M., and Yeung, A. T. (2000) An artificial gene for human porphobilinogen synthase allows comparison of an allelic variation implicated in susceptibility to lead poisoning. *J Biol Chem* **275:**2619-26.

Jahn, D., Hungerer, C., and Troup, B. (1996) Unusual pathways and environmentally regulated genes of bacterial heme biosynthesis. *Naturwissenschaften* **83:**389-400.

Jahn, D., Michelsen, U., and Soll, D. (1991) Two glutamyl-tRNA reductase activities in *Escherichia coli*. *J Biol Chem* **266:**2542-8.

Jahn, D., Verkamp, E., and Soll, D. (1992) Glutamyl-transfer RNA: a precursor of heme and chlorophyll biosynthesis. *Trends Biochem Sci* **17:**215-8.

Jordan, P. M. (1994) Highlights in haem biosynthesis. *Curr Opin Struct Biol* **4:**902-11.

Jordan, P. M., and Warren, M. J. (1987) Evidence for a dipyrromethane cofactor at the catalytic site of *E. coli* porphobilinogen deaminase. *FEBS Lett* **225:**87-92.

Kamlage, B., and Blaut, M. (1992) Characterization of cytochromes from *Methanosarcina strain* Gol and their involvement in electron transport during growth on methanol. *J Bacteriol* **174:**3921-7.

Kandler, O., and Hippe, H. (1977) Lack of peptidoglycan in the cell walls of *Methanosarcina barkeri*. *Arch Microbiol* **113:**57-60.

Kappas, A. S., S. Galbraith, R.A.; Nordmann, Y. (1995) The Metabolic and Molecular Basis of Inherited Diseases, 7th ed. McGraw-Hill, New York.

Karrasch, M., Borner, G., Enssle, M., and Thauer, R. K. (1989) Formylmethanofuran dehydrogenase from methanogenic bacteria, a molybdoenzyme. *FEBS Lett* **253:**226-30.

Kawashima, T., Amano, N., Koike, H., Makino, S., Higuchi, S., Kawashima-Ohya, Y., Watanabe, K., Yamazaki, M., Kanehori, K., Kawamoto, T., Nunoshiba, T., Yamamoto, Y., Aramaki, H., Makino, K., and Suzuki, M. (2000) Archaeal adaptation to higher temperatures revealed by genomic sequence of *Thermoplasma volcanium*. *Proc Natl Acad Sci U S A* **97:**14257-62.

Kersey, P., Bower, L., Morris, L., Horne, A., Petryszak, R., Kanz, C., Kanapin, A., Das, U., Michoud, K., Phan, I., Gattiker, A., Kulikova, T., Faruque, N., Duggan, K., McLaren, P., Reimholz, B., Duret, L., Penel, S., Reuter, I., and Apweiler, R. (2005) Integr8 and Genome Reviews: integrated views of complete genomes and proteomes. *Nucleic Acids Res* **33:**D297-302.

Kiel, J. A., Boels, J. M., Beldman, G., and Venema, G. (1990) Nucleotide sequence of the *Synechococcus sp*. PCC7942 branching enzyme gene (*glgB*): expression in *Bacillus subtilis*. *Gene* **89:**77-84.

Kikuchi, G., Kumar, A. M., Tamlage, P., and Shemin, D. (1958) The enzymatic synthesis of δ-aminolevulinic acid. *J. Biol. Chem.* **233:**1214-1219.

Koch, M., Breithaupt, C., Kiefersauer, R., Freigang, J., Huber, R., and Messerschmidt, A. (2004) Crystal structure of protoporphyrinogen IX oxidase: a key enzyme in haem and chlorophyll biosynthesis. *EMBO J* **23:**1720-8.

Kohashi, M., Clement, R. P., Tse, J., and Piper, W. N. (1984) Rat hepatic uroporphyrinogen III co-synthase. Purification and evidence for a bound folate coenzyme participating in the biosynthesis of uroporphyrinogen III. *Biochem J* **220:**755-65.

Kuhn, W., and Gottschalk, G. (1983) Characterization of the cytochromes occurring in *Methanosarcina* species. *Eur J Biochem* **135:**89-94.

Labbe, P., Camadro, J. M., and Chambon, H. (1985) Fluorometric assays for coproporphyrinogen oxidase and protoporphyrinogen oxidase. *Anal Biochem* **149:**248-60.

Laemmli, U. K. (1970) Cleavage of structural proteins during the assembly of the head of bacteriophage T4. *Nature* **227:**680-5.

Layer, G., Verfurth, K., Mahlitz, E., and Jahn, D. (2002) Oxygen-independent coproporphyrinogen-III oxidase HemN from *Escherichia coli*. *J Biol Chem* **277:**34136-42.

Leech, H. K., Raux-Deery, E., Heathcote, P., and Warren, M. J. (2002) Production of cobalamin and sirohaem in *Bacillus megaterium*: an investigation into the role of the branchpoint chelatases sirohydrochlorin ferrochelatase (SirB) and sirohydrochlorin cobalt chelatase (CbiX). *Biochem Soc Trans* **30:**610-3.

Lermontova, I., Kruse, E., Mock, H. P., and Grimm, B. (1997) Cloning and characterization of a plastidal and a mitochondrial isoform of tobacco protoporphyrinogen IX oxidase. *Proc Natl Acad Sci U S A* **94:**8895-900.

Lubben, M., and Morand, K. (1994) Novel prenylated hemes as cofactors of cytochrome oxidases. Archaea have modified hemes A and O. *J Biol Chem* **269:**21473-9.

Luer, C., Schauer, S., Mobius, K., Schulze, J., Schubert, W. D., Heinz, D. W., Jahn, D., and Moser, J. (2005) Complex formation between glutamyl-tRNA reductase and glutamate-1-semialdehyde 2,1-aminomutase in *Escherichia coli* during the initial reactions of porphyrin biosynthesis. *J Biol Chem* **280:**18568-72.

Luo, J., and Lim, C. K. (1993) Order of uroporphyrinogen III decarboxylation on incubation of porphobilinogen and uroporphyrinogen III with erythrocyte uroporphyrinogen decarboxylase. *Biochem J* **289 (Pt 2):**529-32.

Maeder, D. L., Anderson, I., Brettin, T. S., Bruce, D. C., Gilna, P., Han, C. S., Lapidus, A., Metcalf, W. W., Saunders, E., Tapia, R., and Sowers, K. R. (2006) The *Methanosarcina barkeri* genome: comparative analysis with *Methanosarcina acetivorans* and *Methanosarcina mazei* reveals extensive rearrangement within methanosarcinal genomes. *J Bacteriol* **188:**7922-31.

Maneli, M. H., Corrigall, A. V., Klump, H. H., Davids, L. M., Kirsch, R. E., and Meissner, P. N. (2003) Kinetic and physical characterisation of recombinant wild-type and mutant human protoporphyrinogen oxidases. *Biochim Biophys Acta* **1650:**10-21.

Mathews, M. A., Schubert, H. L., Whitby, F. G., Alexander, K. J., Schadick, K., Bergonia, H. A., Phillips, J. D., and Hill, C. P. (2001) Crystal structure of human uroporphyrinogen III synthase. *EMBO J* **20:**5832-9.

Matias, P. M., Pereira, I. A., Soares, C. M., and Carrondo, M. A. (2005) Sulphate respiration from hydrogen in *Desulfovibrio bacteria*: a structural biology overview. *Prog Biophys Mol Biol* **89:**292-329.

Matringe, M., Camadro, J. M., Labbe, P., and Scalla, R. (1989) Protoporphyrinogen oxidase as a molecular target for diphenyl ether herbicides. *Biochem J* **260:**231-5.

Matseliukh, B. P. (2006) Regulation of antibiotic biosynthesis in *Streptomycetes*. *Mikrobiol Z* **68:**85-95.

McConville, M. L., and Charles, H. P. (1979) Mutants of *Escherichia coli* K12 permeable to haemin. *J Gen Microbiol* **113:**165-8.

McCoy, A. J., Grosse-Kunstleve, R. W., Storoni, L. C., and Read, R. J. (2005) Likelihood-enhanced fast translation functions. *Acta Crystallogr D Biol Crystallogr* **61:**458-64.

McNeill, L. A., and Shoolingin-Jordan, P. M. (1998) Dipyrromethane cofactor assembly in porphobilinogen deaminase. *Biochem Soc Trans* **26:**S286.

Meissner, P. N., Dailey, T. A., Hift, R. J., Ziman, M., Corrigall, A. V., Roberts, A. G., Meissner, D. M., Kirsch, R. E., and Dailey, H. A. (1996) A R59W mutation in human protoporphyrinogen oxidase results in decreased enzyme activity and is prevalent in South Africans with variegate porphyria. *Nat Genet* **13:**95-7.

Meissner, P. N., Day, R. S., Moore, M. R., Disler, P. B., and Harley, E. (1986) Protoporphyrinogen oxidase and porphobilinogen deaminase in variegate porphyria. *Eur J Clin Invest* **16:**257-61.

Mock, H. P., and Grimm, B. (1997) Reduction of Uroporphyrinogen Decarboxylase by Antisense RNA Expression Affects Activities of Other Enzymes Involved in Tetrapyrrole Biosynthesis and Leads to Light-Dependent Necrosis. *Plant Physiol* **113:**1101-1112.

Mock, H. P., Heller, W., Molina, A., Neubohn, B., Sandermann, H., Jr., and Grimm, B. (1999) Expression of uroporphyrinogen decarboxylase or coproporphyrinogen oxidase antisense RNA in tobacco induces pathogen defense responses conferring increased resistance to tobacco mosaic virus. *J Biol Chem* **274:**4231-8.

Mohr, C. D., Sonsteby, S. K., and Deretic, V. (1994) The *Pseudomonas aeruginosa* homologs of *hemC* and *hemD* are linked to the gene encoding the regulator of mucoidy AlgR. *Mol Gen Genet* **242:**177-84.

Moser, J., Lorenz, S., Hubschwerlen, C., Rompf, A., and Jahn, D. (1999) *Methanopyrus kandleri* glutamyl-tRNA reductase. *J Biol Chem* **274:**30679-85.

Moser, J., Schubert, W. D., Beier, V., Bringemeier, I., Jahn, D., and Heinz, D. W. (2001) V-shaped structure of glutamyl-tRNA reductase, the first enzyme of tRNA-dependent tetrapyrrole biosynthesis. *EMBO J* **20:**6583-90.

Murshudov, G. N., Vagin, A. A., and Dodson, E. J. (1997) Refinement of macromolecular structures by the maximum-likelihood method. *Acta Crystallogr D Biol Crystallogr* **53:**240-55.

Mustajoki, P. (1980) Variegate porphyria. Twelve years' experience in Finland. *Q J Med* **49:**191-203.

Nishimura, K., Nakayashiki, T., and Inokuchi, H. (1993) Cloning and sequencing of the *hemE* gene encoding uroporphyrinogen III decarboxylase (UPD) from *Escherichia coli* K-12. *Gene* **133:**109-13.

Noriega, G., Mattei, G., Batlle, A., and Juknat, A. A. (2002) Rat kidney porphobilinogen deaminase kinetics. Detection of enzyme-substrate complexes. *Int J Biochem Cell Biol* **34:**1230-40.

O´Brian, M. R., and Thöny-Meyer, L. (2002) Biochemistry, Regulation and Genomics of Haem Biosynthesis in Prokaryotes. *Microbial Physiology* **46:**258-317.

Ohno, Y., Buescher, E. S., Roberts, R., Metcalf, J. A., and Gallin, J. I. (1986) Reevaluation of cytochrome b and flavin adenine dinucleotide in neutrophils from patients with chronic granulomatous disease and description of a family with probable autosomal recessive inheritance of cytochrome b deficiency. *Blood* **67:**1132-8.

Otwinowski, Z., and Minor, W. (1997) Processing of X-ray diffraction data collected in oscillation mode. *Methods in Enzymology* **276:**307-326.

Padmanaban, G., and Rangarajan, P. N. (2000) Heme metabolism of *Plasmodium* is a major antimalarial target. *Biochem Biophys Res Commun* **268:**665-8.

Panek, H., and O'Brian, M. R. (2002) A whole genome view of prokaryotic haem biosynthesis. *Microbiology* **148:**2273-82.

Petricek, M., Petrickova, K., Havlicek, L., and Felsberg, J. (2006) Occurrence of two 5-aminolevulinate biosynthetic pathways in *Streptomyces nodosus* subsp. *asukaensis* is linked with the production of asukamycin. *J Bacteriol* **188:**5113-23.

Poulson, R. (1976) The enzymic conversion of protoporphyrinogen IX to protoporphyrin IX in mammalian mitochondria. *J Biol Chem* **251:**3730-3.

Poulson, R., and Polglase, W. J. (1975) The enzymic conversion of protoporphyrinogen IX to protoporphyrin IX. Protoporphyrinogen oxidase activity in mitochondrial extracts of *Saccharomyces cerevisiae*. *J Biol Chem* **250:**1269-74.

Raux-Deery, E., Leech, H. K., Nakrieko, K. A., McLean, K. J., Munro, A. W., Heathcote, P., Rigby, S. E., Smith, A. G., and Warren, M. J. (2005) Identification and characterization of the terminal enzyme of siroheme biosynthesis from *Arabidopsis thaliana*: a plastid-located sirohydrochlorin ferrochelatase containing a 2FE-2S center. *J Biol Chem* **280:**4713-21.

Raux, E., Leech, H. K., Beck, R., Schubert, H. L., Santander, P. J., Roessner, C. A., Scott, A. I., Martens, J. H., Jahn, D., Thermes, C., Rambach, A., and Warren, M. J. (2003) Identification and functional analysis of enzymes required for precorrin-2 dehydrogenation and metal ion insertion in the biosynthesis of sirohaem and cobalamin in *Bacillus megaterium*. *Biochem J* **370:**505-16.

Righetti, P. G. (1990) Recent developments in electrophoretic methods. *J Chromatogr* **516:**3-22.

Roberts, A. G., Puy, H., Dailey, T. A., Morgan, R. R., Whatley, S. D., Dailey, H. A., Martasek, P., Nordmann, Y., Deybach, J. C., and Elder, G. H. (1998) Molecular characterization of homozygous variegate porphyria. *Hum Mol Genet* **7:**1921-5.

Rodgers, K. R. (1999) Heme-based sensors in biological systems. *Curr Opin Chem Biol* **3:**158-67.

Romana, M., Dubart, A., Beaupain, D., Chabret, C., Goossens, M., and Romeo, P. H. (1987) Structure of the gene for human uroporphyrinogen decarboxylase. *Nucleic Acids Res* **15:**7343-56.

Romana, M., Le Boulch, P., and Romeo, P. H. (1987) Rat uroporphyrinogen decarboxylase cDNA: nucleotide sequence and comparison to human uroporphyrinogen decarboxylase. *Nucleic Acids Res* **15:**7211.

Sambrook, J., Fritsch, E.F. & Maniatis, T. (1989) Molecular cloning: a laboratory manual, 2nd ed. Cold Spring Harbor Laboratory Press, Cold Spring Harbor, New York.

Sano, S., and Granick, S. (1961) Mitochondrial coproporphyrinogen oxidase and protoporphyrin formation. *J Biol Chem* **236:**1173-80.

Sarkany, R. P. (1999) Porphyria. From Sir Walter Raleigh to molecular biology. *Adv Exp Med Biol* **455:**235-41.

Sasarman, A., Chartrand, P., Lavoie, M., Tardif, D., Proschek, R., and Lapointe, C. (1979) Mapping of a new *hem* gene in *Escherichia coli* K12. *J Gen Microbiol* **113:**297-303.

Sasarman, A., Letowski, J., Czaika, G., Ramirez, V., Nead, M. A., Jacobs, J. M., and Morais, R. (1993) Nucleotide sequence of the *hemG* gene involved in the protoporphyrinogen oxidase activity of *Escherichia coli* K12. *Can J Microbiol* **39:**1155-61.

Sasarman, A., Nepveu, A., Echelard, Y., Dymetryszyn, J., Drolet, M., and Goyer, C. (1987) Molecular cloning and sequencing of the *hemD* gene of *Escherichia coli* K-12 and preliminary data on the Uro operon. *J Bacteriol* **169:**4257-62.

Schleifer, K. H., and Kocur, M. (1973) Classification of staphylococci based on chemical and biochemical properties. *Arch Mikrobiol* **93:**65-85.

Schomburg, I., Chang, A., Ebeling, C., Gremse, M., Heldt, C., Huhn, G., and Schomburg, D. (2004) BRENDA, the enzyme database: updates and major new developments. *Nucleic Acids Res* **32:**D431-3.

Schutz, M., Brugna, M., Lebrun, E., Baymann, F., Huber, R., Stetter, K. O., Hauska, G., Toci, R., Lemesle-Meunier, D., Tron, P., Schmidt, C., and Nitschke, W. (2000) Early evolution of cytochrome bc complexes. *J Mol Biol* **300:**663-75.

Selmer, T., Kahnt, J., Goubeaud, M., Shima, S., Grabarse, W., Ermler, U., and Thauer, R. K. (2000) The biosynthesis of methylated amino acids in the active site region of methyl-coenzyme M reductase. *J Biol Chem* **275:**3755-60.

Shemin, D. (1976) 5-Aminolaevulinic acid dehydratase: structure, function, and mechanism. *Philos Trans R Soc Lond B Biol Sci* **273:**109-15.

Shemin, D., and Russel, C. S. (1953) Delta-aminolevulinic acid, its role in the biosynthesis of porphyrins and purins. *J. Am. Chem. Soc.* **75:**4873-4875.

Shoolingin-Jordan, P. M. (1995) Porphobilinogen deaminase and uroporphyrinogen III synthase: structure, molecular biology, and mechanism. *J Bioenerg Biomembr* **27:**181-95.

Shoolingin-Jordan, P. M., and Cheung, K. M. (1999) The biosynthesis of heme, vol. 4. Elsevier, Pergamon.

Siepker, L. J., Ford, M., de Kock, R., and Kramer, S. (1987) Purification of bovine protoporphyrinogen oxidase: immunological cross-reactivity and structural relationship to ferrochelatase. *Biochim Biophys Acta* **913:**349-58.

Skerman, V. B. D., McGowan, V., and Sneath, P. H. A. (1980) Approved Lists of Bacterial Names. *Int. J. Syst. Bacteriol* **30:**225-420.

Spencer, J. B., Stolowich, N. J., Roessner, C. A., and Scott, A. I. (1993) The *Escherichia coli cysG* gene encodes the multifunctional protein, siroheme synthase. *FEBS Lett* **335:**57-60.

Tang, L., Stith, L., and Jaffe, E. K. (2005) Substrate-induced interconversion of protein quaternary structure isoforms. *J Biol Chem* **280:**15786-93.

Thauer, R. K., and Bonacker, L. G. (1994) Biosynthesis of coenzyme F_{430}, a nickel porphinoid involved in methanogenesis. *Ciba Found Symp* **180:**210-22; discussion 222-7.

Thauer, R. K., and Sauer, K. (1999) The role of corrinoids in methanogenesis. John Wiley & Sons, Inc.

Tsai, S. F., Bishop, D. F., and Desnick, R. J. (1987) Coupled-enzyme and direct assays for uroporphyrinogen III synthase activity in human erythrocytes and cultured lymphoblasts. Enzymatic diagnosis of heterozygotes and homozygotes with congenital erythropoietic porphyria. *Anal Biochem* **166:**120-33.

Tsai, S. F., Bishop, D. F., and Desnick, R. J. (1987) Purification and properties of uroporphyrinogen III synthase from human erythrocytes. *J Biol Chem* **262:**1268-73.

Verkamp, E., and Chelm, B. K. (1989) Isolation, nucleotide sequence, and preliminary characterization of the *Escherichia coli* K-12 *hemA* gene. *J Bacteriol* **171:**4728-35.

Vevodova, J., Graham, R. M., Raux, E., Schubert, H. L., Roper, D. I., Brindley, A. A., Ian Scott, A., Roessner, C. A., Stamford, N. P., Elizabeth Stroupe, M., Getzoff, E. D., Warren, M. J., and Wilson, K. S. (2004) Structure/function studies on a *S*-adenosyl-*L*-methionine-dependent uroporphyrinogen III C methyltransferase (SUMT), a key regulatory enzyme of tetrapyrrole biosynthesis. *J Mol Biol* **344:**419-33.

von Eiff, C., McNamara, P., Becker, K., Bates, D., Lei, X. H., Ziman, M., Bochner, B. R., Peters, G., and Proctor, R. A. (2006) Phenotype microarray profiling of *Staphylococcus aureus menD* and *hemB* mutants with the small-colony-variant phenotype. *J Bacteriol* **188:**687-93.

von und zu Fraunberg, M., Timonen, K., Mustajoki, P., and Kauppinen, R. (2002) Clinical and biochemical characteristics and genotype-phenotype correlation in Finnish variegate porphyria patients. *Eur J Hum Genet* **10:**649-57.

Wang, K. F., Dailey, T. A., and Dailey, H. A. (2001) Expression and characterization of the terminal heme synthetic enzymes from the hyperthermophile *Aquifex aeolicus*. *FEMS Microbiol Lett* **202:**115-9.

Warnich, L., Kotze, M. J., Groenewald, I. M., Groenewald, J. Z., van Brakel, M. G., van Heerden, C. J., de Villiers, J. N., van de Ven, W. J., Schoenmakers, E. F., Taketani, S., and Retief, A. E. (1996) Identification of three mutations and associated haplotypes in the protoporphyrinogen oxidase gene in South African families with variegate porphyria. *Hum Mol Genet* **5:**981-4.

Warren, M. J., and Jordan, P. M. (1988) Investigation into the nature of substrate binding to the dipyrromethane cofactor of *Escherichia coli* porphobilinogen deaminase. *Biochemistry* **27:**9020-30.

Warren, M. J., Raux, E., Schubert, H. L., and Escalante-Semerena, J. C. (2002) The biosynthesis of adenosylcobalamin (vitamin B_{12}). *Nat Prod Rep* **19:**390-412.

Weinstein, J. D., and Beale, S. I. (1983) Separate physiological roles and subcellular compartments for two tetrapyrrole biosynthetic pathways in *Euglena gracilis*. *J Biol Chem* **258:**6799-807.

Zeghouf, M., Fontecave, M., and Coves, J. (2000) A simplifed functional version of the *Escherichia coli* sulfite reductase. *J Biol Chem* **275:**37651-6.